HITACHI

GE Hitachi Nuclear Energy

NEDO-33284
Revision 1
Class I
DRF 0000-0036-8667
November 2007

Licensing Topical Report

Marathon-5S Control Rod Assembly

INFORMATION NOTICE

This is a non-proprietary version of the document NEDE-33284P, Revision 1, which has the proprietary information removed. Portions of the document that have been removed are indicated by an open and closed bracket as shown here [[ ]].

IMPORTANT NOTICE REGARDING THE CONTENTS OF THIS REPORT

Please Read Carefully

The information contained in this document is furnished **for the purpose of obtaining NRC approval for the use of the Marathon-5S control rod in Boiling Water Reactors**. The only undertakings of GE Hitachi Nuclear Energy respecting information in this document are contained in the contracts between GE Hitachi Nuclear Energy and the participating utilities in effect at the time this report is issued, and nothing contained in this document shall be construed as changing those contracts. The use of information by anyone other than that for which it is intended is not authorized; and with respect to **any unauthorized use**, GE Hitachi Nuclear Energy makes no representation or warranty, and assumes to liability as to the completeness, accuracy, or usefulness of the information contained in this document.

Table Of Contents

List of Tables

List of Figures

ACRONYMS AND ABBREVIATIONS

Acronym / Abbreviation	Description
AOO	Anticipated operational occurrence
ASME	American Society of Mechanical Engineers
ATWS	Anticipated Transient Without Scram
CFR	Code of Federal Regulations
CRB	Control rod blade
CRD	Control rod drive
CRDA	Control Rod Drop Accident
ECCS	Emergency core cooling system(s)
ECP	Engineering Computer Code
ESF	Engineered Safety Feature
FHA	Fuel Handling Accident
GEH	General Electric Hitachi Nuclear Energy
GNF	Global Nuclear Fuels
IASCC	Irradiation Assisted Stress Corrosion Cracking
LOCA	Loss of Coolant Accident
LTR	Licensing topical report
MCPR	Minimum Critical Power Ratio
MSLBA	Main Steamline Break Accident
NRC	U.S. Nuclear Regulatory Commission
OBE	Operating Basis Earthquake
QA	Quality assurance
RAI	Request for additional information
SRSS	Square root sum of squares
SSE	Safe Shutdown Earthquake
STS	Standard Technical Specifications
TS	Technical Specifications

EXECUTIVE SUMMARY

The GEH Marathon-5S control rod is a derivative of the Marathon design approved by Reference 1. The primary difference between the Marathon-5S and the original Marathon design, in Reference 1, is a simpler absorber tube geometry. The new simplified absorber tubes use the same crack resistant, GEH proprietary, 304S "Rad Resist" stainless steel as the current Marathon design.

The Marathon-5S uses a B_4C capsule [[

]]

A nuclear evaluation of the Marathon-5S control rod shows that the initial cold and hot reactivity worths are within ±5% of the original equipment control rod ("matched worth criteria"). Therefore, the Marathon-5S is a direct nuclear replacement for previous control rod designs, and no special nuclear calculation or BWR plant change is required.

The structure of the Marathon-5S control rod has been evaluated during all normal and upset conditions, and has been found to be mechanically acceptable. The fatigue usage of the control rod has also been found to be well below lifetime limits.

[[

]] For all cases, the mechanical lifetime exceeds the nuclear lifetime. Therefore, the Marathon-5S control rod is nuclear lifetime limited.

The operational performance of the Marathon-5S is also evaluated. The scram time, no settle characteristics, and control rod drop speeds are all better than or equal to the original Marathon design. Installation of Marathon-5S control rods does not affect any item in the Standard Plant Technical Specifications, and no plant operational change is required. Further, there is no effect on plant safety analyses or on design basis analysis models.

The licensing acceptance criteria applied to the original Marathon design in Reference 1 are re-evaluated and are judged to be sufficient and complete. Therefore, the Marathon-5S is evaluated against the licensing acceptance criteria in Reference 1, and is found to be acceptable. GEH requests NRC approval for the use of Marathon-5S control rods in Boiling Water Reactors.

1. INTRODUCTION AND BACKGROUND

GEH currently manufactures the long life Marathon Control Rod Blade (CRB). The Nuclear Regulatory Commission (NRC) acceptance of the Marathon CRB is documented by a Licensing Topical Report (LTR), Reference 1. The Marathon CRB consists of 'square' absorber tubes, edge welded together to form the control rod wings, and welded to individual tie rod segments to form the cruciform assembly shape. The square absorber tubes are filled with a combination of boron carbide (B_4C) capsules, empty capsules, hafnium rods, and spacers. Previously, GEH manufactured original equipment and replacement Duralife Control Rod Blades, which consisted of a full-length tie rod, with boron carbide absorber rods and hafnium plates and/or strips enclosed within a sheath to form each wing. The most recent Duralife Licensing Topical Report is shown as Reference 2.

The Marathon-5S is a derivative version of the Marathon CRB in that the basic design is the same. For example, the outer absorber tubes are edge welded together to form the cruciform CRB shape, and they are filled with capsules containing boron carbide (B_4C) powder. However, several design changes are made to the Marathon CRB, resulting in a more producible, medium duty version of the Marathon CRB.

Potential effects of the proposed change are evaluated to ensure

(i) the integrity of the reactor coolant pressure boundary;

(ii) the capability to shut down the reactor and maintain it in a safe shutdown condition; and

(iii) the capability to prevent or mitigate the consequences of accidents which could result in potential offsite exposures comparable to the applicable guideline exposures set forth in 10 CFR50.34(a)(1) and 10 CFR 100.11.

The following sections address the potential effect of the proposed changes on fission product barriers (e.g., fuel cladding) and other involved structures, systems and components, safety functions, design basis events, special events and Standard Technical Specifications (STS) to ensure continued compliance with design and regulatory acceptance criteria.

No design changes have been made to the Marathon-5S control rod since revision 0 of this report. This revision is made to incorporate responses to NRC Requests for Additional Information (RAI), per NRC request.

GEH requests NRC approval for the use of Marathon-5S control rods in Boiling Water Reactors.

2. DESIGN CHANGE DESCRIPTION

There are six design changes made to the long life Marathon CRB, as described in Reference 1, to produce the medium duty Marathon-5S CRB. These changes are described in the following subsections.

2.1 ABSORBER TUBE GEOMETRY

The geometry of the Marathon absorber tube is shown in Figure 2-3 of Reference 1. The geometry of the Marathon-5S absorber tube in shown in Figure 2-1 of this report. Table 2-1 provides a comparison of typical parameters for the Marathon and Marathon-5S CRBs. Figure 2-2 is a scale overlay of the original Marathon absorber tube (light blue) with the Marathon-5S absorber tube (dark blue). As shown in Figure 2-2 and Table 2-1, both the width [[
]]. As demonstrated in Figure 2-2, due to the geometry difference, [[ ]].

This comparison shows that the use of the new absorber tube geometry has no effect on the thickness of the wing, nor on the material composition of the absorber tube, GEH proprietary type 304S. The advantage of the Marathon-5S is an absorber tube whose shape is simpler to manufacture than the Marathon absorber tube.

As in the Marathon control rod, the absorber tubes are edge welded together to form the wing of the control rod. A sketch of the control rod wing is shown in Figure 2-3.

2.2 CAPSULE GEOMETRY

The Marathon-5S CRB uses a capsule body tube geometry with [[
]]. A comparison of the Marathon-5S and Marathon capsule dimensions is contained in Table 2-1. Due to irradiation induced B_4C powder swelling, a B_4C capsule expands as the absorber is depleted. [[

]].

2.3 CAPSULE LENGTH

The Marathon CRB LTR (Reference 1) identifies the nominal length of the B_4C capsules as 11.4 inches. Current Marathon CRB designs use 36" capsules [[ ]] and 24" [[ ]] B_4C capsules. [[

]]

The Marathon-5S CRB also uses 36" and 24" B_4C capsules. These capsule lengths are reflected in Table 2-1. Diagrams of absorber material columns are shown in Figure 2-4.

2.4 FABRICAST VELOCITY LIMITER

The velocity limiter currently used for Marathon CRBs is a cast/fabricated hybrid called the FabriCast. The FabriCast velocity limiter uses a casting for the "vane" of the velocity limiter (see Figrue 2-5), which has identical geometry to the "vane" portion of the single piece cast velocity limiter (called "original" in Reference 1). Because the geometry is the same, the FabriCast velocity limiter has the same drop speed and scram insertion performance as the original single piece cast velocity limiter design. The Marathon-5S CRB may use a FabriCast velocity limiter or the previous cast velocity limiters used on Duralife and Marathon CRBs.

2.5 PLAIN HANDLE

The Marathon LTR (Reference 1) allows for the use of the traditional handle with rollers or handles with wear pads. To eliminate the possibility of stress corrosion cracking initiating within the handle pin-hole, Marathon-5S CRBs for C lattice (BWR/4,5) and S lattice (BWR/6) plants incorporate the use of plain, roller-less handles. These are handles with no handle pins and rollers, but also with no protruding wear pad. An evaluation of the use of plain, roller-less handles in C lattice (BWR/4,5) and S lattice (BWR/6) applications is provided in Appendix A.

Marathon-5S control rods for D lattice (BWR/2-4) applications will use spacer pads.

2.6 FULL LENGTH TIE ROD

The Marathon CRB uses multiple tie rod segments along the center of the cruciform shape. The Marathon-5S CRB utilizes a single tie rod that runs the entire length of the assembly similar to that used on Duralife control rods (see Reference 2). The cross-sectional geometry of this full-length tie rod is designed such that it does not alter the interface between the control rod and the adjacent fuel channels. This is achieved by ensuring that contact occurs between the wing of the control rod and the face of the fuel channel and not at the fuel channel corner and tie rod.

Sketches of Marathon-5S control rods are shown in Figures 2-6, 2-7 and 2-8 for D lattice BWR/2-4, C lattice BWR/4,5, and S lattice BWR/6 applications, respectively.

Table 2-1
Comparison of Typical Parameters of Marathon and Marathon-5S CRBs

Parameter		BWR/2-4 D Lattice		BWR/4-5 C Lattice		BWR/6 S Lattice	
		Marathon CRB [1]	M-5S CRB	Marathon CRB [1]	M-5S CRB	Marathon CRB [1]	M-5S CRB
Control Rod Weight (lb) [2]		[[					
Absorber Tubes per Wing							
Nominal Wing Thickness (in)							
Absorber Tube							
	Length (in)						
	Inside Diameter (in)						
	Nominal Thin Section Wall Thickness (in)						]]
	Material	304S	304S	304S	304S	304S	304S
	Cross-sectional area (in^2)	[[					]]
B_4C Absorber Capsule							
	Length (in)	[[					
	Inside Diameter (in)						
	Wall Thickness (in)						
	Material						
	B4C Density (g/cc)						
	B4C Density (% theoretical)						]]

1. Values from Table 2-1 of the Marathon LTR (Reference 1), except for absorber tube cross-sectional area from design calculations. Current Marathon absorber capsule lengths are also updated, see Section 2.3.
2. For 'no settle' considerations, the Marathon-5S CRB has been designed to have dry and wet weights not less than 5 lbs lighter than the current Marathon CRBs, which weigh less than the original equipment.
3. [[

]].

[[

]]

Figure 2-1. Marathon-5S CRB Absorber Tube Geometry

[[

]]

Figure 2-2. Marathon and Marathon-5S Absorber Tube Geometry

[[

Figure 2-3. Marathon-5S Absorber Wing Weld Locations

[[

]]

Figure 2-4. Typical Absorber Material Configurations within Absorber Tubes

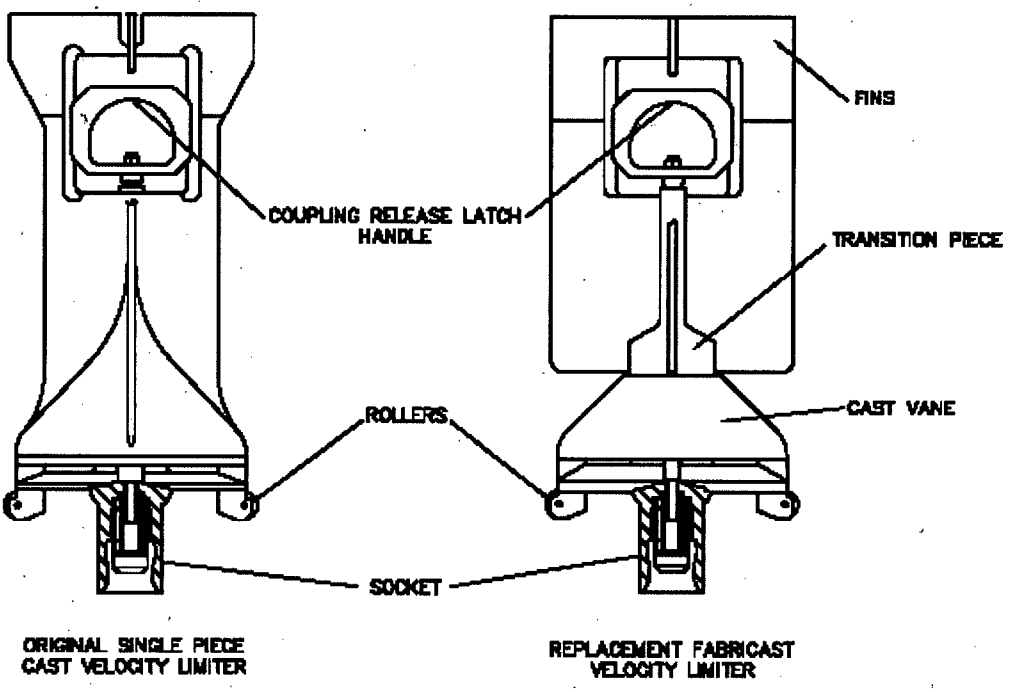

Figure 2-5. Original Single Piece Cast and Replacement FabriCast Velocity Limiters

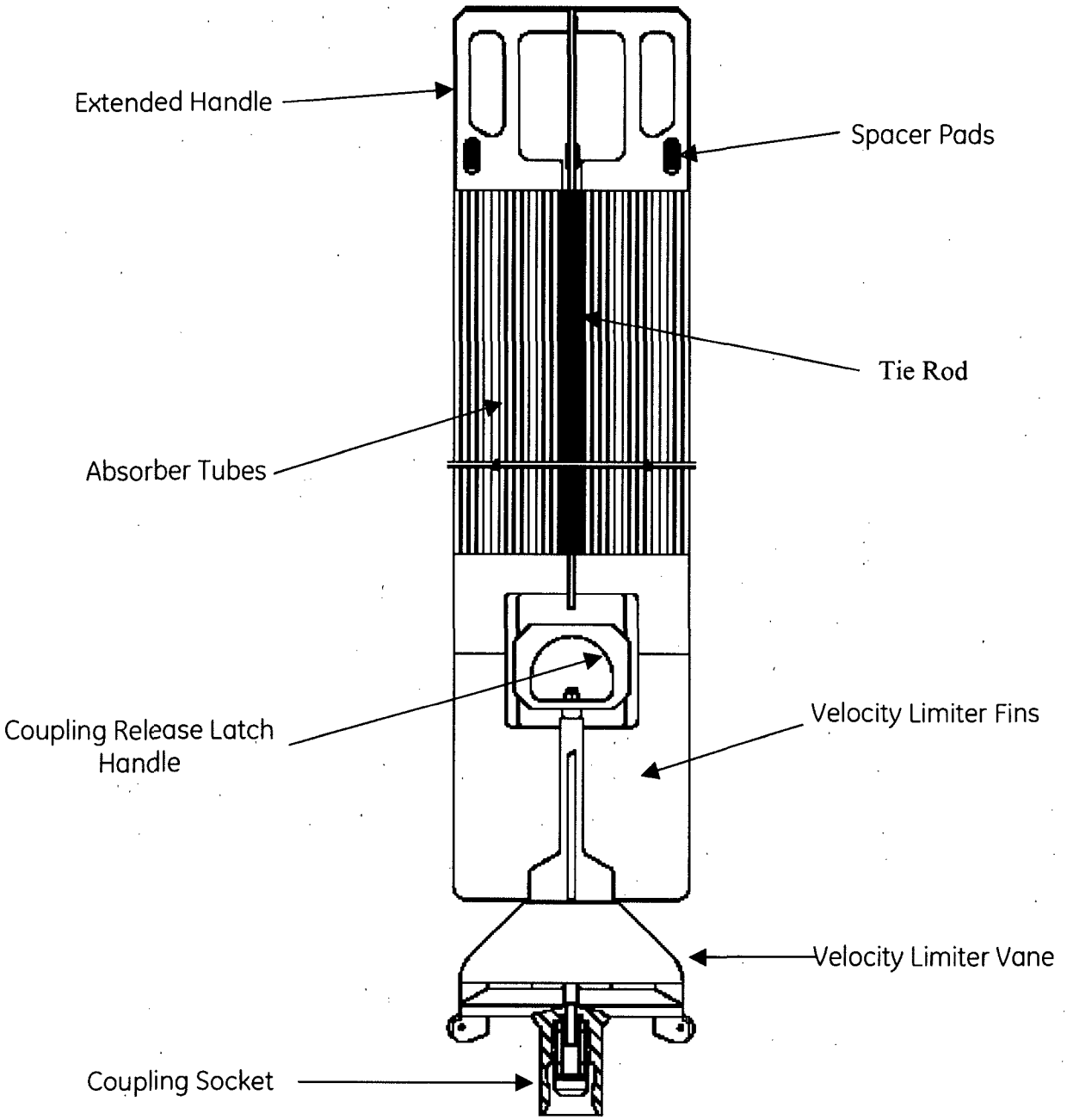

Figure 2-6. BWR/2-4 D Lattice Marathon-5S Control Rod

(Extended Handle Shown)

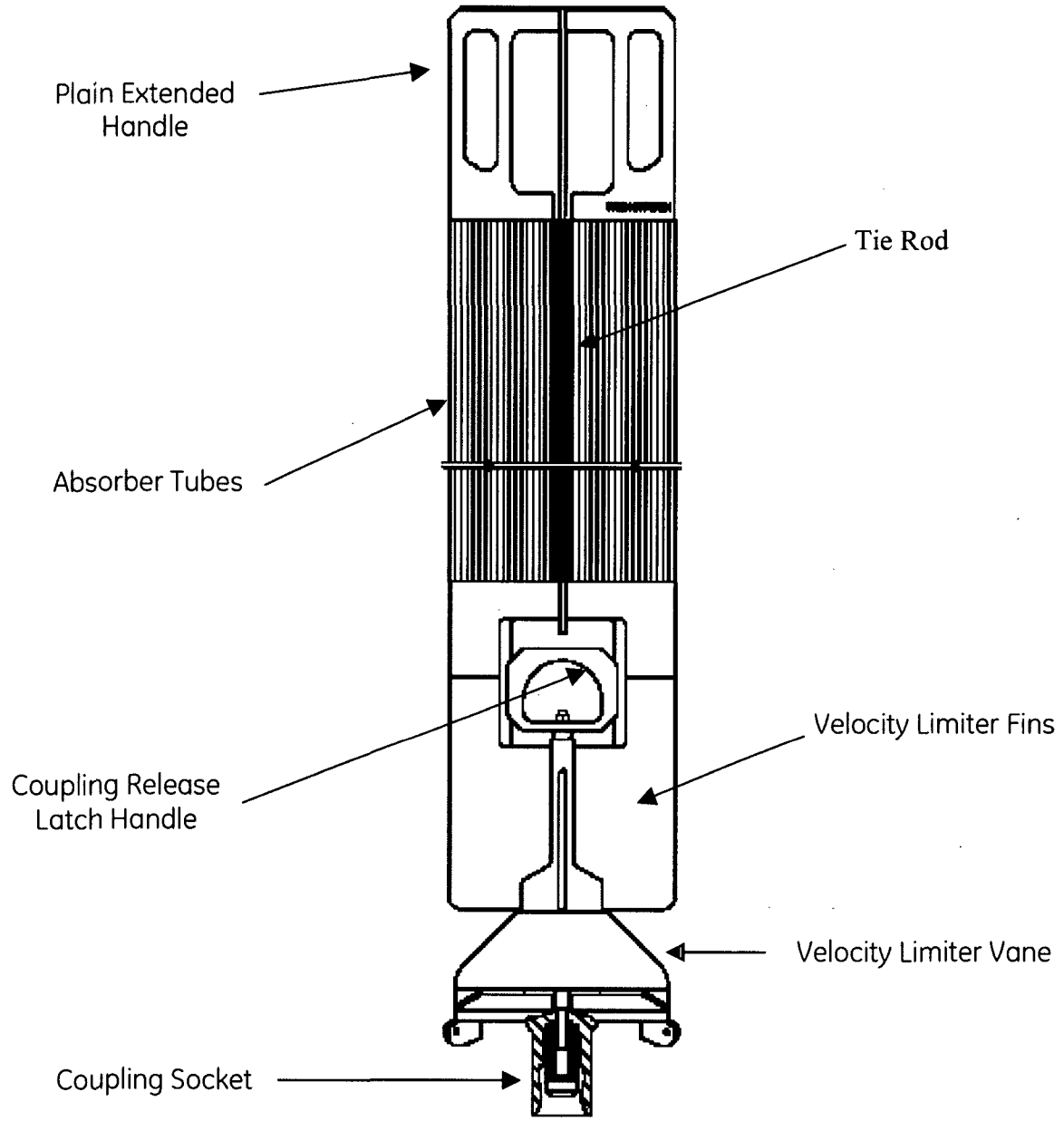

Figure 2-7. BWR/4,5 C Lattice Marathon-5S Control Rod

(Extended Handle Shown)

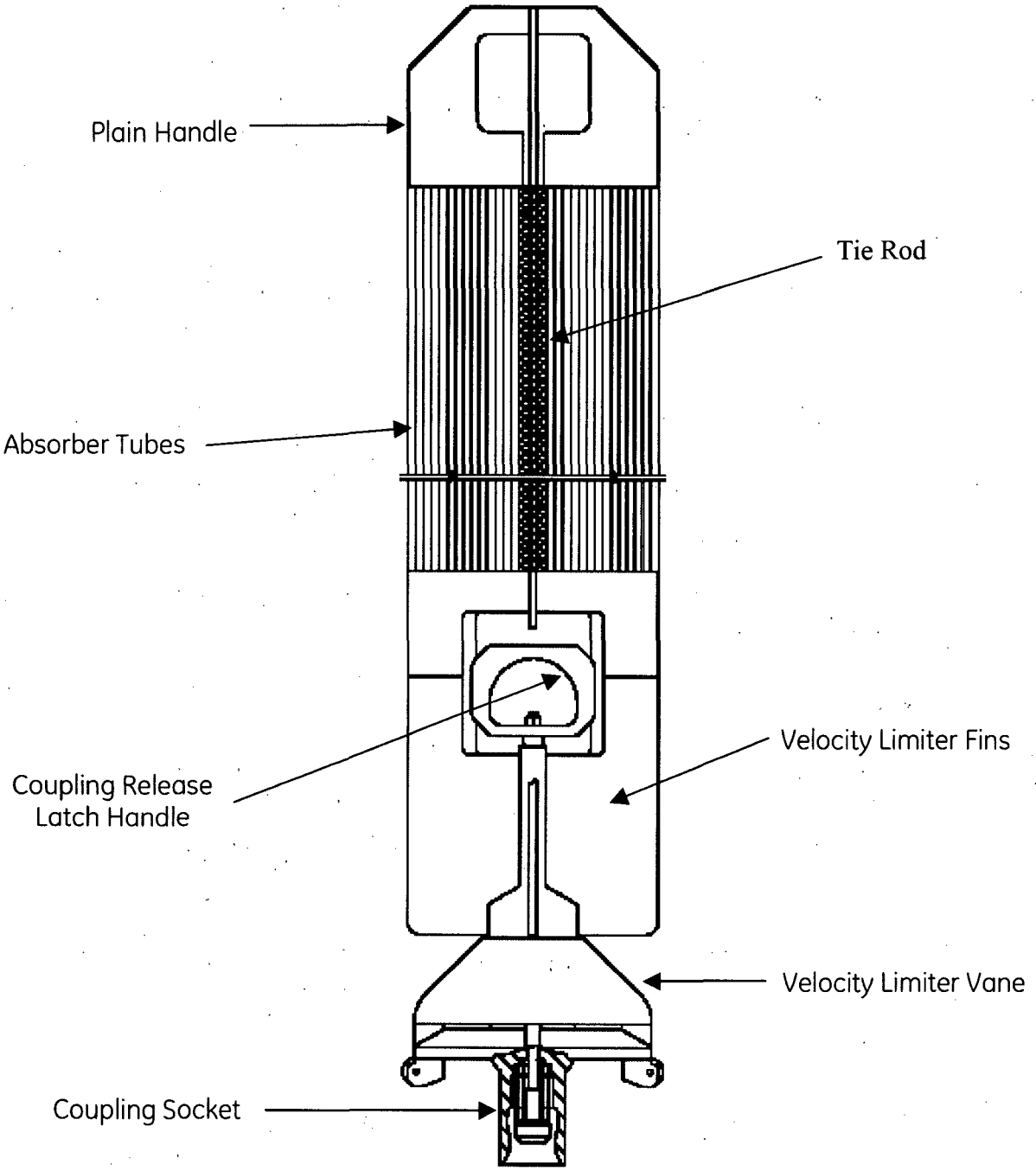

Figure 2-8. BWR/6 S Lattice Marathon-5S Control Rod

3. SYSTEM DESIGN

3.1 ANALYSIS METHOD

For each control rod load application, worst case or bounding loads are identified. Stresses are calculated using worst-case dimensions and limiting material properties. For analyses involving many tolerances, square root sum of squares (SRSS) or statistical tolerancing may be used. Corrosion, wear, and crud deposition are accounted for when appropriate.

3.1.1 Combined Loading

As in Reference 1, effective stresses and strains are determined using the distortion energy theory (Von Mises), and compared to allowable limits. Using the principal stresses: σ_1, σ_2, and σ_3, the equivalent Von Mises stress is calculated as:

$$\sigma_{VM} = \sqrt{1/2[(\sigma_1 - \sigma_2)^2 + (\sigma_2 - \sigma_3)^2 + (\sigma_3 - \sigma_1)^2]}$$

Both the Von Mises and Tresca stress criteria are used to predict the conditions for yielding under both uniaxial and multiaxial stress states. The Tresca Criterion can be called the maximum shear criterion since it measures the maximum shear stress present The Von Mises takes into account all principal stresses in the calculation of the conditions where yielding occurs. For thin walled tubes, under combined loads, the Von Mises Criterion appears to more accurately represent the condition under which yielding occurs (Reference 11). The use of the Von Mises criterion takes into consideration the hydrostatic component of stress and the corresponding strain value. It should be recognized that failure modes in thin walled structures such as control rod absorber tubes are initiated at the surface, a location where one of the three principal stresses is zero. The use of the von Mises criterion is therefore adequate to evaluate the potential for any of the important failure modes. First, ductile failure is associated with plastic flow. The criterion was developed to best assess that mode. Fatigue and crack growth processes would initiate on the surface. Again, plastic flow at the surface is necessary for these processes to start. As supported by the stress analyses results in Section 3.3 through 3.8, the stresses are below the un-irradiated stress limits. Therefore, the absorber tubes will only experience elastic deformation. This condition is also true in the irradiated condition where the stress ratio will decrease when compared to the actual irradiated yield strength value.

Given this, the effects of irradiation are well known. Specifically, the material will have a significant increase in yield strength and ultimate strength. Therefore, the design criteria used, one based on un-irradiated properties, will insure that as fluence is accumulated, the component continues to remain elastic and well below the actual yield strength. As stated in Reference 1, this approach has been previously accepted.

3.1.2 Unirradiated Versus Irradiated Material Properties

Each structural analysis is first evaluated to determine whether unirradiated or irradiated material properties are appropriate. In general, as stainless steel is irradiated, the yield and ultimate tensile strengths increase, while the ductility, or allowable strain decreases. In order to determine the correct technique, the analyses are broken into two categories:

1. Analyses with an applied load (ie, scram). For these analyses, a maximum stress is calculated, and compared to the limiting unirradiated stress limit.
2. Analyses with an applied displacement (ie, seismic bending). For these analyses, a maximum strain is calculated, and compared to the limiting irradiated strain limit.

Austenitic stainless steels do not display a ductile to brittle transition (DBTT). The material fracture toughness and ductility (in the unirradiated condition) does not vary significantly in the temperature range of interest (70 - 550°F). In turn, the effect of irradiation on austenitic stainless steel is to reduce the toughness and ductility somewhat; however, austenitic stainless steel still retains ductility after irradiation. There are existing data at high fluence that confirm the tensile ductility and fracture toughness. Specifically, ductility levels and fracture toughness data for irradiated components are documented in Reference 9. These data substantiate their ductile behavior at both room temperature as well as operating temperature.

3.2 MATERIAL PROPERTY LIMITS

The limiting unirradiated material strengths are first identified for the control rod structural materials, and shown in Table 3-1. For most materials, limiting values from the ASME Boiler and Pressure Vessel Code are used. In other cases, minimum material strengths are specified in GEH material specifications.

GEH requires that the mechanical properties of all material used in the fabrication of control rods be certified as meeting material specification limits. For example, the mechanical properties of finished, annealed, and un-irradiated type 304S absorber tubes are defined by a fabrication specification. These mechanical limits, along with the certification results of three recent absorber tube lots are shown in Table 3-26. As shown, all mechanical properties met the specification requirements. See section 3.2.4 for more information on GEH's stabilized type 304S stainless steel.

3.2.1 Stress Criteria

The licensing acceptance criteria of Reference 1 are used, in which the control rod stresses and strains and cumulative fatigue shall be evaluated to not exceed the ultimate stress or strain of the material.

The figure of merit employed for the stress-strain limit is the design ratio, where:

Design ratio = effective stress/stress limit, or, effective strain/strain limit.

The design ratio must be less than or equal to 1.0. Conservatism is included in the evaluation by limiting stresses for all primary loads to one-half of the ultimate tensile value.

Resulting allowable stresses for primary loads are shown in Table 3-2.

3.2.2 Absorber Tube Material Isotropy

The irradiation resistant special melt austenitic stainless steel (type 304S) used for the control rod absorber tubes is manufactured using standard industrial processes and solution annealing. There is no significant anisotropy produced in wrought product by these procedures. Photos of finished absorber tubes, at 300X magnification, in different orientations, are shown in Figures 3-14 through 3-16. The axial loading direction is the direction of design concern and is aligned with the direction of standard tensile tests on irradiated material. The necking observed in these irradiated tensile tests can be interpreted as supporting the adequacy of the strength and ductility of the material in the radial direction.

3.2.3 Welded Connections

For welded connections, a weld quality factor, q, is used to further reduce the allowable stress. Therefore, the allowable stress for a welded connection, Sm', is:

$$S_m' = (q)Sm$$

Weld quality factors are determined based on the inspection type and frequency of the weld. Weld quality factors are shown in Table 3-3.

3.2.4 Laser Welding Process

Laser Beam Weld (LBW) processes are used extensively in the manufacture of Marathon and Marathon-5S control rods. Welding processes for control rods are developed and qualified against a set of acceptance standards which includes: (1) meeting minimum penetration requirements, (2) smooth blends between welded members, and (3) no cracks, holes, lack of fusion or porosity. During weld process development for the Marathon-5S control rod, it was found that good results for the absorber tube-to-tube laser welds were achieved using the same parameters as the Marathon control rod.

As a result of the complexity of the control rod geometry, GEH qualifies the welding process in a manner meeting the intent of the ASME Code. The qualification method selected is to confirm the mechanical properties of the weld by using a representative mockup of the laser weld. Mechanical tests confirm that the mechanical properties of the weld were higher than the minimum properties of the base metal.

The weld quality factor (q) provides a safety margin against manufacturing defects during processing. The critical to quality components of the weld are defined by ASME B&PV code weld procedure QW-264.1, Welding Procedure Specifications, Laser Beam Welding (LBW). GEH further refines its internal critical to quality requirements from the ASME B&PV code for its day-to-day operations. [[
]].

To evaluate the strength of the absorber section to handle/velocity limiter laser weld, test panels consisting of four edge-welded absorber tubes and end plates representing the handle/fin were fabricated. These test specimens used the same weld processes and parameters as production

welds in order to provide a real-world test of the weld strength. A tensile test was then performed.

The results of this test showed that the test specimens ruptured first in the absorber tube material, prior to the rupturing of the laser weld, as shown in the Figure 3-17.

GEH performs metallographic evaluation on sample laser welds on a weekly basis to confirm that the results of the welding process remain within parameters. These results are documented. Photomicrographs of a typical laser weld, taken as part of a recent qualification test, are shown in Figure 3-16. Comparing the grain structure at the edge of the weld to an area away from the weld shows that there is no effective heat affected zone for a laser weld. This combined lack of heat affected zone, Ta stabilization, and low carbon chemistry, accounts for the good carbide test results mentioned above.

Austenitic stainless steels have no inherent age hardening capability and lend themselves readily to the welding process. GEHs' proprietary Type 304 S composition is as follows:

[[

]]

A common concern in austenitic stainless steel welds is carbide precipitation. Carbide formation in a weld heat affected zone would encourage intergranular stress corrosion cracking in this location. The combination of low heat input welding practices, tantalum stabilization, and restrictive carbon limits, provides an effective barrier to such intergranular cracking.

3.2.5 Absorber Tube Axial Shrink Due to Welding

Due to the absorber tube-to-tube laser welding process, the absorber tubes shrink by varying amounts in the axial direction. Prior to welding, the length of the absorber tube is [[

]]. The lengths of the absorber tubes after welding were measured on a production Marathon control.

The biggest difference in relative length between the absorber tubes after welding is [[ ]].

The length of the finished absorber section is [[ ]]. Therefore, the maximum axial strain due to the differential weld shrinking of the absorber tubes is:

Strain (ε)= $\Delta L/L_{initial}$ = [[ ]].

A [[ ]] strain is metallurgically insignificant in terms of driving microstructural changes in the bulk tubing. This strain is an elastic driver towards overall distortion. Distortion is minimized through production controls. Please see section 3.2.4 for further discussion with regard to the mechanical properties of the laser welds.

3.3 SCRAM

The largest axial structural loads on a control rod blade are experienced during a control rod scram, due to the high terminal velocity. To be conservative, structural analyses of the control rod are performed assuming a 100% failed control rod drive buffer. A dynamic model of mass, spring and gap elements is used to simulate a detailed representation of the load bearing components of the assembly during a scram event. Simulations are run at atmospheric temperatures, pressures, speeds, and properties as well at operating temperatures, pressures, speeds, and properties. The resulting loads are shown in Table 3-4.

Structural stresses are determined from the scram loads shown in Table 3-4 using the limiting material properties, weld quality factors, and worst-case geometry for the area subject to the load. Figures 3-1 and 3-2 show the welds and cross-sections analyzed.

Resulting maximum stresses during a failed buffer scram are shown in Tables 3-5, 3-6 and 3-7 for D lattice BWR/2-4, C lattice BWR/4-5, and S lattice BWR/6 applications. These stresses are evaluated against the stress limits shown in Table 3-2. Specific details for each calculation are shown in Appendix B. As shown by the design ratios in Tables 3-5 through 3-7, sufficient margin exists against failure for all cross-sections and welds.

3.4 SEISMIC AND FUEL CHANNEL BOW INDUCED BENDING

Fuel channel deflections, which result from seismic events, impose lateral loads on the control rods. The Marathon-5S control rod is analyzed for Operating Basis Earthquake (OBE) events and Safe Shutdown Earthquake (SSE) events.

3.4.1 Wing Outer Edge Bending

The OBE analysis is performed by evaluating the strain in the Marathon-5S absorber section with maximum OBE deflection. In addition, maximum control rod deflections due to fuel channel bulge and bow are conservatively added to the calculated seismic bending deflections. [[

]]

The limiting location for strain due to bending of the control rod cross-section occurs at the outer edge of the control rod wing. At this location, a combined strain due to simultaneous application of the following loads is calculated: (1) control rod bending due to an OBE seismic event, (2) control rod bending due to worst case channel bulge and bow, (3) axial absorber tube stress due to maximum internal pressure, and (4) a failed buffer scram. The results of these strain calculations are shown in Table 3-8. As shown, even under these combined worst-case conditions, the maximum strain is well below the limiting maximum allowable strain at irradiated conditions.

3.4.2 Absorber Tube to Tie Rod Weld

The combined effect of control rod bending due to OBE and channel bulge and bow deflection combined with maximum absorber tube internal pressure is also evaluated at the full-length tie rod to absorber tube weld. A finite element model is used, as shown in Figure 3-3. Resulting worst-case stresses are shown in Table 3-9. As shown, the resulting stresses are acceptable against the design criteria.

3.4.3 Absorber Tube Lateral Load

Finally, the lateral load imposed on the control rod absorber tube due to an excessively bowed channel is evaluated. The finite element model is shown in Figure 3-19. As shown, the entire lateral load is applied to a single square absorber tube, along with reactor internal pressure. For conservatism, no internal pressure is applied to the tube, which would offset the external pressure and reduce the stresses in the tube.

The resulting stress intensity plot is shown in Figure 3-20. The maximum stress intensity is calculated as [[ ]], which is less than the absorber tube allowable load of [[ ]] from Table 3-2.

3.4.4 Marathon-5S Seismic Scram Tests

For the SSE analysis, the control rod must be capable of full insertion during fuel channel deflections. As discussed in Section 5.2, because the Marathon-5S control rod has a stiffness less than or equal to the Marathon assembly, and because the weight of the Marathon-5S control rod is less than previous designs, the Marathon-5S has seismic scram capability equal to or better than the Marathon control rod.

To confirm the seismic scram capability of the Marathon-5S control rod, seismic scram tests were performed. This test facility consists of a simulated pressure vessel and reactor internals, and a control rod drive. Prototype Marathon-5S control rods were installed, and the control rod drive was set to simulate D, C, and S lattice operation.

The Marathon-5S prototypes used for the test incorporated plain, roller-less handles. The acceptance criterion for the test was that scram time requirements were to be met up to fuel bundle oscillation consistent with an OBE (Operational Basis Earthquake) event. The results of the tests were very successful, in that scram time requirements were met through the much more severe SSE (Safe Shutdown Earthquake) event for both the C lattice and S lattice applications.

The D lattice application met scram time requirements with OBE fuel channel deflections. During the tests, the control rods received very little wear.

3.5 STUCK ROD COMPRESSION

Maximum compression loads from the control rod drive (CRD) are evaluated for a stuck control rod. Both buckling, and compressive yield are analyzed for the entire control rod cross-section (buckling mode A), and conservatively assuming that the entire compression load is applied to a single control rod wing (buckling mode B). Figure 3-4 shows the buckling modes. An additional axial load of 600 lb due to channel bulge and bow is also added to the compression load.

Results of the stuck rod compression loads are contained in Table 3-10 for the entire control rod cross-section (mode A), and in Table 3-11 for the single wing (mode B). As can be seen, neither compressive yielding nor buckling will occur for either buckling mode. Additionally, for both buckling modes, the compressive yield load is reached prior to the critical buckling load.

3.6 ABSORBER BURN-UP RELATED LOADS

The structure of a control rod must provide for positioning and containment of the neutron absorber material (Boron Carbide powder, Hafnium, etc) throughout its nuclear and mechanical life and prohibit migration of the absorber out of its containment during normal, abnormal, emergency and faulted conditions. The Marathon-5S CRB, like the Marathon CRB, contains boron carbide powder within capsules contained within absorber tubes (capsule within a tube design).

The boron neutron absorption reaction releases helium atoms. Some of this helium gas is retained within the compacted boron carbide powder matrix, causing the powder column to swell. This swelling causes the B_4C capsule to expand. The remainder of the helium is released as a gas. The capsule end caps for the Marathon and Marathon-5S designs are crimped to the capsule body tubes. This allows the helium gas to escape from the capsule and fill the absorber tube gap and any empty capsule plenum volume provided.

For the Marathon capsule design, [[

]].

For the Marathon-5S capsule design, [[

]].

Using the pressurization capability of the absorber tube, limits are determined for each absorber tube configuration (see Figure 2-4), in terms of B_4C column depletion.

These individual absorber tube depletion limits are then combined with radial depletion profiles and axial depletion profiles to determine the mechanical depletion limit for the control rod assembly. See Section 4.6.

3.6.1 Irradiated Boron Carbide Swelling Design Basis

Mechanical test data of the irradiated behavior of boron carbide was obtained by irradiating test capsules for a period of approximately ten years in a reactor. Test capsules were placed in neutron monitor tubes and irradiated in a reactor. The configurations of two types of test capsules used are shown in Figure 3-8.

The dimensions of the test capsules were measured prior to irradiation, and post-irradiation in a hot cell using standard laboratory practice. For test capsules with a mandrel, the diametral strains were mathematically corrected to compensate for the mandrel, resulting in an increase of reported strain value.

Diametral swelling results are shown in the Table 3-17 and Figure 3-9. The Marathon-5S swelling analysis conservatively uses the +3σ upper bound value of [[ ]].

Axial swelling data is shown in Table 3-18. As shown, the axial swelling is [[

]].

3.6.2 Clearance Between Capsule and Absorber Tube

As a result of the welding process forming the control rod wings, the inside diameter of the absorber tubes shrink. Therefore, a minimum inside diameter is established, and is 100% inspected following the welding, before the absorber section is loaded with capsules.

The worst-case capsule dimensions are used, which result in the maximum outside diameter at 100% local depletion. These consist of the original maximum outside diameter, and minimum wall thickness, resulting in the maximum beginning boron carbide diameter

The strain at the ID of the capsule is equal to the diametral strain of the boron carbide powder. The +3 σ upper limit of [[ ]] from Table 3-17 is used. Then, assuming constant volume deformation of the capsule, the strain on the outside diameter of the capsule is:

[[ ]]

Then, the capsule outside diameter at 100% local depletion is:

$OD_{100\%} = OD_0(1+ \varepsilon_{OD})$.

A summary of this calculation is shown in Table 3-19 for both the D/S lattice and C lattice absorber tube and capsule combinations. [[

]].

3.6.3 Thermal Analysis

Pressure in the absorber tube due to helium release is calculated accounting for worst-case capsule and absorber tube dimensions and B_4C helium release fraction. Because the amount of helium released from the B_4C powder increases with temperature, a finite element thermal analysis is performed to determine the peak B_4C temperature (see Figure 3-6). This thermal analysis is performed using worst-case dimensions, maximum end-of-life crud buildup, combined with maximum beginning-of-life heat generation.

For the thermal model, corrosion is modeled as the build-up of an insulating layer of crud. This crud may be corrosion products from the control rod absorber tube, or deposited from other reactor internals. For all thermal analyses, a crud layer corresponding to a 32-year residence time is used ([[ ]]).

A temperature distribution is shown in Figure 3-6 for the D/S lattice case. The model used assumes that the tube is interior to the wing, in that there is another absorber tube to the left and right. The boundary on the left and right is conservatively assumed to be insulated (zero heat flux).

Results for both D/S lattice and C lattice are shown in Tables 3-24 and 3-25, and in Figures 3-11 and 3-12. The following conservatisms are applied to the thermal model:

- Peak beginning-of-life heat generation rates are used, these are combined with:
- End-of-life combined corrosion and crud build-up of [[ ]], twice that used in previous analyses.
- Peak heat generation rates are used from the highest heat generation tube, which is actually the outermost edge tube. In reality, this tube will have coolant on one side, rather than be insulated. Further some heat transfer will occur from the peak heat generation tube to the adjacent tube, rather than be perfectly insulated.
- Maximum wall thickness dimensions are used.

Peak B_4C temperatures are shown in Table 3-12. The temperatures shown in this table are based on peak beginning-of-life boron carbide heat generation rates (see section 4.5), and are from the peak heat generation absorber tube at the peak axial location. They are radially averaged only across the cross-section of an individual boron carbide capsule.

Helium release fractions are based on models developed using data from multiple sources. The data shows a significant dependence of helium release fraction on the irradiation temperature. The helium release fractions used for each lattice type are shown in Table 3-12. The helium release model is based on data from 500 °F to 1000 °F, which envelopes the temperatures shown in Table 3-12.

3.6.4 Absorber Tube Pressurization Capability

[[

]]. Finite element analyses are performed to determine the pressurization capability of the absorber tube. These analyses incorporate the use of worst-case dimensions, maximum expected wear, and the largest allowable surface defects (see Figure 3-5).

Absorber Tube Defects

The limiting case used for establishment of the absorber tube allowable pressure simultaneously combines worst-case absorber tube dimensions (thinnest wall per drawings), surface defects at the center of the flat portion of the tube, on the round portion of the tube, and a crack-like defect on the thinnest portion of the inside diameter of the tube.

The largest sized allowable surface defects are based on the manufacturing capability of the absorber tube. A collaborative effort was undertaken with the supplier of the absorber tubes to determine a maximum surface defect size that would maintain reasonable yield rates, but would not reduce the pressurization capability of the tube below acceptable values. A surface defect depth limit of [[ ]] in depth was determined, applied to the absorber tubing specification, and factored into the pressurization analysis.

At receipt inspection, the acceptance criteria for surface defects is based primarily on the depth of the defect. Additionally, matching sets of visual standards are used by both the supplier and by GEH to identify acceptable and unacceptable surface features.

The finite element analysis shows that smaller diameter defects result in larger stress concentrations around the defect. A survey was performed of surface defects, and the smallest area defect was found to be [[ ]] in diameter. Therefore, a diameter of [[ ]] was used for the finite element model surface defects.

After factoring in maximum allowable surface defects and worst-case (thinnest wall) absorber tube geometry, the finite element analysis is performed. An example stress distribution is shown in Figure 3-5. The surface defect geometry is also shown.

The burst pressure is defined as the internal pressure at which any point in the tube reaches a stress intensity equal to the true ultimate strength of the material. Then, to calculate an allowable pressure, a safety factor of 2.0 is applied to the differential pressure across the absorber tube wall such that:

$$P_{allow} = \frac{(P_{burst} - P_{external})}{2} + P_{external}$$

The calculated burst and allowable pressures are shown in Table 3-20. The results at operating temperature are limiting, and are used as the design basis allowable pressure of the tubes.

Absorber Tube Wear and Corrosion

Corrosion and wear are significant to the pressurization capability analysis of the absorber tube. In the pressurization analysis, the peak stress concentrations occur on the 'flat' portion of the tube. Combined corrosion and wear on this surface are modeled as a removal of material.

The analysis shows that combined corrosion and wear, modeled as a removal of material for the pressurization analysis, can exceed [[ ]] without affecting the design basis allowable pressure of the outer absorber tube shown in Table 3-20. For the D/S lattice absorber tube, the upper limit for combined corrosion and wear that occurs after control rod installation is [[ ]]. For the C lattice absorber tube, the upper limit is [[ ]]. This amount of wear is considered sufficiently conservative.

Maximum Stress Components

Stress components at the point of maximum stress intensity were analyzed for the absorber tube with the maximum allowable internal pressure. The point of maximum stress intensity is found to be on the outer edge of the absorber tube, at the middle of the flat portion. Principle stress components are shown in Table 3-21. All stress values shown in Table 3-21 are within the allowable stress value for 304S tubing of [[ ]] shown in Table 3-2.

Effect of the Welded Connection Between Absorber Tubes

The effect of the welded connection between adjacent absorber tubes on the stresses in the tube due to internal pressure was evaluated using a multiple tube finite element model. In this model, three adjacent absorber tubes were pressurized. A stress intensity distribution is shown in Figure 3-11. As shown, the maximum stress is at the flat portion of the tube exposed to the coolant. The effect of the adjacent pressurized tubes is to produce compressive rather than tensile stresses in the flat portions of the tube that are welded together. In this way, the opposing pressures from opposite sides of this welded ligament is actually beneficial in terms of the pressurization capability of the tubes.

A comparison of this multiple tube model to the single tube model showed that the single tube model predicts lower burst pressures. Therefore, the single tube model is used to determine design basis allowable pressures, and there is no degrading effect due to the lack of gaps between the absorber tubes in the Marathon-5S design.

The Marathon and Marathon-5S Control Rod Blades (CRB) are manufactured using very low heat input laser weld processes. The resulting regions of microstructural change including the associated heat affected zones (HAZ) are very small (see section 3.2). Based on general understanding, the fine HAZ microstructure will have mechanical properties that are equivalent to, or exceed, those of the wrought base material. Therefore, the HAZ will have mechanical properties that exceed the required minimum properties of the associated wrought material.

Two potential issues arise from welding of the absorber section: (1) sensitization and (2) residual stress. These issues are addressed below:

Sensitization: The low heat input laser welding processes have minimal impact on the wrought tube material, in that they typically do not result in sensitized material. To confirm this

conclusion, the processes are continually evaluated metallographically to confirm the acceptability of the weld region (i.e., lack of sensitization). In addition, [[

]]. Note also from section 3.6.2 that these contact hoop stresses (and associated strains) have been eliminated for the Marathon-5S control rod.

Residual stress: One major effect of the welding process is that it will introduce tensile residual stresses in the narrow weld/HAZ region. These stresses are not a significant concern for two reasons: (1) The field cracking has not been associated with the weld HAZ and (2) the irradiation experienced by the CRB over the initial time of operation can significantly reduce these stresses by 60% or more through radiation creep processes (Reference 12). At this level of reduced stress, there is little concern for any effect on stress corrosion cracking (SCC) initiation or their applied stresses and strains. In that the major concern are strains from swelling, this level of stress is well below those levels required to even produce yielding. See also section 3.2.

Absorber Tube Expansion

As the outer absorber tube is pressurized, a small amount of radial expansion is experienced. The radial expansion is evaluated using the two-dimensional finite element pressurization model. For this evaluation, the maximum allowable internal pressure is applied. The model showed that the maximum expansion of the width of the tube is [[ ]] for D/S lattice and [[ ]] for C lattice. This amount of expansion is very small, and will have no adverse effect on the fit, form or function of the control rod.

The pressurization of the absorber tubes will also cause an axial expansion of the tubes. This is due to the internal pressure pushing against the end plugs that seal the ends of the absorber tubes. Using the maximum allowable internal pressure, the area of the end plugs, and the number of pressurized tubes in the absorber section, the maximum axial load is calculated and shown in Table 3-22.

Assuming stresses remain in the elastic range, the axial strain on the absorber tubes is calculated as $\varepsilon = \sigma/E = P/AE$, with the elongation being $\Delta L = \varepsilon L$. For an absorber section that is nominally [[ ]] long, the total elongation is also shown in Table 3-22. These maximum elongations are relatively small, and will not affect the fit, form or function of the control rod.

The analyses presented in part b above independently evaluate the diametral and axial expansion of the absorber tubes due to the internal pressure in the tubes. In reality, expansion in the diametral direction will generally reduce expansion in the axial direction, and vice versa. Therefore, the strains and displacements shown in Table 3-22 are conservative.

Effect of Irradiated Material

The pressurization finite element model uses unirradiated material properties. To test the assertion that the use of unirradiated properties in the pressurization finite element model is conservative, a test case is performed. The D lattice, 550 °F case is chosen for the test, with worst-case dimensions and maximum allowable surface defects. An internal pressure of [[

]] is applied, which is the burst pressure found using unirradiated materials, as shown in Table 3-20. At this internal pressure, the maximum stress intensity using irradiated materials is [[ ]], which is less than the true ultimate strength of the irradiated material, [[ ]]. Therefore, since the test case using irradiated material properties does not reach the ultimate strength of the irradiated material, the burst pressure analysis using unirradiated material properties is conservative. Further, the maximum strain intensity in the tube for the irradiated property test is low, at [[ ]].

Burst Pressure Tests

As discussed above, the allowable pressure for the absorber tube for the Marathon-5S is based on a finite element model incorporating worst-case dimensions, along with maximum specification permitted surface defects and expected wear. The finite element analysis shows that the worst-case burst pressure, on which the allowable pressure of the Marathon-5S tube is based, is [[ ]] lower than the burst pressure using nominal dimensions and no surface defects. See Table 3-22.

To confirm the finite element results, burst pressure tests were performed on two test specimens consisting of a short panel of welded absorber tubes, in which all tubes are pressurized, see Figures 3-12 and 3-13. The resulting tested burst pressures are compared to the finite element calculated burst pressures in Table 3-23.

As shown, the test results exceed the nominal predicted burst pressure by approximately [[ ]], and exceed the worst-case burst pressure (worst-case dimensions and surface defects) by a wide margin (~[[ ]]). Since the design basis allowable pressure for the absorber tube is based on the worst-case burst pressure combined with a safety factor of 2.0, the design is conservative.

Conclusions

The analysis is conservative because it considers the combined effects of: (1) worst case tube dimensions (thinnest wall), (2) maximum allowable surface defects, (3) a large amount of combined corrosion and wear, and (4) unirradiated material properties. The true ultimate strength of the material will increase with irradiation. Burst pressure tests further validate the design basis allowable pressures.

3.6.5 Irradiation Assisted Stress Corrosion Cracking Resistance

In order for the stress corrosion cracking mechanism to activate it requires a material that is susceptible, a conducive environment and a sustained tensile stress. If one of these three mechanisms is not present to a sufficient degree, the likelihood of a stress corrosion crack to form is significantly reduced.

The Marathon absorber tube is made from a GEH proprietary stainless steel, "Rad Resist 304S", which is optimized to be resistant to Irradiation Assisted Stress Corrosion Cracking (IASCC). The Marathon-5S absorber tubes are also fabricated from this material, and thus, are expected to

have the same crack resistant properties. The chemistry of this material is shown in section 3.2.4.

In addition to using IASCC resistant material, the Marathon-5S is designed such that [[

]]. See section 3.6.2. This significantly reduces the amount of stress/strain present in the absorber tubes at the end of life, and significantly reduces the likelihood of stress-corrosion cracking.

3.7 HANDLING LOADS

The Marathon-5S control rod is designed to accommodate twice the weight of the control rod during handling, to account for dynamic loads. The handle is analyzed using a finite element model, using worst-case geometry (see Figure 3-7). Table 3-13 shows the results of the handle loads analysis.

3.8 LOAD COMBINATIONS AND FATIGUE

The Marathon-5S control rod is designed to withstand load combinations including anticipated operational occurrences (AOOs) and fatigue loads associated with those combinations. The fatigue analysis is based on the following assumed lifetime, which is consistent with previous analyses,

[[

]]

For scram, each cycle represents a single scram insertion. Scram simulations show that the oscillations in the control rod structure damp out quickly. Further, it is extremely conservative to assume [[ ]] scrams with a 100% inoperative control rod drive buffer, as the loads experienced by the control rod in a normal buffered scram are much less severe.

For the Operational Basis Earthquake (OBE), a total of [[ ]] seismic events, in which each event consists of [[ ]] cycles of control rod lateral bending. The assumption of [[ ]] lifetime OBE events is also considered very conservative.

Based on the reactor cycles, the combined loads are then evaluated for the cumulative effect of maximum cyclic loadings. The fatigue usage is evaluated against a limit of 1.0. The maximum cyclic stress is determined using a conservative stress concentration factor of 3.0. Table 3-14 shows the fatigue usage due to control rod SCRAM at three limiting weld locations. In this analysis, it is assumed that each scram occurs with a 100% failed CRD buffer.

Table 3-15 shows the fatigue usage at the control rod outer edge due to bending from OBE seismic events and severe channel bow, control rod scram, and maximum absorber tube internal pressure. As can be seen, the combined fatigue usage is much less than 1.0.

Table 3-16 shows the fatigue usage at the tie rod to first absorber tube weld. The combined loading due to failed buffer scram, maximum absorber tube internal pressure, OBE seismic

events and severe channel bow is considered. As shown, the combined fatigue usage is much less than 1.0.

It is well known that the cycles for fatigue initiation are dependent on the stress or strain range. The number of loading cycles that the control rod blade experience are limited to 100 for all of the different designs. The stress amplitudes are all in the elastic range. As shown in Tables 3-14 through 3-16, based upon the ASME Section III fatigue design curve for un-irradiated austenitic material (ref. 6), the low number of cycles represents only a small amount of cumulative damage, well below the design limit. The ½ ultimate tensile stress value represents the ASME design limit for ~30,000 cycles. It has been established that an increase in the strength level, consistent with the effect of irradiation, would only increase the margin. This is supported by data on high strength materials, which confirm that the endurance limit is close to ½ ultimate tensile stress (Reference 7).

The last consideration with regard to fatigue is an evaluation of whether there is any flow-induced vibration that could in turn provide the potential for fatigue initiation. An assessment was performed to evaluate the loads induced by transverse loading. The evaluation that treated the control blade as a cantilever beam, found that the loads were very small and would not be sufficient to even close the gap between the blade and the fuel assembly. This load is considered so small as to be negligible, and would not lead to any risk of fatigue.

Table 3-1
Marathon-5S Material Properties

Material Type	Control Rod Components	Ultimate Tensile Strength, S_U (ksi)		Yield Strength, S_Y (ksi)		Modulus of Elasticity, E (x 10^6 psi)		Poisson's Ratio, v	
		70 °F	550 °F	70 °F	550 °F	70 °F	550 °F	70 °F	550 °F
316 Plate	Handles and pads; VL fins, VL Hardware	[[							
316 Bar	Handle pads; VL hardware								
XM-19 Bar	VL socket								
CF3 Casting	VL vane casting, latch handle casting								
ER 308L	Capsule end caps, absorber tube end plugs, weld filler metal								
304S Bar	Tie rods								
304S Tubing	Absorber Tubes								
Hardened 304L Tubing	Capsule body tubes								]]

Table 3-2
Design Allowable Stresses for Primary Loads

Material Type	CR Components	½ Ultimate Tensile Stress S_m (ksi)	
		70 °F	550 °F
316 Plate	Handles and pads; VL fins, VL Hardware	[[	
316 Bar	Handle pads; VL hardware		
XM-19 Bar	VL socket		
CF3 Casting	VL vane casting, latch handle casting		
ER 308L	Capsule end caps, absorber tube end plugs, weld filler metal		
304S Bar	Tie rods		
304S Tubing	Absorber Tubes		
Hardened 304L Tubing	Capsule body tubes		]]

Table 3-3
Weld Quality Factors

Weld	Weld Inspection	Weld Quality Factor, q
Socket to Transition Piece	[[	
Transition Piece to Fin		
Fin to Absorber Section		
Handle to Absorber Section		
End Plug to Absorber Tube		
Vane to Transition Piece		]]

Table 3-4
Maximum Control Rod Failed Buffer Dynamic Loads

Components	Maximum Equivalent Loads in Kips (10^3 lbs) (Tension Listed as Negative)					
	D Lattice		C Lattice		S Lattice	
	70 °F	550 °F	70 °F	550 °F	70 °F	550 °F
Coupling	[[					
Velocity Limiter (VL)						
VL/Absorber Section Interface						
Absorber Section						
Handle/Absorber Section Interface						
Handle						
Capsules (Per Capsule)						]]

Table 3-5
D Lattice BWR/2-4 Failed Buffer Scram Stresses

Location	Room Temperature (70 °F)			Operating Temperature (550 °F)		
	Maximum Stress	Allowable Limit	Design Ratio	Maximum Stress	Allowable Limit	Design Ratio
Socket Minimum Cross-Sectional Area	[[					
Socket to Transition Piece Weld						
VL Transition Piece to Fin Weld						
VL Fin Minimum Cross-Sectional Area						
Velocity Limiter to Absorber Section Weld						
Absorber Section						
Handle to Absorber Section Weld						
Handle Minimum Cross-Sectional Area						]]

Table 3-6
C Lattice BWR/4-5 Failed Buffer Scram Stresses

Location	Room Temperature (70 °F)			Operating Temperature (550 °F)		
	Maximum Stress	Allowable Limit	Design Ratio	Maximum Stress	Allowable Limit	Design Ratio
Socket Minimum Cross-Sectional Area	[[					
Socket to Transition Piece Weld						
VL Transition Piece to Fin Weld						
VL Fin Minimum Cross-Sectional Area						
Velocity Limiter to Absorber Section Weld						
Absorber Section						
Handle to Absorber Section Weld						
Handle Minimum Cross-Sectional Area						]]

Table 3-7
S Lattice BWR/6 Failed Buffer Scram Stresses

Location	Room Temperature (70 °F)			Operating Temperature (550 °F)		
	Maximum Stress	Allowable Limit	Design Ratio	Maximum Stress	Allowable Limit	Design Ratio
Socket Minimum Cross-Sectional Area	[[					
Socket to Transition Piece Weld						
VL Transition Piece to Fin Weld						
VL Fin Minimum Cross-Sectional Area						
Velocity Limiter to Absorber Section Weld						
Absorber Section						
Handle to Absorber Section Weld						
Handle Minimum Cross-Sectional Area						]]

Table 3-8
Outer Edge Bending Strain due to Seismic and Channel Bow Bending, Internal Absorber Tube Pressure and Failed Buffer Scram

Description	D Lattice	C Lattice	S Lattice
	550 °F	550 °F	550 °F
Outer Edge Bending Strain, Seismic (%)	[[		
Outer Edge Bending Strain, Seismic + Channel Bow (%)			
Max Internal Pressure Axial Stress (ksi)			
Max Failed Buffer Scram Stress (ksi)			
Total Outer Edge Strain, Seismic + Failed Buffer Scram + Absorber Tube Internal Pressure (%)			
Total Outer Edge Strain, Seismic + Channel Bow + Failed Buffer Scram + Absorber Tube Internal Pressure (%)			
Allowable Strain (%) ½ Ultimate, Irradiated			
Design Ratio			]]

Table 3-9
Absorber Tube to Tie Rod Weld Stress

Description	D Lattice 550 °F	C Lattice 550 °F	S Lattice 550 °F
Seismic + Internal Pressure, Max S_{INT} (ksi)	[[		
Seismic + Channel Bow + Internal Pressure, Max S_{NT} (ksi)			
Ultimate Tensile Stress (ksi)			
Design Ratio			]]

Table 3-10
Stuck Rod Compression Buckling – Entire Control Rod (Mode A)

Description	D Lattice		C Lattice		S Lattice	
	70 °F	550 °F	70 °F	550 °F	70 °F	550 °F
Critical Buckling Load, P_{cr} (lb)	[[					
Compressive Yield Load (lb)						
Maximum Stuck Rod Compression Load (lb)						
Added Compression Load due to Channel Bow (lb)						
Total Compressive Load (lb)						
Design Ratio,Buckling						
Design Ratio, Compressive Yield						]]

Table 3-11
Stuck Rod Compression Buckling – Control Rod Wing (Mode B)

Description	D Lattice		C Lattice		S Lattice	
	70 °F	550 °F	70 °F	550 °F	70 °F	550 °F
Critical Buckling Load, P_{cr} (lb)	[[					
Compressive Yield Load (lb)						
Total Compressive Load (lb)						
Design Ratio, Buckling						
Design Ratio, Compressive Yield						]]

Table 3-12
Boron Carbide Peak Temperatures

Parameter	Nominal Dimensions		Worst Case Dimensions	
	D/S Lattice	C Lattice	D/S Lattice	C Lattice
B_4C Centerline Temperature (°F)	[[			
Average B_4C Temperature (°F)				
Helium Release Fraction (%)				]]

Table 3-13
Handle Lifting Load Stress

Lattice Type	Handle Type	Maximum Stress Intensity (ksi)	Design Ratio, ½ Ultimate Stress
D Lattice BWR/2-4	BWR/4 Extended Handle	[[	
	BWR/3 Extended Handle		
	Standard Handle		
C Lattice BWR/4-5	Extended Handle		
	Standard Handle		
S Lattice BWR/6	Standard Handle		]]

Table 3-14
Fatigue Usage due to Failed Buffer Scram

Location	D Lattice				C Lattice				S Lattice			
	Stress Amp. (ksi)	Allow Cycles (N)	Actual Cycles	Usage	Stress Amp. (ksi)	Allow Cycles (N)	Actual Cycles	Usage	Stress Amp. (ksi)	Allow Cycles (N)	Actual Cycles	Usage
Socket to Transition Piece Weld	[[											
Transition Piece to Fin Weld												
VL Fin to Absorber Section Weld												]]

Table 3-15
Fatigue Usage at Absorber Section Outer Edge

Stress Type	D Lattice				C Lattice				S Lattice			
	Stress Amp. (ksi)	Allow Cycles (N)	Actual Cycles	Usage	Stress Amp. (ksi)	Allow Cycles (N)	Actual Cycles	Usage	Stress Amp. (ksi)	Allow Cycles (N)	Actual Cycles	Usage
Absorber Section Outer Edge - Scram + Internal Pressure	[[											
Absorber Section Outer Edge – Seismic + Channel Bow												]]
	Total Usage =		[[	]]	Total Usage =		[[	]]	Total Usage =		[[	]]

Table 3-16
Fatigue Usage at Absorber Tube to Tie Rod Weld

Stress Type	D Lattice				C Lattice				S Lattice			
	Stress Amp. (ksi)	Allow Cycles (N)	Actual Cycles	Usage	Stress Amp. (ksi)	Allow Cycles (N)	Actual Cycles	Usage	Stress Amp. (ksi)	Allow Cycles (N)	Actual Cycles	Usage
Absorber Tube to Tie Rod Weld - Scram	[[											
Absorber Tube to Tie Rod Weld – Seismic + Channel Bow + Internal Pressure												]]
	Total Usage =		[[	]]	Total Usage =		[[	]]	Total Usage =		[[	]]

Table 3-17
Irradiated Boron Carbide Diametral Swelling Data

[[

]]

Table 3-18
Irradiated Boron Carbide Axial Swelling Data

[[

]]

Table 3-19
Irradiated Boron Carbide Capsule Swelling Calculation

Parameter	D/S Lattice	C Lattice
Absorber Tube ID Before Welding (in)	[[	
Minimum Absorber Tube ID After Welding (in)		
Capsule OD (in)		
Capsule Wall Thickness (in)		
Maximum Capsule OD_0 (in)		
Maximum Capsule ID_0 (in)		
Capsule ID strain (in/in)		
Capsule OD strain (in/in)		
Capsule OD at 100% local depletion		]]

Table 3-20
Absorber Tube Pressurization Results: Minimum Material Condition with OD and ID Surface Defects

Lattice	Temp (°F)	External Pressure (psi)	FEA Burst Pressure (psi)	**Allowable Pressure (psi)**
C	70	14.7	[[	
C	550	1050		
D	70	14.7		
D	550	1050		]]

Table 3-21
Absorber Tube Pressurization Results: Principle Stress Results at Operating Temperature and Pressure and Maximum Allowable Pressure

Stress Component	D/S Lattice	C Lattice
S1 (Hoop)	[[	
S2 (Axial)		
S3 (Radial)		
Stress Intensity		
Equivalent Stress		]]

Table 3-22
Control Rod Axial Elongation due to Absorber Tube Pressurization

Parameter	D Lattice	C Lattice	S Lattice
Axial Load due to Pressurization (kips)	[[		
Absorber Section Cross-Sectional Area (in^2)			
Modulus of Elasticity, E (ksi)			
Strain (in/in)			
Elongation, ΔL (inch)			]]

Table 3-23
D/S Lattice Burst Pressure Results from FEA and Testing

Parameter (D/S Lattice)	Burst Pressure (psia)
Nominal Dimensions (FEA)	[[
Worst-Case Dimensions and Maximum Surface Defects (Design Basis) (FEA)	
Specimen 1 Tested Burst Pressure	
Specimen 2 Tested Burst Pressure	]]

Table 3-24
D/S Lattice Thermal Analysis Results

Location	Nominal Dimensions		Worst Case Dimensions	
	Radius (in)	Nodal Temp (°F)	Radius (in)	Nodal Temp (°F)
Centerline	[[			
Ring1 OD				
Ring2 OD				
Ring3 OD				
Ring4 OD				
Ring5 OD				
Ring6 OD				
Ring7 OD				
Ring8 OD				
Capsule ID				
Capsule OD				
Abs Tube ID				
Abs Tube OD				
Crud Surface				
Avg B4C				
Avg He Void				]]

Table 3-25
C Lattice Thermal Analysis Results

Location	Nominal Dimensions		Worst Case Dimensions	
	Radius (in)	Nodal Temp (°F)	Radius (in)	Nodal Temp (°F)
Centerline	[[			
Ring1 OD				
Ring2 OD				
Ring3 OD				
Ring4 OD				
Ring5 OD				
Ring6 OD				
Ring7 OD				
Ring8 OD				
Capsule ID				
Capsule OD				
Abs Tube ID				
Abs Tube OD				
Crud Surface				
Avg B4C				
Avg He Void				]]

Table 3-26
Type 304S Absorber Tube Mechanical Properties

Property	Room Temperature Yield Stress (ksi)	550 °F Yield Stress (ksi)	Room Temperature Ultimate Tensile Stress (ksi)	550 °F Ultimate Tensile Stress (ksi)	Room Temperature Elongation (% in 2 inches)
Specification Requirement*	[[				
Example Lot 1					
Example Lot 2					
Example Lot 3					]]

* These material requirements are specified in the fabrication specification for the absorber tubes. The tubing supplier certifies each lot of absorber tubes as meeting these requirements.

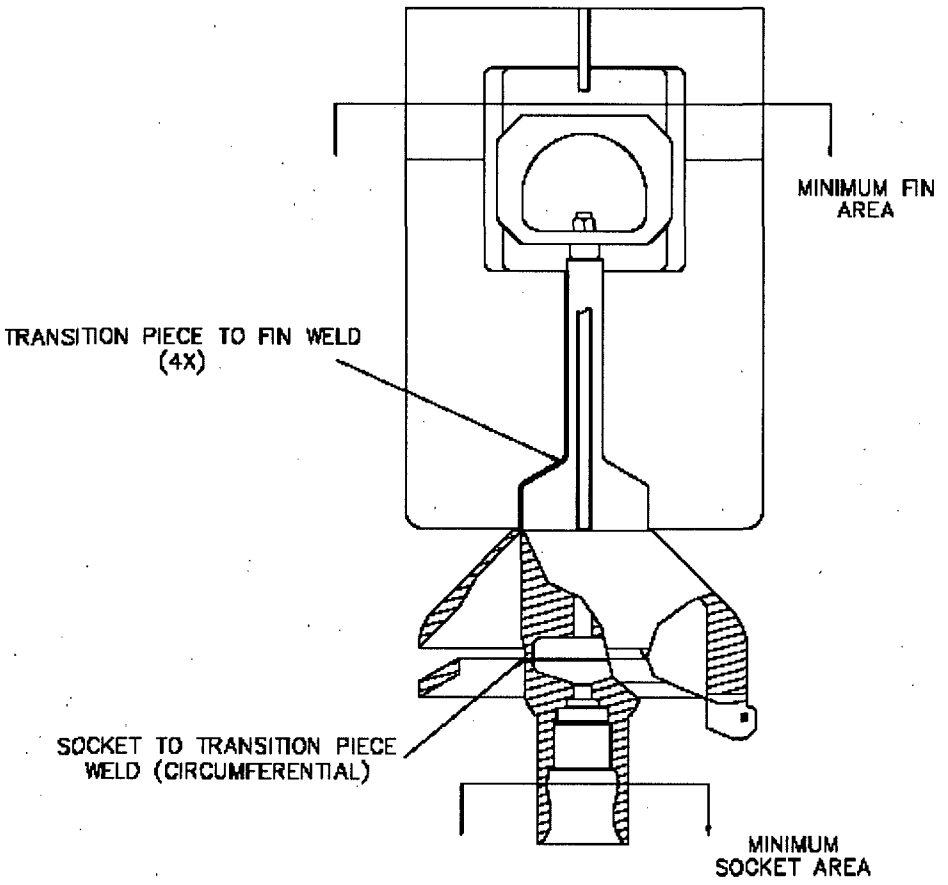

Figure 3-1. Velocity Limiter Welds and Cross-Sections Analyzed

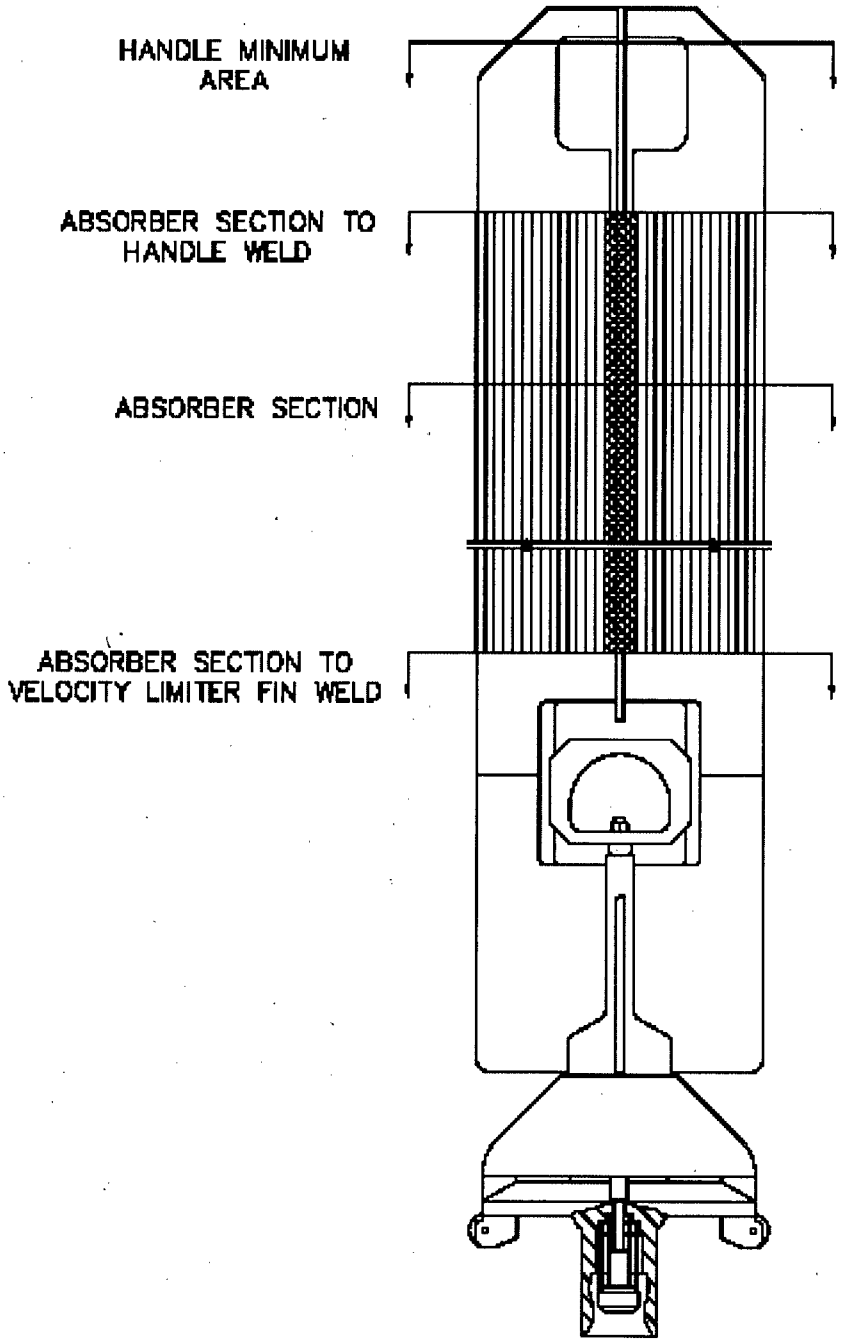

Figure 3-2. Control Rod Assembly Welds and Cross-Sections Analyzed

[[

]]

Figure 3-3. Absorber Tube to Tie Rod Finite Element Model

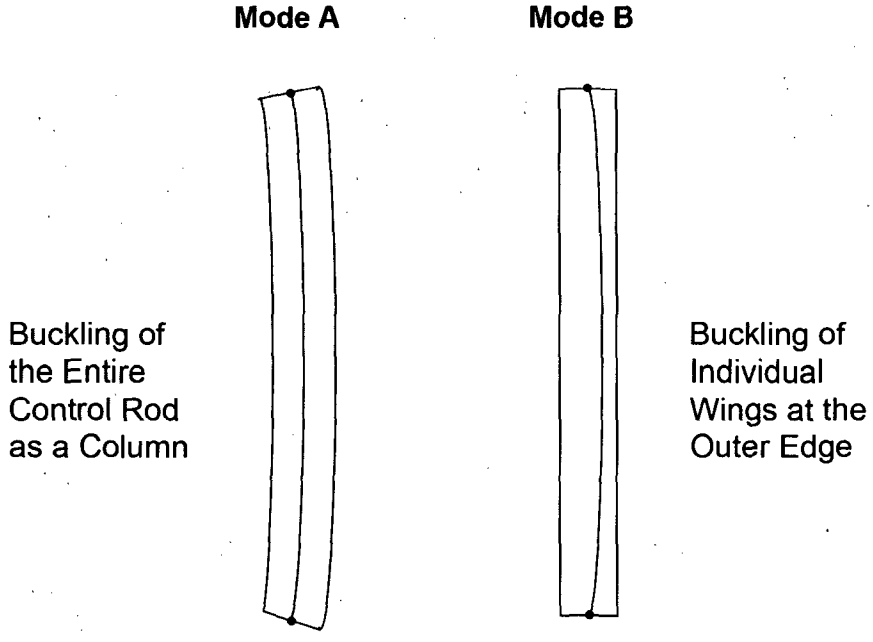

Figure 3-4. Control Rod Buckling Modes

[[

]]

Figure 3-5. Absorber Tube Pressurization Finite Element Model

[[

]]

Figure 3-6. Absorber Tube and Capsule Thermal Finite Element Model

[[

]]

Figure 3-7. Handle Lifting Loads Finite Element Model

[[

]]

Figure 3-8. Irradiated Test Capsule Configurations

[[

]]

Figure 3-9. Irradiated Boron Carbide Diametral Swelling Data

[[

]]

Figure 3-10. Neutron Radiograph of Irradiated Marathon Absorber Capsules

[[

]]

Figure 3-11. D/S Lattice Thermal Analysis Results

[[

]]

Figure 3-12. C Lattice Thermal Analysis Results

[[

]]

Figure 3-11. Stress Intensity Distribution for Multiple Tube Pressurization Finite Element Model, All Tubes Pressurized

[[

]]

Figure 3-12. Absorber Tube Burst Pressure Test Specimen – After Test

[[

]]

Figure 3-13. Absorber Tube Burst Pressure Test Specimen Rupture

[[

]]

Figure 3-14. Absorber Tube Material, 300X Magnification

[[

]]

Figure 3-15. Absorber Tube Material, 300X Magnification

[[

]]

Figure 3-16. Absorber Tube Material, 300X Magnification

[[

]]

Figure 3-17. Absorber Section Tensile Test Specimen After Rupture

[[

]]

Figure 3-18. Typical Autogenous Laser Weld of 304S Absorber Tubes

[[

]]

Figure 3-19. Lateral Load Finite Element Model

[[

]]

Figure 3-20. Lateral Load Finite Element Results (C Lattice)

4. NUCLEAR EVALUATIONS

4.1 DESIGN CRITERIA

A control rod's nuclear worth characteristics shall be compatible with reactor operation requirements. As approved in Reference 1, a replacement control rod can meet these requirements by demonstrating that the initial hot and cold CRB reactivity worths are within ± 5% Δk/k (where Δk/k is $1-k_{con}/k_{unc}$) of the original equipment control rod blade design worth. Replacement rods with reactivity worth outside this tolerance require, as a minimum, evaluations on cold shutdown margin, AOO CPR, control rod drop accident, fuel cycle economics, nuclear methods, and control rod lifetime.

For GEH original equipment control rods, the nuclear lifetime is defined as the quarter-segment depletion at which the control rod cold worth (Δk/k) is 10% less than its zero-depletion cold worth. The original equipment (DuraLife 100) control rods consist of thin sheaths enclosing boron carbide filled tubes. The sheaths are welded to a central tie rod to form the cruciform shape of the control rods. The original equipment control rods are shown in Figure 4-7.

As discussed above, a retrofit design may have an initial cold worth that differs from the original equipment control rod that it is replacing, within ±5% of the initial worth of that control rod (the "matched worth" criterion). The nuclear lifetime for such a retrofit control rod is defined as the quarter-segment depletion at which the cold worth is the same as the end-of-nuclear-life cold worth of the original equipment control rod that it is replacing.

4.2 METHODOLOGY

The nuclear lifetime for a particular control blade design is determined with a two-dimensional step-wise depletion of the control blade poisons. This is done by computing the eigenvalue for hot, voided conditions with a Monte Carlo neutron transport code. The poison reaction rates from the analysis are then assumed to be constant for a fixed period of time (Δt) to obtain the number of absorptions for each discrete area of the blade. The poison number densities are then updated in the Monte Carlo code input and another eigenvalue calculation is performed. This process continues until the reduction in cold worth – as computed by companion cold Monte Carlo eigenvalue calculations – reaches the end-of-nuclear-life criterion.

For locations within the blade that use boron carbide as a poison, the change in the number of absorber atoms is computed as:

$$\frac{dN_{B-10}}{dt} = -(N \cdot \sigma)_{B-10}$$

Here, σ is the reaction rate for B-10 from the Monte Carlo code.

The number of absorptions from each of the regions is summed to obtain the total number of absorptions (A) for the time interval. This total number of absorptions is normalized by the total number of B-10 atoms if the design would have incorporated only boron carbide as an absorber. The resulting value is the B-10 equivalent depletion:

$$\%_{depletion} = \frac{A}{N_{B-10}}$$

Reactivity worth calculations for the Marathon-5S are performed using a GEH controlled version of MCNP4A developed by the Los Alamos National Laboratory (Reference 3). MCNP is a Monte Carlo code for solving the neutral-particle transport equation as a fixed source or an eigenvalue problem in three dimensions. Continuous energy cross section data is used in the calculation, thus making creation of multi-group cross sections unnecessary. The use of MCNP is the only process change from the original Marathon nuclear analysis which used MERIT. Otherwise, depletion calculations remain unchanged.

Two additional utility codes are used in conjunction with MCNP. The GEH utility code "MODL" is used to set up the MCNP input deck, based on lattice design data and control rod design data. The GEH utility code "HO" is coupled to MCNP for the depletion calculation. It reads the MCNP tallies (cell fluxes and absorber cross sections) and then performs the control blade depletion calculation. The depleted absorber atom densities are then used to update the MCNP inputs for the next time step. MCNP input data for cold case are also generated with "HO" by modifying the input data from the hot inputs.

For the depletion calculations that are performed for each fuel lattice, the time step used is 100 days. In order to reach the 10% cold worth reduction for the nuclear lifetime evaluation, a total of 21 time steps are used for the re-calculation of DuraLife 100 (original equipment), and a total of 30 time steps are used for the calculation of Marathon-5S lifetime. Tables 4-13 through 4-15 contain input parameters used to model the original equipment and Marathon-5S control rods.

B-10 drift, defined as the faster depletion of B-10 on the outer edge of B_4C column than the average pin due to spatial self-shielding of B-10 is accounted for in the MCNP calculations. The calculations use a ring model that divides each B_4C column into four concentric rings of equal cross-sectional area. The radii of the boron carbide rings used in the updated analysis are shown in Table 4-12.

4.3 CONTROL ROD NUCLEAR LIFETIME

A description of the fuel bundles used for the D, C, and S lattice control rod nuclear lifetime calculations are shown in Figures 4-1 through 4-3. Both the hot and cold calculation results for the peak ¼ segment are shown in Tables 4-1 through 4-3. The cold calculation results, on which the nuclear lifetime is based, are shown graphically in Figures 4-4 through 4-6. The nuclear lifetimes, based on a cold worth equal to a cold worth reduction of 10% for an original equipment control rod are summarized in Table 4-4.

4.4 INITIAL CONTROL ROD WORTH

As discussed above, a control rod with an initial (non-depleted) reactivity worth within ±5% of the original equipment control rod is considered "matched worth" and therefore, does not require any special treatment in plant core analyses. The initial cold and hot worths (0% depletion) of the Marathon-5S control rod designs are found in Tables 4-1 through 4-3. These values of Δk/k

are then compared to the worths of the original equipment control rods in Tables 4-5 through 4-7. Although the Marathon-5S control rod has a lower initial worth than the previous Marathon control rod (Reference 1), all cold and hot initial control rod worths are within ±5% of the original equipment, and can be considered to be direct nuclear replacements of the original equipment.

4.5 HEAT GENERATION RATES

The capture of neutrons by boron-10 atoms results in the release of energy, or heat generation. As discussed in Section 3.6, a thermal model of the absorber tube and capsule is used to calculate boron carbide temperatures within the capsules, which affects the rate of helium release. The heat generation rates for the Marathon-5S designs are calculated assuming 2.79 MeV per neutron capture in boron-10. Then, a radial peaking factor is employed to determine the heat generation rate in the highest fluence absorber tube, which is the outermost tube.

Both average and peak heat generation rates are shown in Table 4-8. The peak heat generation rates are used in the thermal model discussed in Section 3.6 to determine the capsule boron carbide temperatures shown in Table 3-12.

4.6 CONTROL ROD MECHANICAL LIFETIME

As discussed in Section 3.6, the lifetime limiting mechanism for the Marathon-5S control rod is the pressurization of the absorber tubes due to the helium release from the irradiated boron carbide. An absorber tube mechanical limit as a function of average B-10 per cent depletion is calculated based on peak heat generation, temperatures and helium release fractions, combined with worst-case component geometries. As discussed in Section 3.6, the method for evaluating the swelling phenomenon of irradiated boron carbide is very conservative, using worst-case capsule and absorber tube dimensions, along with a $+3\sigma$ upper limit swelling rate assumption. Using these conservatisms, the Marathon-5S capsule is designed [[

]].

The calculation of the control rod mechanical lifetime limit, in terms of a four-segment average B-10 depletion, is shown in Tables 4-9, 4-10 and 4-11 for D, C, and S lattice applications. Along the top of the table is the absorber tube number, where tube 1 is the first absorber tube, welded to the cruciform tie rod. Also shown are the span-wise radial peaking factors, which show the relative absorption rate of each absorber tube. A limiting axial depletion profile is used to calculate the B-10 depletion for each absorber tube and axial node. At the bottom of the table, the average depletion for each tube is shown, along with the depletion limit for that tube, which varies depending on the number of empty capsule plenums employed at the bottom of the absorber column. Through an iterative process, the peak ¼ segment depletion is raised until the limiting absorber tube reaches its mechanical limit. The 4-segment mechanical lifetime of the control rod is then the average of the four ¼ segments.

The 4 segment mechanical lifetime limits are summarized in Table 4-4, along with the peak ¼ segment nuclear lifetime limits. [[

]]. Therefore, the nuclear lifetime of the

Marathon-5S control rod is limiting, in that the mechanical lifetime exceeds the nuclear lifetime for all cases.

4.7 CONTROL ROD DEPLETION MONITORING

The nuclear depletion calculation summarized above is performed to establish limits on the lifetime of the control rod, expressed as a maximum ¼ -segment depletion. The nodal and ¼ -segment depletions for each control rod are tracked by the core monitoring computer. For those plants that use GNF's 3D Monicore for core monitoring, control rod depletions are updated hourly.

"Quarter-segment depletion" is defined as the average depletion of nodal depletion values in a given axial ¼ segment (6 nodes) of the control rod, averaged over four wings. So for any depletion time step, there are 4 quarter-segment depletion values for a given axial depletion profile. In GEH control rod design, the nuclear lifetime is defined as the depletion value of any quarter segment at which the control rod cold worth is 10% less than the zero-depletion cold worth of the Original Equipment. "Local depletion" is normally defined as the depletion value for each absorber rod in a one-inch segment.

As part of a destructive examination of a DuraLife type control rod, the nodal depletions taken from the monitoring computer were compared to measured values from the control rod being examined. The two sets of depletions were found to be in good agreement.

Table 4-1
D Lattice Depletion Calculation Results

Irradiation Time (days)	Equivalent B-10 Depletion (%)	Hot, Voided Eigenvalue	Hot Worth (Δk/k)	Hot Change in Worth (%)	Cold Eigenvalue	Cold Worth (Δk/k)	Cold Change in Worth (%)
[[							]]

Table 4-2
C Lattice Depletion Calculation Results

Irradiation Time (days)	Equivalent B-10 Depletion (%)	Hot, Voided Eigenvalue	Hot Worth (Δk/k)	Hot Change in Worth (%)	Cold Eigenvalue	Cold Worth (Δk/k)	Cold Change in Worth (%)
[[							]]

Table 4-3
S Lattice Depletion Calculation Results

Irradiation Time (days)	Equivalent B-10 Depletion (%)	Hot, Voided Eigenvalue	Hot Worth (Δk/k)	Hot Change in Worth (%)	Cold Eigenvalue	Cold Worth (Δk/k)	Cold Change in Worth (%)
[[							]]

Table 4-4
Marathon-5S Control Rod Nuclear and Mechanical Depletion Limits

Application	End of Life B-10 Equivalent Depletion (%)	
	Nuclear Peak Quarter Segment	Mechanical Four Segment Average
D Lattice, BWR/2-4	[[	
C Lattice, BWR/4,5		
S Lattice, BWR/6		]]

Table 4-5
Initial Reactivity Worth, D Lattice (BWR/2-4) Original Equipment and Marathon-5S CRBs

Condition	Original Equipment Δk/k	Marathon-5S Δk/k	Marathon-5S Change from Original Equipment
Cold	[[		
Hot (40% Void)			]]

Table 4-6
Initial Reactivity Worth, C Lattice (BWR/4,5) Original Equipment and Marathon-5S CRBs

Condition	Original Equipment Δk/k	Marathon-5S Δk/k	Marathon-5S Change from Original Equipment
Cold	[[		
Hot (40% Void)			]]

Table 4-7
Initial Reactivity Worth, S Lattice (BWR/6) Original Equipment and Marathon-5S CRBs

Condition	Original Equipment Δk/k	Marathon-5S Δk/k	Marathon-5S Change from Original Equipment
Cold	[[		
Hot (40% Void)			]]

Table 4-8
Heat Generation Rates

Application	Average Heat Generation Rate (Watts/gram B_4C)	Radial Peaking Factor	Peak Tube Heat Generation Rate (Watts/gram B_4C)
D Lattice, BWR/2-4	[[		
C Lattice, BWR/4,5			
S Lattice, BWR/6			]]

Table 4-9
D Lattice Mechanical Lifetime Calculation

[[

]]

Table 4-10
C Lattice Mechanical Lifetime Calculation

[[

]]

Table 4-11
S Lattice Mechanical Lifetime Calculation

[[

]]

Table 4-12
Boron Carbide Ring Radii in MCNP Model

Ring Number	Ring Radial Thickness (cm)	
	Marathon-5S, D and S Lattice	Marathon-5S, C Lattice
1 (inner)	[[	
2		
3		
4 (outer)		]]

Table 4-13
D Lattice Original Equipment and Marathon-5S Dimensions

Description		**DuraLife 100 D**		**Marathon-5S D**	
		(inches)	(cm)	(inches)	(cm)
Span		[[			
Half Span	SBL				
Wing Thickness (Square Tube Width)					
Half Wing Thickness	TBL				
Tie Rod Half Thickness	TTR				
Radius of Central Support Filet	RBLF				
Radius of Blade Tip	RBLT				
Span of Central Support (Tie Rod)					
Half Span of Central Support	SCS				
Thickness of Sheath	TSH				
Inner Diameter of Tube (Capsule)	**TID**				
Outer Diameter of Tube	TOD				
Wall Thickness of Tube					
Type	IBLADE				
Number of B4C Tubes (Capsules)	**NOPT**				
Number of Hafnium Rods	NOHFT				
Number of Empty Tubes	NOBT				]]

Table 4-14
C Lattice Original Equipment and Marathon-5S Dimensions

Description		DuraLife 100 C		Marathon-5S C	
		(inches)	(cm)	(inches)	(cm)
Span		[[			
Half Span	SBL				
Blade Thickness (Square Tube Width)					
Half Blade Thickness	TBL				
Tie Rod Half Thickness	TTR				
Radius of Central Support Filet	RBLF				
Radius of Blade Tip	RBLT				
Span of Central Support (Tie Rod)					
Half Span of Central Support	SCS				
Thickness of Sheath	TSH				
Inner Diameter of Tube (Capsule)	**TID**				
Outer Diameter of Tube (Hafnium Rod)	TOD				
Wall Thickness of Tube					
Type	IBLADE				
Number of B4C Tubes (Capsules)	**NOPT**				
Number of Hafnium Rods	NOHFT				
Number of Empty Tubes	NOBT				]]

Table 4-15
S Lattice Original Equipment and Marathon-5S Dimensions

Description		DuraLife 100 S		Marathon-5S S	
		(inches)	(cm)	(inches)	(cm)
Span		[[			
Half Span	SBL				
Wing Thickness (Square Tube Width)					
Half Wing Thickness	TBL				
Tie Rod Half Thickness	TTR				
Radius of Central Support Filet	RBLF				
Radius of Blade Tip	RBLT				
Span of Central Support (Tie Rod)					
Half Span of Central Support	SCS				
Thickness of Sheath	TSH				
Inner Diameter of Tube (Capsule)	**TID**				
Outer Diameter of Tube	TOD				
Wall Thickness of Tube					
Type	IBLADE				
Number of B4C Tubes (Capsules)	**NOPT**				
Number of Hafnium Rods	NOHFT				
Number of Empty Tubes	NOBT				]]

[[

]]

Figure 4-1. D Lattice Fuel Bundle Rod Position and Enrichment

[[

]]

Figure 4-2. C Lattice Fuel Bundle Rod Position and Enrichment

[[

]]

Figure 4-3. S Lattice Fuel Bundle Rod Position and Enrichment

[[

]]

Figure 4-4. D Lattice Control Rod Cold Worth Reduction with Average Depletion

[[

]]

Figure 4-5. C Lattice Control Rod Cold Worth Reduction with Average Depletion

[[

]]

Figure 4-6. S Lattice Control Rod Cold Worth Reduction with Average Depletion

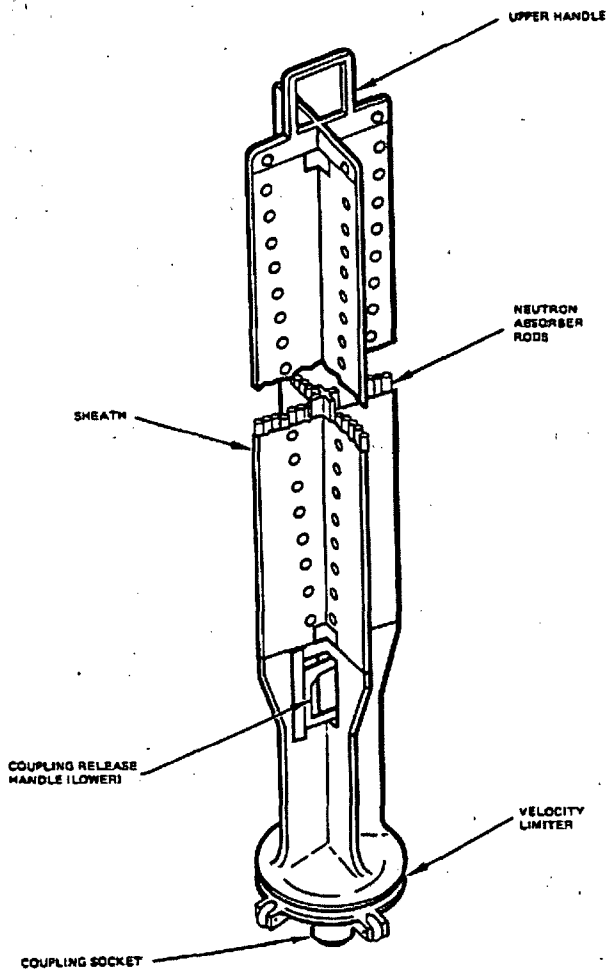

ORIGINAL EQUIPMENT CONTROL ROD DESIGN

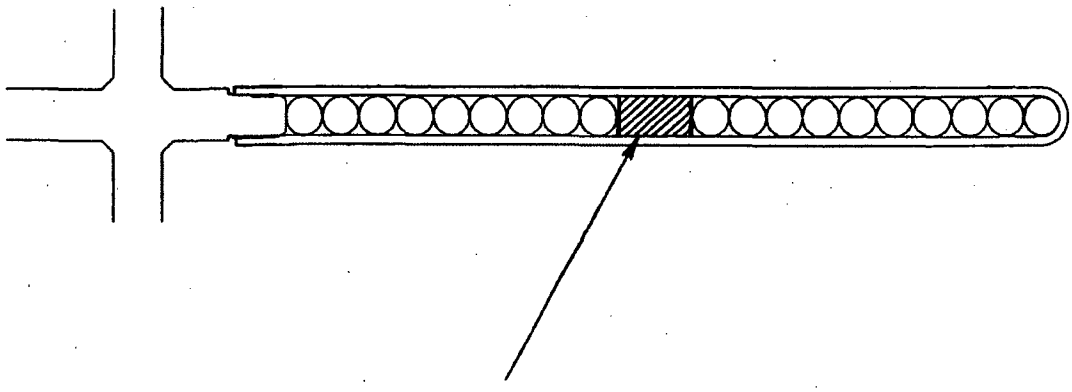

Figure 4-7. BWR/2-6 Original Equipment

5. OPERATIONAL EVALUATIONS

5.1 DIMENSIONAL COMPATIBILITY

The width of the absorber tube and the width of the control rod wing of the Marathon-5S CRB are identical to the Marathon CRB (see Table 2-1). Plus, all other envelope dimensions, including tie rod, handle, and velocity limiter are identical. Therefore, the fit and clearance of the Marathon-5S CRB in the fuel cell is identical to the Marathon CRB.

Reference 10 provides a summary of the inspection history of the Marathon control rod. For all of these inspections, no issues have been identified with respect to the lack of dimensional stability of the Marathon control rod assembly. The inspections have not shown signs of excessive wear on the control rod due to any distortion of the control rod assembly.

Therefore, the inspection history of the Marathon control rod demonstrates that the Marathon design is dimensionally stable, even with significant amounts of irradiation and residence time.

5.2 SCRAM TIMES

An OBE or SSE earthquake condition could cause the fuel channels to temporarily bow or bend. In addition, as fuel channels age, they tend to both bulge and bow, which can negatively affect the insertion capability of the control rod blade.

Previous Marathon prototype scram testing shows that the insertion capability of the CRB is affected by the stiffness of the assembly The stiffer (less flexible) the control rod assembly, the longer the scram times. The stiffness of the Marathon-5S CRB has been evaluated to be equal to or less stiff than the Marathon CRB, in terms of the assembly cross-sectional area moment of inertia. Therefore, the Marathon-5S CRB will have a scram insertion capability equal to or better than the Marathon CRB, in the event of temporary or permanent channel deformation.

The overall assembly weight of the Marathon-5S CRB is not greater than the maximum weights of Marathon CRB designs produced. This, combined with the bending stiffness characteristics, ensure that the Marathon-5S CRB design will not have an adverse effect on scram times.

The results of seismic scram tests are discussed in section 3.4.4. As discussed, for all lattice types, the control rods successfully inserted within scram time requirements under OBE fuel channel deflection conditions, and successfully inserted under SSE fuel channel deflection conditions.

5.3 'NO SETTLE' CHARACTERISTICS

A 'no settle' condition may occur in the event of excessive friction between the control rod and the fuel channels. If this additional friction does not allow the weight of the CRB to settle the assembly into a control rod drive (CRD) positional notch, a 'no settle' condition occurs. As previously discussed, the envelope dimensions for the Marathon-5S CRB are identical to the Marathon CRB. Further, the wet (buoyant) weight of the Marathon-5S assembly is within five pounds of the lightest Marathon CRB design. Therefore, the ability of the Marathon-5S assembly to settle into a CRD notch is equal to that of the Marathon CRB.

5.4 DROP SPEEDS

The parameters that affect the drop speed of the control rod in the event of a rod drop accident are the weight of the control rod assembly, and the geometry of the "bell" of the velocity limiter. The Marathon-5S CRB uses the same cast or FabriCast (hybrid cast/fabricated) velocity limiters as those on the Duralife and Marathon CRBs. Alternately, the Marathon-5S control rod may also use a cast velocity limiter, similar to the original equipment. Because, with either velocity limiter, the weight of the Marathon-5S CRB is less than the weight of the Duralife CRBs used for the original drop tests, the Marathon-5S CRB will have drop speeds less than the [[ ]] required. Therefore, the Marathon-5S CRB will limit the reactivity insertion rate during a CRDA within the existing safety analysis parameters.

5.5 FUEL CELL THERMAL HYDRAULICS

The surface geometry of the Marathon-5S is different than the Marathon control rod due to the different outer absorber tube geometry. In order to evaluate the effect on the thermal hydraulics of the fuel cell, the total displaced volume of the Marathon-5S control rod is compared to the Marathon control rod, approved in Reference 1. The S lattice, BWR/6 version of these control rods are chosen for this comparison.

The total displaced volume for the Marathon control rod is [[ ]]. The total displaced volume of the Marathon-5S control rod is [[ ]], for a difference of [[ ]] from the Marathon control rod. This small difference is judged to be negligible in its effect on the thermal hydraulics of the fuel cell.

The topographic differences between the Marathon-5S and the Marathon control rods is less significant than the differences between the Marathon control rods and DuraLife type control rods and control rods from other vendors. These small topographic changes will have no significant effect on the thermal hydraulics of the fuel cell.

6. LICENSING CRITERIA

The NRC Safety Evaluation Report for the Marathon Control Rod Blade (within Reference 1) identifies five criteria for the licensing and evaluation of the Marathon CRB. These same five criteria are used for the Marathon-5S control rod, with the fifth criteria modified to require a surveillance program.

6.1 STRESS, STRAIN, AND FATIGUE

6.1.1 Criteria

The control rod stresses, strains, and cumulative fatigue shall be evaluated to not exceed the ultimate stress or strain of the material.

6.1.2 Conformance

As discussed in Section 3, the design changes for the Marathon-5S CRB have been evaluated using the same or more conservative design bases and methodology than the Marathon CRB. All components of the Marathon-5S control rod are found to be acceptable when analyzed for stresses due to normal, abnormal, emergency, and faulted loads. The design ratio, which is the effective stress divided by the stress limit or the effective strain divided by the strain limit, is found to be less than or equal to 1.0 for all components. Conservatism is included in the evaluation by limiting stresses for all primary loads to one-half of the ultimate strength (i.e., a safety factor of two is employed).

The fatigue usage of the Marathon-5S CRB is calculated using the same methodology as the Marathon CRB. The fatigue analysis assumes [[
]]. It is found that the calculated fatigue usage is less than the material fatigue capability (the fatigue usage factor is much less than 1.0).

6.2 CONTROL ROD INSERTION

6.2.1 Criteria

The control rod shall be evaluated to be capable of insertion into the core during all modes of plant operation within the limits assumed in the plant analyses.

6.2.2 Conformance

The thickness of the wing of the Marathon-5S CRB, [[
]], is identical to the Marathon CRB. Other envelope dimensions, including those for control rods with plain handles or with spacer pads, are also identical. Therefore, the fit and clearance of the Marathon-5S CRB in the fuel cell is identical to the Marathon CRB.

An OBE or SSE earthquake condition potentially could cause the fuel channels to temporarily bow or bend. In addition, as fuel channels age, they tend to both bulge and bow, which can negatively affect the insertion capability of the control rod blade.

Previous Duralife and Marathon prototype seismic scram testing has shown that the insertion capability of the CRB is affected by the stiffness of the assembly and by the assembly weight. If the control rod assembly is stiffer (less flexible), then the scram times are longer. The stiffness of the Marathon-5S CRB has been evaluated to be equal to or less stiff than the Marathon CRB, in terms of the assembly cross-sectional area moment of inertia. This, combined with the fact that the Marathon-5S assembly is lighter than previous control rod designs shows that the Marathon-5S CRB has a scram insertion capability equal to or better than the Marathon CRB in the event of temporary or permanent channel deformation.

The results of seismic scram tests are discussed in section 3.4.4. As discussed, for all lattice types, the control rods successfully inserted within scram time requirements under OBE fuel channel deflection conditions, and successfully inserted under SSE fuel channel deflection conditions.

6.3 CONTROL ROD MATERIAL

6.3.1 Criteria

The material of the control rod shall be shown to be compatible with the reactor environment.

6.3.2 Conformance

The Marathon-5S CRB uses the same materials as the Marathon CRB (see Section 3.6). No new material has been introduced. The new design absorber tubes are made from the same high purity stabilized type 304 stainless steel (Radiation Resist 304S) as the Marathon absorber tubes. Material testing and the service history of the Marathon control rod blades confirm the resistance to IASCC.

6.4 REACTIVITY

6.4.1 Criteria

The reactivity worth of the control rod shall be included in the plant core analyses.

6.4.2 Conformance

The compatibility of the Marathon-5S CRB is evaluated using the matched worth criterion approved in the Marathon CRB LTR (Reference 1); that is, replacement control rods whose initial reactivity worth is ± 5 % $\Delta k/k$ with respect to the original equipment do not need special treatment in plant core analyses. The nuclear design of the Marathon-5S CRB meets this criterion as discussed in Section 4. Therefore, Marathon-5S CRBs can be used without change to current GEH lattice physics codes and design procedures.

6.5 SURVEILLANCE

6.5.1 Criteria

As the new design absorber tube is judged a sufficiently significant design change, a surveillance

program is required.

6.5.2 Conformance

With the assistance of the BWR plant sites, GEH will monitor the depletions of installed Marathon-5S control rods and will make arrangements to visually inspect the two highest depletion Marathon-5S control rods during each refueling outage until the control rods have reached as close to end of life as practical and are removed from the high depletion locations.

Should evidence of a problem with material integrity arise; (1) arrangements will be made to inspect additional Marathon-5S control rods to the extent necessary to identify the root cause and (2) if appropriate, GEH will recommend a revised lifetime limit to the NRC based on the inspections and other applicable information.

GEH will report to NRC the status of the Marathon-5S surveillance program, including the results of all visual inspections, at least annually.

7. EFFECT ON STANDARD PLANT TECHNICAL SPECIFICATIONS

The purpose and function of control rods are discussed in the Bases sections of the standard BWR/4 and BWR/6 Standard Technical Specifications (STS), References 4 and 5. Section B3.1.3, of both states:

"*...the CRD System provides the means for the reliable control of reactivity changes to ensure under conditions of normal operation, including anticipated operational occurrences, that specified fuel design limits are not exceeded. In addition, the control rods provide the capability to hold the reactor core subcritical under all conditions and to limit the potential amount and rate of reactivity increase caused by a malfunction in the CRD System.*"

The nuclear worth characteristics of the Marathon-5S CRB are compatible with the core cold shutdown requirements and hot operational requirements of the original equipment control rods. This is achieved by meeting the matched worth criteria, described in the Marathon LTR (Reference 1), as a reactivity worth within ± 5 % Δk/k of the reactivity worth of the original equipment CRB. Therefore, the Marathon-5S CRB provides the means for the reliable control of reactivity changes to ensure that under conditions of normal operation, including AOOs, specified fuel design limits are not exceeded. Furthermore, the Marathon-5S CRB provides the capability to hold the reactor core subcritical under all conditions, while meeting current Technical Specification shutdown margin requirements. The overall Marathon-5S assembly weight and velocity limiter design will limit the amount and rate of reactivity increase caused by a malfunction of the CRD system, i.e.) a Control Rod Drop Accident (CRDA).

Therefore, there is no effect on the STS from introduction of the Marathon-5S control rod blade.

8. PLANT OPERATIONAL CHANGES

The fit, form and function of the Marathon-5S CRB are equivalent to the existing Duralife and Marathon CRB designs. The Marathon-5S CRB meets all scram insertion criteria, reactivity control criteria, and CRDA.

No changes to the STS or their Bases (References 3 and 4) are needed. Therefore, it is expected that no plant-specific Technical Specifications (TS) or their Bases will require a change to implement the Marathon-5S control rod. Thus, no plant operating procedure change is expected, except for CRB replacement schedules. Therefore, the introduction of the Marathon-5S CRB has no effect on plant operations.

9. EFFECTS ON SAFETY ANALYSES AND DESIGN BASIS ANALYSIS MODELS

9.1 ANTICIPATED OPERATIONAL OCCURRENCES AND OTHER MALFUNCTIONS

As previously discussed, the reactivity worth of the Marathon-5S CRB is an equivalent replacement for previous control rod designs. Furthermore, the Marathon-5S CRB meets all scram time criteria. Therefore, use of the Marathon-5S CRB does not adversely affect the mitigating response function (i.e., scram) for AOOs.

Introduction of the Marathon-5S CRB is unrelated to the initiating events of the analyzed AOOs, and thus, the probabilities of the different AOOs occurring are unaffected.

Because the Marathon-5S CRB meets the existing design and licensing requirements for Marathon CRBs, the probability of any CRB-related malfunction or of causing a malfunction is not increased, and no new malfunction scenario is created.

The introduction of the Marathon-5S CRB does not (1) introduce a new failure mode or sequence of events that could result in the MCPR safety limit being challenged, (2) cause a 10 CFR 50.2 design bases criterion or limit to be changed or exceeded (such that a safety-related function is adversely affected), (3) create a possibility of a new safety-related component interaction. Therefore, the change does not create a possibility for a malfunction of equipment important to safety different than previously evaluated.

In the safety analyses, the equipment modeled or assumed to function for mitigating the radiological consequences of all design basis abnormal events is not affected by the use of Marathon-5S CRBs. Therefore, the analyzed consequences of the malfunctions in plant Safety Analysis Reports are not affected.

9.2 ACCIDENTS

The ECCS-LOCA performance, LOCA radiological, containment performance, and Main Steamline Break Accident (MSLBA) analyses all assume reactor scram within Technical Specifications requirements, and these are met by Marathon-5S CRBs. The Engineered Safety Feature (ESF) functions, which are modeled/assumed in the accident radiological consequence analyses, are also not affected by the use of Marathon-5S CRBs. Therefore, these analyses' models, scenarios, and the final radiological consequences are not affected.

The failures assumed in the initiating events for the LOCA and MSLBA are not related to the CRBs, and thus, the probabilities of these accidents occurring are not affected.

Other than the event evaluation assumption that the CRBs maintain structural integrity, the Fuel Handling Accident (FHA) initiating event and its related mitigation functions do not involve the CRBs. Therefore, the probability and consequences of a FHA are unaffected.

There is no additional friction between the Marathon-5S CRB relative to the Marathon CRB, and the CRD coupling mechanism is unchanged. Therefore, the probability of a stuck and decoupled

control rod occurring does not change, and thus, the probability of a CRDA cannot significantly increase.

The reactivity insertion rate during a CRDA is controlled by the weight of the control rod and by the shape of the velocity limiter. The Marathon-5S CRB remains within all rod drop parameters assumed or modeled in the safety analysis. Therefore, the analysis and consequences of a CRDA are unchanged.

The change to Marathon-5S CRBs does not create a new fission product release path, result in a new fission product barrier failure mode, or create a new sequence of events that results in significant fuel cladding failures. Therefore, the use of Marathon-5S CRBs cannot create an accident of a different type.

9.3 SPECIAL EVENTS

The ATWS event assumes a failure to scram (without a specific cause) and that the Standby Liquid Control System is used for reactor shutdown. Therefore, the ATWS analysis scenario and results are independent of control rod blade design, and thus, the ATWS analysis is unaffected.

The station blackout, shutdown from outside control room, and safe shutdown fire analyses all assume reactor scram within TS requirements, which are not affected by the use of Marathon-5S CRBs. The other safe shutdown functions, which are modeled/assumed in the analyses, are also not related to or affected by the use of Marathon-5S CRBs. Therefore, these analyses' models, scenarios, and the final results are not affected.

9.4 FISSION PRODUCT BARRIER DESIGN BASIS LIMITS

During all design basis events, Marathon-5S CRB performance is equal to or better than existing CRBs. The margins to the thermal limits on fuel cladding, Minimum Critical Power Ration (MCPR) Safety Limit, Reactor Coolant Pressure Boundary stress limits (e.g., temperature and pressure), and containment structural stress limits are unaffected by the use of Marathon-5S CRBs. Therefore, the fission product barrier design basis limits are not affected.

9.5 SAFETY AND DESIGN BASIS ANALYSIS MODELS

Marathon-5S CRB implementation does not change any safety analysis input, model, or result. No design analysis methodology change is used or needed in the design of the Marathon-5S CRB. Therefore, this change does not involve a departure from a method of evaluation used in establishing a design basis or in a safety analysis

10. HAFNIUM NEUTRON ABSORBER OPTION

In the future, hafnium may be offered as an optional neutron absorber material in high absorption rate absorber tubes. As was approved for the original Marathon control rod in Reference 1, the hafnium will be the in the form of a rod, sealed inside the absorber tube. However, before the hafnium option is offered, a related technical safety evaluation shall demonstrate that the hafnium containing control rods meet all the safety, design and operational acceptance criteria presented within the report.

11. SUMMARY AND CONCLUSIONS

The Marathon Marathon-5S control rod blade is designed as an acceptable direct replacement control rod for BWR/2-6. Conservative mechanical evaluations show acceptability of the control rod structure. Conservative nuclear analyses show that the Marathon-5S is a 'matched worth' control rod and is interchangeable with the original equipment.

Operational evaluations show no adverse effect on plant operations, including control rod scram, 'no settle' characteristics, and control rod drop.

The Marathon-5S control rod, which is a derivative of the Marathon design, meets all licensing acceptance criteria of the Marathon design (Reference 1).

The introduction of the Marathon-5S CRB does not affect the Standard Technical Specifications (References 3 and 4) or their Bases, any plant safety analysis, or any plant design basis. In addition, no adverse effect is found when examining safety analyses and design basis analysis models. The Marathon-5S CRB meets all applicable design and regulatory requirements. Therefore, the use of the Marathon-5S CRB is judged to be acceptable.

12. REFERENCES

1. GE Nuclear Energy, "GE Marathon Control Rod Assembly," NEDE-31758P-A, GE Proprietary, October 1991.

2. GE Nuclear Energy, "Safety Evaluation of the General Electric Duralife 230 Control Rod Assembly," NEDE-22290-P-A Supplement 3, GE Proprietary, May 1988.

3. MNCP4A – A General Monte Carlo N-Particle Radiation Transport Code, Version 4A, LA-12625, March 1994.

4. USNRC, "Standard Technical Specifications General Electric Plants, BWR/4," NUREG-1433 Vol. 1 & 2, Revision 3.0, June 2004.

5. USNRC, "Standard Technical Specifications General Electric Plants, BWR/6," NUREG-1434 Vol. 1 & 2, Revision 3.0, June 2004.

6. 1989 ASME Section III, Division 1, Appendix I, Figure I-9.2.1.

7. JA Bannantine, JJ Comer and JL Handrock, 'Fundamentals of Metal Fatigue Analysis', Prentice Hall, 1990.

8. BWR Vessel and Internals Project: Fracture Toughness and Tensile Properties of Irradiated Austenitic Stainless Steel Components Removed from Service (BWRVIP-35)," EPRI TR-108279, June 1997.

9. BWR Vessel and Internals Project: Review of Test Data for Irradiated Stainless Steel Components (BWRVBIP-66)," EPRI TR-112611, March 1999.

10. MFN 07-138, "Marathon Control Rod Assembly Surveillance Program Status", February 26, 2007.

11. *Mechanical Behavior of Materials*, F. A. McClintock and A. S. Argon, pages 277-278, Addison-Wesley Publishing Company, Inc., 1966.

12. "Boiling Water Reactor Vessel and Internal Project: Crack Growth Rates in Irradiated Stainless Steels in BWR Internal Components (BWRVIP-99)", EPRI TR 1003018 Final Report, December 2001.

APPENDIX A – PLAIN HANDLE EVALUATION

GEH currently recommends the use of plain, roller-less handles for our 'C' Lattice (BWR/4,5) and 'S' Lattice (BWR/6) Marathon Control Rod Blades (CRBs). While the majority of our operational history with the pin-and-roller design, which dates to at least the 1970's, has been very positive, on a few occasions, GEH has had reported cracking at the handle pin-hole. The pin to pin-hole interface represents a crevice condition, which is a potential corrosion concern. Extensive investigation of the handle cracking has led to several improvements in the manufacturing process, but the pin and roller design inherently transfers cracking prevention to control of processes. Therefore, the potential for cracking cannot be unconditionally eliminated with the current pin and roller design. It is, however, eliminated with the plain handle design.

A-1 PLAIN HANDLE DESCRIPTION

With the plain handle control rod blade design, the handle pins and rollers and associated holes are eliminated, leaving the flat plate material of the handle intact, as shown in Figure A-1.

A-1.1 Fuel Channel and CRB Dimensions

In-service CRBs travel in the gap between fuel bundle channels. The dimensions of this gap vary with the type of fuel channel employed. Three cases for 'C' Lattice applications are shown in Figure A-2. Two cases for 'S' Lattice applications are shown in Figure A-3.

As shown in Figure A-2 for 'C' Lattice BWR/4,5 control rods, the protrusion of the handle roller from the face of the handle is nominally [[ ]]. Therefore, for uniform thick channels, a plain handle control rod is able to lean up to [[ ]] closer to one set of fuel channels than the same control rod with handle rollers. For thick/thin channels (120/75 and 100/65/50), removal of the roller has no effect nominally, because the roller protrusion is less than the depth of the channel 'groove' (see Figure A-2) so the CRB is supported by the thicker 'corner' of the fuel channel.

As shown in Figure A-3 for 'S' Lattice BWR/6 control rods, the protrusion of the handle roller from the face of the handle is nominally [[ ]]. Therefore, for uniform thick channels, a plain handle control rod is able to lean up to [[ ]] closer to one set of fuel channels than the same control rod with handle rollers. For 120/75 thick/thin channels, removal of the roller has no effect nominally, because the roller protrusion is less than the depth of the channel 'groove' (see Figure A-3) so the CRB is supported by the thicker 'corner' of the fuel channel.

GEH evaluated the nuclear effect of eliminating the handle pins and rollers for both C and S lattice applications. The review considered two possible effects: (1) the effect of the control rod leaning closer to one set of fuel bundles, (2) the effect of additional stainless steel due to not having drilled roller holes in the handle.

The conclusion for the effect of the small amount of lean of the control rod was that the effect of leaning slightly closer to one set of fuel bundles would be offset be leaning slightly further away from the opposite set of fuel bundles. The conclusion is that the net effect would not be observable in any neutron transport calculation performed.

The evaluation of the additional stainless steel in the handle plate concluded that the effect would be offset by the removal of the handle rollers. The evaluation concluded that even if the entire core of control rods were replaced with plain handles, no net change in reactivity would be expected.

A-1.2 Handle Vertical Position

In order to determine if removal of the handle rollers creates the opportunity for the CRB to 'snag' or 'hang-up' during insertion or withdrawal, the position of the handle relative to the fuel channel is examined.

For 'C' Lattice, BWR/4,5 applications, when fully withdrawn, the top of the absorber section (absorber section to handle weld) is a minimum [[ ]] above the bottom of the fuel channel. When fully inserted, the top of the extended handle is a minimum [[ ]] below the top of the fuel channel.

For 'S' Lattice, BWR/6 applications, when fully withdrawn, the top of the absorber section (absorber section to handle weld) is a minimum [[ ]] above the bottom of the fuel channel. When fully inserted, the top of the handle is a minimum [[ ]] below the top of the fuel channel.

Therefore, for both 'C' and 'S' Lattice applications, the handle remains within the axial (vertical) bounds of the fuel channel throughout its insertion or withdrawal stroke. Because the fuel channels have only smooth transitions in the axial direction, there are no opportunities for the control rod to 'snag' or 'hang-up' during insertion or withdrawal.

A-1.3 Effect of Channel Bulge

As fuel channels age, they can bulge outward at the fuel channel centerline. As can be seen in Figure A-4, the position of the roller is offset [[ ]] from the centerline of the fuel channel for both 'C' Lattice and 'S' Lattice applications. The offset and roller diameter were designed so that in the case of excessive bulge, the fuel channels would bind inboard of the roller rather than on the roller itself. This has been confirmed by inspections done on control rods from fuel cells with highly bulged channels which have shown contact occurring inboard of the roller. Also note that, if the roller were to be impinged by the channels on both sides, the roller would not rotate but 'skid' or slide. Because of this, there is no negative effect from the removal of the handle rollers on the performance of the CRB in fuel cells with highly bulged channels.

A-1.4 Friction and Wear

Lateral loads on the handle rollers were determined during testing of alternate roller materials. The tests showed that the lateral loads on the rollers were small, typically between [[ ]], with a maximum of [[ ]]. To determine the axial friction load at this contact, the lateral load is multiplied by a friction coefficient between stainless steel and zircaloy (fuel channels) of [[ ]] (see Figure below). This results in a maximum axial friction load of [[ ]]. For conservatism, this load is rounded up to [[ ]], which is much less than control rod drive normal insertion and scram forces. Therefore, removal of the handle rollers has no significant effect on normal insertion, or on scram speeds and times.

GEH has completed seismic scram testing for the Marathon-5S control rod. This test uses a simulated reactor pressure vessel, including fuel bundles and other reactor internals. In the test, the core plate is oscillated to produce fuel bundle oscillation that would be experienced during a seismic event.

The Marathon-5S prototypes used for the test incorporated plain, roller-less handles. The acceptance criterion for the test was that scram time requirements were to be met up to fuel bundle oscillation consistent with an OBE (Operational Basis Earthquake) event. The results of the tests were very successful, in that scram time requirements were met through the much more severe SSE (Safe Shutdown Earthquake) event for both the C lattice and S lattice applications. This is further evidence that the implementation of the plain, roller-less handle will not degrade the ability of the control rod to scram.

Fuel cells with highly bulged and/or bowed channels can experience a 'no settle' condition in which the CRB does not settle into a control rod drive notch due to increased friction. [[

]]. Therefore, removal of the handle rollers does not exacerbate a 'no settle' condition.

[[

]]. Therefore, wear between the fuel channel and the control rod is not a concern.

A-1.5 Reactor Clearances

As noted above, for uniform thickness channels, removal of the handle rollers allows the CRB to lean closer to one set of fuel channels. All clearances potentially impacted by this increased lean have been examined for 'C' and 'S' Lattice applications. Sufficient clearances are demonstrated for all reactor components, including the top guide and the orificed fuel support.

A-1.6 Plain Handle CRB Experience

As of July 2007, GEH Nuclear Energy has delivered over 248 plain handle CRBs to BWRs world-wide since 1990. Operational experience from these BWRs has shown no excessive friction, wear or functional concerns.

Table A-1 contains a list of 16 visual inspections of plain handle Marathon control rods at an international BWR. As shown, the inspections have not identified any issues with the plain handle design. There has been no reported cracking, neutronics problems, corrosion, excessive crud formation, nor any other unanticipated or anticipated problems or degradation at any location. Because this reactor has similar internal dimensions to domestic 'C' Lattice GEH BWRs, this experience shows that plain handle CRBs will perform their functions without issue in domestic 'C' Lattice reactors.

A-1.7 Conformance to Design Requirements

The effect of the plain handle design on the following design requirements is evaluated for 'C' Lattice and 'S' Lattice Marathon CRBs.

A-1.7.1 Dimensional Compatibility with Fuel Assemblies

Because the handle roller is the widest component of the absorber wing, removal of the handle pins and rollers will not cause the control rod to exceed maximum allowable control rod wing thicknesses.

A-1.7.2 Dimensional Compatibility with Orificed Fuel Support

The clearance between the control rod and the orificed fuel support has been evaluated throughout the control rod stroke. The small amount of additional lean that the control rod may experience is unlikely to cause contact between the control rod and the fuel support. The likelihood for contact between the plain handle 'C' Lattice CRB and the orificed fuel support is less than 0.3 % when inserted adjacent to 80 mil thick uniform channels. For other 'C' Lattice channels and all 'S' Lattice applications, this likelihood is significantly less.

A-1.7.3 Insertion Capability

Elimination of the handle pins and rollers does not adversely affect the ability of the control rod to be inserted during normal or upset conditions. The amount of axial friction added by introduction of the plain handle [[ ]] does not prevent control rod insertion. Section A-1.4 discusses the results of seismic scram tests for plain handle Marathon-5S control rods, which show that the introduction of plain, roller-less handles will not degrade the insertion capability of the control rod.

A-1.7.4 Scram Time Performance

Introduction of the plain handle control rod does not adversely affect scram speeds or times as the amount of added friction and mass is not significant when compared to control rod drive scram forces.

A-1.7.5 Flow Induced Vibrations (FIV)

The effect of removal of the handle rollers on the likelihood of experiencing flow-induced vibration of inserted control rods has been evaluated analytically. The conclusion is [[

]]. Therefore, the removal of the handle rollers results in no adverse change in control rod FIV.

A-1.7.6 Normal Operation and Transient Loading

The maximum additional axial load due to removal of the handle rollers does not cause the control rod to exceed its design criteria.

A-2 PLANT OPERATIONAL CHANGES

As discussed above, the function of the 'C' Lattice and 'S' Lattice Marathon CRB is unaffected by the removal of the handle rollers. There is no significant effect on scram speeds and times, and no significant effect on normal insertion or withdrawal. All clearances potentially affected by removal of the handle rollers have been evaluated and no interference with any plant components occurs.

No Technical Specification or Bases change is needed, and thus, no plant operating procedure change is expected. Therefore, the removal of the handle pins and rollers has no effect on plant operations.

A-3 EVALUATION OF POTENTIAL AREAS OF CONCERN

Safety Functions

The safety functions of the control rods are to:

- shut down the reactor and maintain the reactor in a shutdown condition with adequate shutdown margin, per the plant TS limits, during and following normal operation, Anticipated Operational Occurrences (AOOs) and accidents;
- allow for rapid insertion (i.e., scram function) of all control rods within TS scram time limits, during all design basis events (i.e., normal operation, AOOs and accidents); and
- limit the reactivity insertion rate during a Control Rod Drop Accident (CRDA).

The nuclear control rod worth is determined by the neutron absorbing material (e.g., B_4C, Hafnium) content and distribution (e.g., control rod capsule distribution), which are unaffected by the use of plain handles. The use of plain handles does not affect the structural integrity of the control rods. Therefore, the use of plain handle CRBs does not affect ability of the control rods to shutdown the reactor and maintain the reactor in a shutdown condition, per the plant TS limits.

As discussed previously, the plain handle CRB has no significant effect on scram speeds or times, and compliance with TS scram time limits is not adversely affected. Therefore, the use of plain handle CRBs does not affect the control rod scram function, during all design basis events.

The reactivity insertion rate during a CRDA is controlled by the weight of the control rod and by the shape of the velocity limiter, which are not changed. Therefore, the use of plain handle control rods does not affect the reactivity insertion rate during a CRDA.

Design Requirements and Limits

As discussed in Section A-1.7, the only design requirements and limits potentially affected by the use of plain handles are: dimensional compatibility with fuel assemblies and the fuel support, insertion capability, scram time performance, flow induced vibrations, and normal and transient loadings. None of these design requirements and limits are violated by the plain handle design. Therefore, the structural integrity and qualification of the Marathon CRB are not affected.

Acceptance Criteria

As discussed in Section A-5, below, the plain handle control rod meets all acceptance criteria from the Marathon CRB Safety Evaluation Report (Reference 1).

Control Rod Drive Reliability

The effect on the control rod drive reliability is minimal, because the added axial loads are very small [[ ]] when compared to the axial loads experienced by the control rod drive.

Materials Compatibility

No new material is introduced by changing to plain handles. GEH inspection experience shows that the rubbing contact, which normally occurs between stainless steel control rods and Zircaloy fuel channels, results in minimal material wear.

Clearance Requirements

All control rod clearances with reactor internals have been thoroughly investigated. No clearance or fit issue is created as a result of the introduction of plain handle CRBs.

Response Time Requirements

As previously discussed, removal of the handle pins and rollers has no significant effect on scram speeds or times, nor on normal control rod insertions and withdrawals.

Flow Induced Vibrational Effects

The potential for flow induced vibrational effects from the use of CRBs has been investigated, and there is no adverse change in control blade vibration. Therefore, there is no adverse vibrational effect related to the removal of the handle rollers.

Potential for Increased Erosion, Corrosion or IGSCC

Elimination of the handle pins and rollers has no negative effect on the potential for increased erosion, corrosion, or Intergranular Stress Corrosion Cracking (IGSCC) of the Marathon square tubes. It does, however, eliminate the potential for IGSCC of the handle at the pin-hole locations.

A-4 EFFECT ON GENERIC PLANT TECHNICAL SPECIFICATIONS

The purpose and function of control rods are discussed in the Bases sections of the standard BWR/4 and BWR/6 Technical Specifications (References 3 and 4). In section B 3.1.3, it states:

"...the CRD System provides the means for the reliable control of reactivity changes to ensure under conditions of normal operation, including anticipated operational occurrences, that specified fuel design limits are not exceeded. In addition, the control rods provide the capability to hold the reactor core subcritical under all conditions and to limit the potential amount and rate of reactivity increase caused by a malfunction in the CRD System."

The removal of the handle pins and rollers adds a small amount of friction [[ ]] to the insertion or withdrawal of the CRBs. This amount of friction does not impede the normal insertion or withdrawal of the control rods, nor does it affect the operation of the control rod drive. Therefore, transitioning to the plain handle control rod has no negative effect on the ability of the CRD system to control reactivity changes under any condition. Further, this added friction has no significant effect on scram speeds or times or on the ability to insert the control rod. Because there also is no significant change to the nuclear worth of the blade, the ability of the control rods to maintain the reactor subcritical is unaffected.

A-5 EFFECT ON LICENSING BASIS

The Safety Evaluation Report for the Marathon Control Rod Blade (within Reference 1) identifies five criteria for the licensing and evaluation of the Marathon CRB. The impact of incorporating plain handle on each of the five criteria is evaluated below.

The control rod stresses, strains, and cumulative fatigue shall be evaluated to not exceed the ultimate stress or strain of the material.

The effect of handle roller removal on control rod stresses, strains and cumulative fatigue have been thoroughly evaluated, and have been found to not exceed the ultimate stress or strain of the materials. The plain handle control rod would not fail because of loads due to shipping, handling, and normal, abnormal, emergency and faulted operating modes. Removal of the handle pins and rollers has no significant effect on axial loads, as the amount of added friction is small. Removal of the handle pins and rollers has no effect on the stress and strain experienced by the square tubes due to B_4C depletion, which is the limiting factor on the mechanical lifetime of the Marathon CRB.

The control rod shall be evaluated to be capable of insertion into the core during all modes of plant operation within the limits assumed in the plant analyses.

The original purpose of the handle rollers was to help guide the control rod between the fuel channels. An evaluation of reactor internal geometries has concluded that there is no interference or fit issue related to the plain handle control rod.

Because of the small amount that the control rod can lean in the channel gap, the lateral loads, and therefore the axial friction loads are small [[ ]]. This small amount of added friction has no significant effect on scram speeds and times. Neither does this small additional axial load impede normal insertion or withdrawal, nor does it result in a 'no settle' condition in which the control rod drive is unable to settle into the appropriate notch.

In the case of excessively bulged or bowed channels, [[ ]]. Therefore, removal of the handle pins and rollers has no adverse effect on the amount of friction experienced in fuel cells with excessively bulged or bowed channels.

An Operational Basis Earthquake (OBE) or Safe Shutdown Earthquake (SSE) condition could cause the fuel channels to temporarily bow or bend. The impact on the control rod – channel interaction is similar to the bulged and bowed channel condition previously discussed. [[

]]. In the event of impingement on the rollers, the rollers would not roll, but slide or skid resulting in friction similar to the plain handle control rod. Therefore, there is no adverse effect on response to an OBE or SSE event from the removal of the control rod handle rollers.

The material of the control rod shall be shown to be compatible with the reactor environment.

Because no new materials are introduced to the control rod by deleting the handle pins and rollers, all CRB materials remain compatible with the reactor environment.

Elimination of the handle rollers results in a small amount of additional rubbing contact between the stainless steel of the control rod, and the Zircaloy fuel channels. GEH's inspection experience from highly bulged and bowed channels has shown that this rubbing results in very little wear on the control rod or on the fuel channel.

The reactivity worth of the control rod shall be included in the plant core analyses.

Elimination of the handle pins and rollers has no effect on vertical position of the neutron absorbing materials. Removal of the rollers may allow the control rod to experience slightly more lean within the fuel cell. A nuclear analysis has concluded that any additional lean of the control rod would have an insignificant effect on the nuclear worth of the CRB.

Prior to the use of new design features on a production basis, lead surveillance control rods may be used.

In the Marathon CRB Safety Evaluation Report (Reference 1), GEH commits to using lead surveillance control rods if a design change impacts the form or function of the control rod assembly, or if new absorber or other materials are used which have not been previously used in reactor cores. As discussed above, removal of the handle pins and rollers has no effect on the form or function of the control rod assembly, and no new materials have been introduced. Therefore, the use of lead surveillance control rods is not required. However, as discussed in Section A-1.4, GEH has supplied over 100 roller-less handle control rod blades to European BWRs, with no reported issues.

A-6 EFFECTS ON SAFETY ANALYSES AND DESIGN BASIS ANALYSIS MODELS

Anticipated Operational Occurrences and Other Malfunctions

Because the use of plain handled CRBs, does not adversely affect the control rod reactivity worth or its scram time, the mitigating response function (i.e., scram) to AOOs is not affected. Therefore, plant AOO (i.e., transient) analyses are unaffected.

The change to plain handled CRBs is unrelated to the initiating events of the analyzed AOOs, and thus, the probabilities of the different AOOs occurring are unaffected.

Because plain handled CRBs meet the existing design and licensing requirements for Marathon CRBs, the probability of any CRB related malfunction or of causing a malfunction is not increased, and no new malfunction scenario is created.

The change to plain handles does not (1) introduce a new failure mode or sequence of events that could result in the MCPR safety limit being challenged, (2) cause a 10 CFR 50.2 design bases criterion to be exceeded (such that a safety-related function is adversely affected), or (3) create possibility of a new safety-related component interaction. Therefore, the change does not create a possibility for a malfunction of equipment important to safety different than previously evaluated.

Accidents

The ECCS-LOCA performance, LOCA radiological, Containment performance and Main Steamline Break Accident (MSLBA) analyses all assume reactor scram within TS requirements, which is not affected by the use of plain handled CRBs. The Engineered Safety Features (ESF) functions, which are modeled/assumed in the accident radiological consequence analyses, are also not related to or affected by the use of plain handled CRBs. Therefore, these analyses' models, scenarios and the final radiological consequences are not affected.

The failures assumed in the initiating events for the LOCA and MSLBA are not related to the CRBs, and thus, the probabilities of these accidents occurring are not affected.

Other than assuming that the CRBs maintain structural integrity, the fuel handling accident (FHA) initiating event and its related mitigation functions do not involve the CRBs. Therefore, the probability and consequences of a FHA are unaffected.

The change in the normal friction force due to the use of the plain handles is judged to be insignificant. The change in handle design is not related to the capability for a control rod to remain coupled to its control rod drive. Therefore, the probability of a stuck and decoupled control rod occurring does not significantly change, and thus, the probability of a CRDA cannot significantly increase.

The reactivity insertion rate during a control rod drop accident (CRDA) is controlled by the weight of the control rod and by the shape of the velocity limiter, which are not affected by the use of a plain handle. The safety-related functions that mitigate the radiological consequences of a CRDA are not related to any CRB handle design. Therefore, the analysis and consequences of a CRDA are unchanged.

The change to CRBs does not allow for a new fission product release path, result in a new fission product barrier failure mode, or create a new sequence of events that results in significant fuel cladding failures. Therefore, the use of plain handles cannot create an accident of a different type.

Special Events

The ATWS event assumes a failure to scram (without a specific cause) and that the Standby Liquid Control System is used for reactor shutdown. Therefore, the ATWS analysis scenario and results are independent of control rod blade handle design, and thus, the ATWS analysis is unaffected.

The station blackout, shutdown from outside control room and safe shutdown fire analyses all assume reactor scram within TS requirements, which is not affected by the use of plain handled CRBs. The other safe shutdown functions, which are modeled/assumed in the analyses, are also not related to or affected by the use of plain handled CRBs. Therefore, these analyses' models, scenarios and the final results are not affected.

Safety and Design Basis Analysis Models

No new analysis methodology is used or needed in the design change to plain handles. Therefore, this change does not involve a departure from a method of evaluation used in establishing a design basis or in a safety analysis.

A-7 SUMMARY AND CONCLUSIONS

The introduction of plain, roller-less handle, 'C' Lattice and 'S' Lattice Marathon control rod blades does not affect the standard plant Technical Specifications or their Bases, any plant safety analysis or any plant design basis. In addition, no adverse effect is found when examining potential areas of concern. Plain handle Marathon CRBs continue to meet all applicable and existing design and regulatory requirements. Therefore, the use of plain handle Marathon CRBs is found to be acceptable.

Table A-1
Plain Handle Control Rod Inspection Results

Manufacture Year	Inspection Date	¼ Segment % Depletion	¼ Segment % Depletion Limit	% of Nuclear Life	Inspection Results
1990	7/92	[[		~0	No issues identified
1990	9/93			~0	No issues identified
1993	9/95			19%	No issues identified
1993	9/96			33%	No issues identified
1993	9/97			49%	No issues identified
1993	7/98			65%	No issues identified
1996	2/99			Unknown	No issues identified
1993	3/00			65%	No issues identified
1993	4/01			65%	No issues identified
1996	9/03			56%	No issues identified
2000	9/03			13%	No issues identified
2000	9/03			25%	No issues identified
2000	9/03			16%	No issues identified
1996	9/04			58%	No issues identified
2000	9/04			47%	No issues identified
2000	9/04		]]	47%	No issues identified

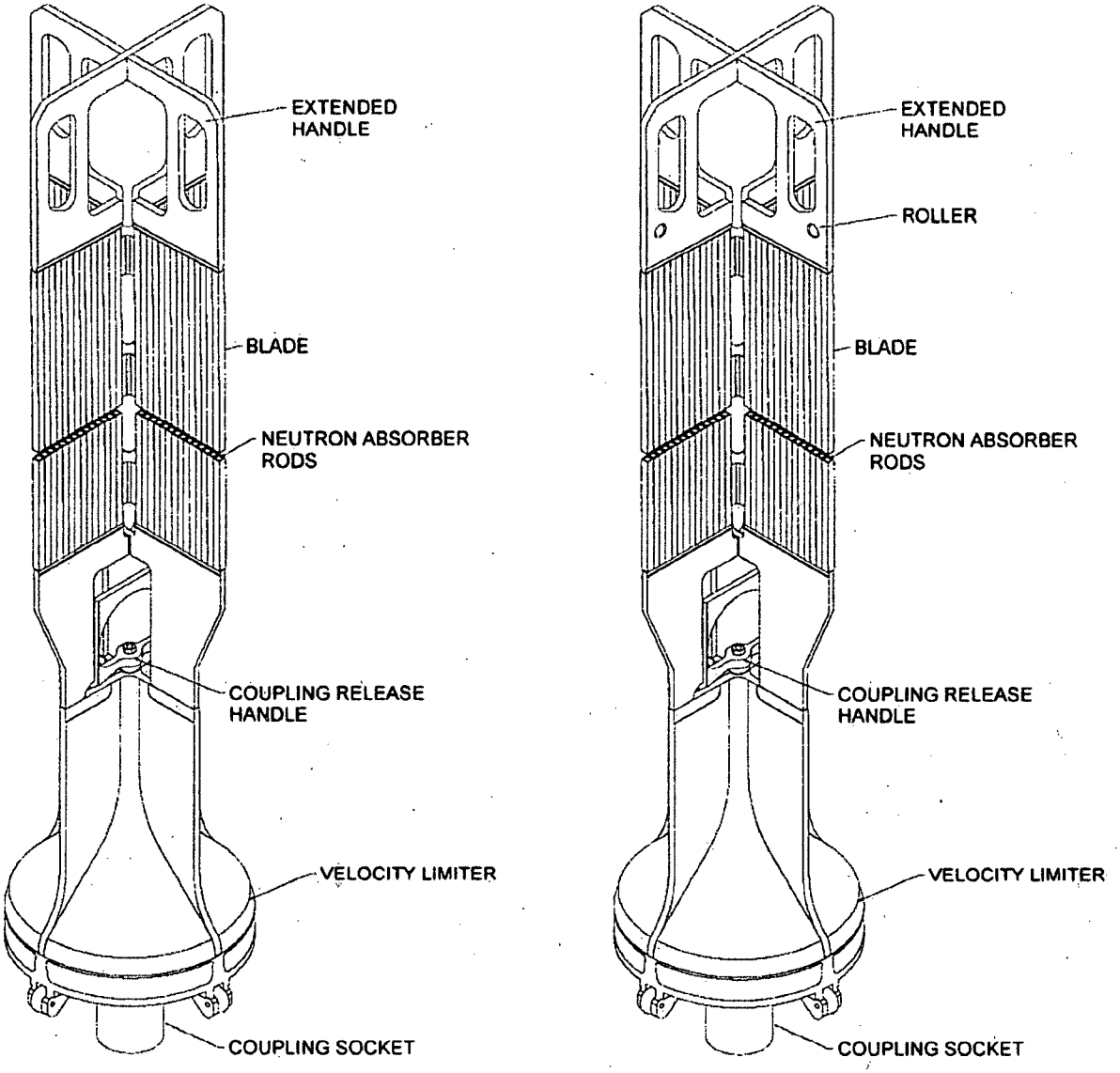

Figure A-1. Plain and Roller Handle Marathon CRBs

('C' Lattice Extended Handle Shown)

[[

]]

Figure A-2. GEH 'C' Lattice (BWR/4,5) Fuel Channel Gap Dimensions

(Not to Scale)

[[

]]

Figure A-3. GEH 'S' Lattice (BWR/6) Fuel Channel Gap Dimensions

(Not to Scale)

[[

]]

Figure A-4. GEH 'C' Lattice (BWR/4,5) and 'S' Lattice (BWR/6) Channel Bulge
(Not to Scale)

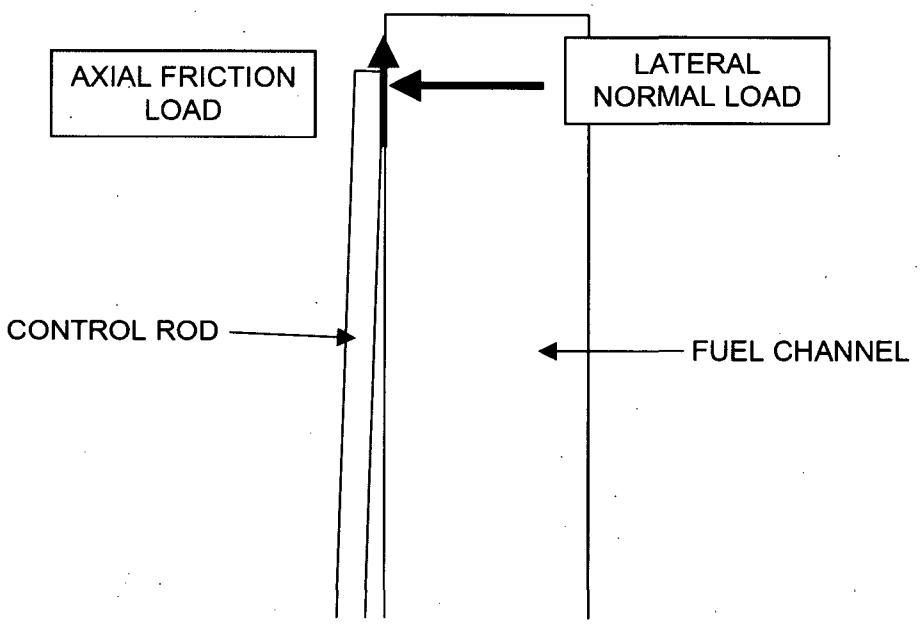

Figure A-5. Diagram of Lateral and Axial Friction Loads on the Control Rod (Control Rod Lean Exaggerated)

APPENDIX B – FAILED BUFFER SCRAM STRESS EVALUATION

Failed buffer scram stress calculations for all cross-sections shown in Figures 3-1 and 3-2 are shown in Table 3-5 through 3-7. During a control rod scram, large axial loads are imparted on the control rod. These axial loads are determined using a dynamic spring and mass model, the results of which are presented in Table 3-4. For this analysis, the scram loads are determined assuming a 100% inoperative control rod drive buffer. The following cross-sections are analyzed.

B-1 SOCKET MINIMUM CROSS-SECTIONAL AREA (FIG. 3-1)

The minimum cross-sectional area of the socket is calculated from the drawing to be [[ ]]. Actual and allowable stress calculations are shown in Table B-1. As shown, all design ratios are less than 1.0. Therefore, the structure is acceptable.

B-2 SOCKET TO TRANSITION PIECE WELD (FIG. 3-1)

The socket to transition piece weld is a full penetration groove weld. It joins the XM-19 socket to the type 316 transition piece, with ER 308L filler metal required. The minimum cross-sectional area is shown in Table B-2. Table B-3 calculates the actual and allowable stresses for this weld. As shown, all design ratios are less than 1.0. Therefore, the weld is acceptable.

B-3 VELOCITY LIMITER TRANSITION PIECE TO FIN WELD (FIG. 3-1)

The transition piece to fin welds are double fillet welds, joining the type 316 transition piece and fins, with ER 308L filler metal required.

For the calculation of the area of these welds, only the vertical portions of the welds are considered. The angled portions of the welds are conservatively neglected (Figure 3-1). Also, since the welds are in shear, the resulting area is multiplied by $(1/\sqrt{3})$ to calculate an equivalent normal area. The minimum equivalent normal weld area is calculated to be [[ ]].

Table B-4 shows the actual and allowable stresses for this weld. As shown, all design ratios are less than 1.0. Therefore, the weld is acceptable.

B-4 VELOCITY LIMITER FIN MINIMUM CROSS-SECTIONAL AREA (FIG. 3-1)

The minimum cross-sectional area of the fins is calculated from the drawing to be [[ ]]. Actual and allowable stress calculations are shown in Table B-5. As shown, all design ratios are less than 1.0. Therefore, the structure is acceptable.

B-5 VELOCITY LIMITER TO ABSORBER SECTION WELD (FIG. 3-2)

The weld connecting the absorber section to the velocity limiter is analyzed using the combined loading of the scram loads and axial loads due to the maximum allowable internal pressure of the absorber tubes.

Since both the scram loads and the load due to the internal pressure of the absorber tubes is considered, a combined weld area of the absorber section to handle weld, and the end plug to

absorber tube weld is calculated. Since the end plug weld is in shear for this loading, the weld area is multiplied by $(1/\sqrt{3})$ to calculate an effective normal weld area. This is added to the minimum absorber section to velocity limiter weld area, which is determined using CAD software:

A_{normal} = (# of tubes}{$(1/\sqrt{3})(\pi)OD_{plug,min}$(weld penetration) + (absorber section to handle/VL area per tube)}.

The weld area per tube is then multiplied by the number of tubes. The weld area calculation is summarized in Table B-6.

Once the effective normal weld area is known, the combined maximum stresses due to scram and internal pressure are calculated as described in Table B-7. As shown, all design ratios are less than 1.0. Therefore, the weld is acceptable.

B-6 ABSORBER SECTION (FIG. 3-2)

The minimum cross-sectional area of the absorber section is calculated in Table B-8. Actual and allowable stresses are shown in Table B-9. As shown, all design ratios are less than 1.0. Therefore, the structure is acceptable.

B-7 ABSORBER SECTION TO HANDLE WELD (FIG. 3-2)

The weld connecting the absorber section to the handle is analyzed using the combined loading of the scram loads and axial loads due to the maximum allowable internal pressure of the absorber tubes.

Since both the scram loads and the load due to the internal pressure of the absorber tubes is considered, a combined weld area of the absorber section to handle weld, and the end plug to absorber tube weld is calculated. Since the end plug weld is in shear for this loading, the weld area is multiplied by $(1/\sqrt{3})$ to calculate an effective normal weld area. This is added to the minimum absorber section to handle weld area, which is determined using CAD software:

A_{normal} = (# of tubes}{$(1/\sqrt{3})(\pi)OD_{plug,min}$(weld penetration) + (absorber section to handle/VL area per tube)}.

The weld area per tube is then multiplied by the number of tubes. The weld area calculation is summarized in Table B-10. Once the effective normal weld area is known, the combined maximum stresses due to scram and internal pressure are calculated as described in Table B-11. As shown, all design ratios are less than 1.0. Therefore, the structure is acceptable.

B-8 HANDLE MINIMUM CROSS-SECTIONAL AREA (FIG. 3-2)

The minimum cross-sectional areas of the handle, and actual and allowable stresses, are shown in the Table B-12. As shown, all design ratios are less than 1.0. Therefore, the structure is acceptable.

Table B-1. Socket Axial Stress Calculations

Description	Source	D Lattice		C Lattice		S Lattice	
		70 °F	550 °F	70 °F	550 °F	70 °F	550 °F
Max Failed Buffer Scram Load (kips)	Table 3-4	[[					
Max Failed Buffer Scram Stress (ksi)	[[ ]]						
Allowable Stress (ksi)	Table 3-2 (XM-19)						
Design Ratio	=stress/allow						]]

Table B-2. Socket to Transition Piece Weld Geometry

Description	Source	All Lattice Types
Minimum Socket/Transition Piece OD (in)	Drawings	[[
Maximum Socket/Transition Piece ID (in)	Drawings	
Min Cross-sectional Area (in^2)	$=PI/4(OD^2-ID^2)$	]]

Table B-3. Socket to Transition Piece Weld Stress Calculations

Description	Source	D Lattice		C Lattice		S Lattice	
		70 °F	550 °F	70 °F	550 °F	70 °F	550 °F
Max Failed Buffer Scram Load (kips)	Table 3-4	[[					
Max Failed Buffer Scram Stress (ksi)	=P/A						
Allowable Stress (ksi)	Table 3-2 (ER 308L)						
Weld Quality Factor	Table 3-3						
Allowable Weld Stress (ksi)	$=S_m*q$						
Design Ratio	=stress/allow						]]

Table B-4. Transition Piece to Fin Weld Stress Calculations

Description	Source	D Lattice		C Lattice		S Lattice	
		70 °F	550 °F	70 °F	550 °F	70 °F	550 °F
Max Failed Buffer Scram Load (kips)	Table 3-4	[[					
Max Failed Buffer Scram Stress (ksi)	=P/A						
Allowable Stress (ksi)	Table 3-2 (ER 308L)						
Weld Quality Factor	Table 3-3						
Allowable Weld Stress (ksi)	$=S_m*q$						
Design Ratio	=stress/Allow						]]

Table B-5. Minimum Fin Area Stress Calculations

Description	Source	D Lattice		C Lattice		S Lattice	
		70 °F	550 °F	70 °F	550 °F	70 °F	550 °F
Max Failed Buffer Scram Load (kips)	Table 3-4	[[					
Max Failed Buffer Scram Stress (ksi)	=P/A						
Allowable Stress (ksi)	Table 3-2 (316 plate)						
Design Ratio	=stress/allow						]]

Table B-6. Velocity Limiter to Absorber Section Weld Geometry

Description	Reference	D Lattice	C Lattice	S Lattice
Absorber Tube to VL Weld Area (in^2)	CAD analysis	[[		
Min End Plug OD (in)	Drawing			
Max End Plug OD (in)	Drawing			
Min End Plug Weld Penetration (in)	Assembly Drawing			
Total Normal Weld Area Per Tube	Equation in Section B-5			
Number of Absorber Tubes per Assembly	Assembly Drawing			
Total Weld Area (in^2)	=(# tubes)(area)			]]

[[

]]

Table B-7. Velocity Limiter to Absorber Section Weld Stress Calculations

Description	Source	D Lattice		C Lattice		S Lattice	
		70 °F	550 °F	70 °F	550 °F	70 °F	550 °F
Max Failed Buffer Scram Load (kips)	Table 3-4	[[					
Maximum Allowable Internal Pressure (ksi)	Finite Element Analysis						
End Plug Pressure Area (in^2)	$=\pi/4*(OD_{plug})^2$						
Number of Pressurized Tubes	Assembly Drawing						
Total Axial Load (kips)	=Scram Load + (press)(area) (# tubes)						
Total Weld Area (in^2)	Table B-6						
Max Failed Buffer Scram + Internal Pressure Stress (ksi)	=Ptot/A						
Allowable Stress (ksi)	Table 3-2 (304S Tubes)						
Weld Quality Factor	Table 3-3						
Allowable Weld Stress (ksi)	$=S_m*q$						
Design Ratio	=Stress/Allow						]]

Table B-8. Absorber Section Geometry Calculation

Description	Source	D Lattice	C Lattice	S Lattice
Min Absorber Tube Area (in^2)	CAD Analysis	[[		
Min Tie Rod Area (in^2)	CAD Analysis			
Number of Absorber Tubes	Assembly Drawing			
Total Minimum Absorber Section Cross-sectional Area (in^2)	=(# tubes)(tube area) + tie rod area			]]

Table B-9. Absorber Section Stress Calculation

Description	Source	D Lattice		C Lattice		S Lattice	
		70 °F	550 °F	70 °F	550 °F	70 °F	550 °F
Max Failed Buffer Scram Load (kips)	Table 3-4	[[					
Max Failed Buffer Scram Stress (ksi)	=P/A						
Allowable Stress (ksi)	Table 3-2 (304S Tubes)						
Design Ratio	=stress/allow						]]

Table B-10. Absorber Section to Handle Weld Area Calculation

Description	Source	D Lattice	C Lattice	S Lattice
Absorber Tube to Handle Weld Area (in^2)	From CAD analysis	[[		
Min End Plug OD (in)	From drawing			
Max End Plug OD (in)	From drawing			
Min End Plug Weld Penetration (in)	From assembly drawing			
Total Normal Weld Area Per Tube (in^2)	Equation above			
Number of Absorber Tubes per Assembly	From assembly drawing			
Total Weld Area (in^2)	=(# tubes)(area)			]]

[[

]]

Table B-11. Absorber Section to Handle Weld Stress Calculations

Description	Source	D Lattice		C Lattice		S Lattice	
		70 °F	550 °F	70 °F	550 °F	70 °F	550 °F
Max Failed Buffer Scram Load (kips)	Table 3-4	[[					
Maximum Allowable Internal Pressure (ksi)	Finite Element Analysis						
End Plug Pressure Area (in^2)	$=\pi/4*(OD_{plug})^2$						
Number of Pressurized Tubes	From assembly drawing						
Total Axial Load (kips)	=Scram Load + (press)(area) (# tubes)						
Total Weld Area (in^2)	Table B-10						
Max Failed Buffer Scram + Internal Pressure Stress (ksi)	=Ptot/A						
Allowable Stress (ksi)	Table 3-2 (304S Tubes)						
Weld Quality Factor	Table 3-3						
Allowable Weld Stress (ksi)	$=S_m*q$						
Design Ratio	=Stress/Allow						]]

Table B-12. Handle Scram Stress Calculations

Description	Reference	D Lattice		C Lattice		S Lattice	
		70 °F	550 °F	70 °F	550 °F	70 °F	550 °F
Max Failed Buffer Scram Load (kips)	Table 3-4	[[					
Handle Minimum Cross-Sectional Area (in^2)	Calculated from Drawings						
Max Failed Buffer Scram Stress (ksi)	=P/A						
Allowable Stress (ksi)	Table 3-2 (316 plate)						
Design Ratio	=stress/allow						]]

RAI #1

Section 2.2 states: [[

]]

a. Provide data to justify that the dimensions selected for the minimum and actual tube-capsule gap increase are adequate.
b. Provide radial expansion data and calculation methods. Justify results.
c. Provide axial expansion data and calculation methods. Justify results.
d. Explain volumetric expansion interactions, axial effects on radial expansion and vice versa. Justify results.
e. Justify finite element analyses (FEA), or any other employed techniques for expansion calculations. Explain if corrosion in the FEA was considered or not, and if it was modeled as a removal of material or as an addition of an insulating material layer.

Response

a,b) Boron carbide swelling data is based on [[ ]] test capsules irradiated in a test reactor and later examined in a hot cell. Measurements of the boron carbide diameter indicated an average diametric swelling of [[ ]]at 100% local depletion, with a +3σ upper limit of [[ ]].

The table below summarizes the calculation to show clearance between the capsule and the absorber tube at 100% local depletion.

As a result of the welding process forming the control rod wings, the inside diameter of the absorber tubes shrink. Therefore, a minimum inside diameter is established, and is 100% inspected following the welding, before the absorber section is loaded with capsules.

The worst-case capsule dimensions are used, which result in the maximum outside diameter at 100% local depletion. These consist of the original maximum outside diameter, and minimum wall thickness, resulting in the maximum beginning boron carbide diameter
The strain at the ID of the capsule is equal to the diametral strain of the boron carbide powder. The +3 σ upper limit of [[ ]]is used. Then, assuming constant volume deformation of the capsule, the strain on the outside diameter of the capsule is:

[[ ]]

Then, the capsule outside diameter at 100% local depletion is:

$OD_{100\%} = OD_0(1+ \varepsilon_{OD})$.

Parameter	D/S Lattice	C Lattice
Absorber Tube ID Before Welding (in)	[[	
Minimum Absorber Tube ID After Welding (in)		
Capsule OD (in)		
Capsule Wall Thickness (in)		
Maximum Capsule OD_0 (in)		
Maximum Capsule ID_0 (in)		
Capsule ID strain (in/in)		
Capsule OD strain (in/in)		
Capsule OD at 100% local depletion		]]

Irradiated Capsule Dimensions Calculation

As shown in the table above, [[

]].

c) Data shows the axial expansion of irradiated boron carbide powder is very small compared to the diametral swelling. Available data shows that the axial swelling is less than or equal to [[.]]. The Marathon-5S design uses the same axial gaps within the capsule, and above the capsule column within the absorber tube as the previous Marathon design, to accommodate any axial swelling. For axial swelling data, please see the response to RAI #8.

d) [[

]]For diametral swelling data and a description of the test apparatus, please see the response to RAI #8.

e) No finite element calculations are used in the boron carbide swelling analysis. The analytical calculation in part a,b) shows that [[

]]

RAI #2

In Table 2-1, explain the absorber tube dimensions for inner diameter (ID), outer diameter (OD), and thickness. In the table, for each lattice, there are [[

]].Is there a typographical error?

Response

The data contained in Table 2-1 of NEDE-33284P (ref. 2) is correct. The figure below is a scale overlay of the original Marathon absorber tube (light blue) with the Marathon-5S absorber tube (dark blue). As shown, [[

]]

[[

]]

Marathon and Marathon-5S Absorber Tube Configurations

RAI #3

Section 3.1. Paragraph 1 states: "Corrosion, wear, and crud deposition are accounted for when appropriate."

a) Provide data calculations of non-corroded, unworn, and without crud deposits, and provide data for appropriate inclusions of corrosion, wear, and crud deposition in analyses.

b) How are the differences accounted for?

c) Do the analyses show that corrosion and wear exceeding [[ ]] deep can be present on the surface, without affecting the design basis allowable pressure of the tube, and that this amount of wear is considered sufficiently conservative?

1. What is the limit to which [[ ]] can be exceeded?
2. Identify the analysis technique and verify that it is a method accepted by the NRC, American Society for Testing and Materials (ASTM), or other recognized scientific body.
3. Present calculations and results.
4. Justify any statement of conservativism.
5. Identify peak stress concentrations in magnitude, direction, and point of application.
6. For peak stress concentrations which are identified [[ ]], explain the stress and strain differences between differently oriented or located flat portions, regarding their proximity to welded joints.
7. Explain and show calculations and results for the effects of welds on the material's microstructure in relation to applied stresses.
8. Are combined corrosion and wear modeled as a removal of material? If so, explain how corrosion is a removal of material, and not an addition of surface material.
9. Identify the model mentioned in RAI questionp 3.c.8 (above) and verify that it is a method accepted by the NRC, ASTM, or other recognized scientific body.
10. Justify finite element analysis thermal calculations, in regard to RAI question 3.c.9 (above) and explain if corrosion in FEA was considered or not.
11. In FEA, was corrosion used as a removal of material or as an addition of an insulating material layer? Justify the answer.
12. In the FEA in Section 3.6, crud is mentioned. Is an additional corrosion layer used in the analysis? Justify the reasoning.
13. Present FEA results for radial and axial directions, and explain directional interactions.

Response
a,b)

Pressurization Analysis:
Corrosion and wear are significant to the pressurization capability analysis of the absorber tube. In the pressurization analysis, the peak stress concentrations occur [[

]] This amount of wear is considered sufficiently conservative.

As an example of the effect of wear on the pressurization capability of the absorber tube is shown in the table below. The table compares the calculated allowable pressure of the absorber tube at worst-case dimensions, with and without [[ ]]of corrosion and wear.

Case	Allowable Pressure (psi)			
	D/S Lattice		C Lattice	
	70 °F	550 °F	70 °F	550 °F
Worst Case Dimensions	[[			
Worst Case Dimensions, [[ ]] Wear				
Design Basis, Based on Largest Allowable Surface Defects				]]

Marathon-5S Absorber Tube Allowable Pressure

Thermal Analysis:
The build-up of crud is significant to the thermal analysis of the absorber tube and capsule. As boron carbide is irradiated, it generates heat. This causes temperature gradients across the capsule body tube and the outer absorber tube, creating a thermal stress. [[

]](see RAI #23).
The presence of a layer of crud on the outer surface of the control rod has the effect of insulating the absorber tube, raising the temperature of the boron carbide.

The finite element thermal analysis of the Marathon-5S absorber tube and capsule assembly is discussed in Section 3.6 of NEDE-33284P (ref. 2). For all thermal analyses, a crud layer corresponding to a 32-year residence time is used [[ ]].

c.1) The analysis shows that combined corrosion and wear, modeled as a removal of material for the pressurization analysis, can exceed [[ ]] without affecting the design basis allowable pressure of the outer absorber tube. For the D/S lattice absorber tube, the upper limit for combined corrosion and wear that occurs after control rod installation is [[ ]]. For the C lattice absorber tube, the upper limit is [[ ]].

c.2,9) The finite element method for performing stress and thermal analyses is a widely accepted analysis technique. For the pressurization analysis, the finite element results are conservative to burst pressure tests, as described in the response to RAI #4d.

c.3) The limiting case used for establishment of the absorber tube allowable pressure combines worst-case absorber tube dimensions (thinnest wall per drawings), surface defects at the center of the flat portion of the tube, on the round portion of the tube, and a crack-like defect on the thinnest portion of the inside diameter of the tube. The geometry and boundary conditions used are shown below. Also shown is an example stress intensity distribution.

[[

]]

¼ Symmetry Absorber Tube Model with OD and ID Surface Defects, Geometry and Boundary Conditions

[[

]]

Absorber Tube with OD and ID Surface Defects, Stress Intensity Distribution

The burst pressure is defined as the internal pressure at which any point in the tube reaches a stress intensity equal to the true ultimate strength of the material. Then, to calculate an allowable pressure, a safety factor of 2.0 is applied to the differential pressure across the absorber tube wall such that:

$$P_{allow} = \frac{(P_{burst} - P_{external})}{2} + P_{external}$$

The calculated burst and allowable pressures are shown in the following table. The results at operating temperature are limiting, and are used as the design basis allowable pressure of the tubes.

Lattice	Temp (°F)	External Pressure (psi)	FEA Burst Pressure (psi)	**Allowable Pressure (psi)**
C	70	[[		
C	550			
D	70			
D	550			]]

Absorber Tube Pressurization Results: Minimum Material Condition with OD and ID Surface Defects

c.4) The analysis is conservative because it considers the combined effects of: (1) worst case tube dimensions (thinnest wall), (2) maximum allowable surface defects, (3) a large amount of combined corrosion and wear, and (4) unirradiated material properties. The true ultimate strength of the material will increase with irradiation. Also note that the burst pressure test summarized in the response to RAI #4d resulted in burst pressures higher than the finite element analysis results.

To test the assertion that the use of unirradiated properties in the pressurization finite element model is conservative, a test case is performed. The D lattice, 550 °F case is chosen for the test, with worst-case dimensions and maximum allowable surface defects. An internal pressure of [[ ]] is applied, which is the burst pressure found using unirradiated materials, as shown in the table above. At this internal pressure, the maximum stress intensity using irradiated materials is [[ ]], which is less than the true ultimate strength of the irradiated material, [[ ]]. Therefore, since the test case using irradiated material properties does not reach the ultimate strength of the irradiated material, the burst pressure analysis using unirradiated material properties is conservative. Further, the maximum strain intensity in the tube for the irradiated property test is low, at [[ ]]

c.5,13) Stress components at the point of maximum stress intensity were analyzed for the absorber tube with the maximum allowable internal pressure. The point of maximum stress intensity is found to be [[
]]. Principle stress components are shown in the following table.

Stress Component	D/S Lattice	C Lattice
S1 (Hoop)	[[	
S2 (Axial)		
S3 (Radial)		
Stress Intensity		
Equivalent Stress		]]

Principle Stress Results at Operating Temperature and Pressure – Maximum Allowable Internal Pressure

c.6) The effect of the welded connection between adjacent absorber tubes on the stresses in the tube due to internal pressure was evaluated using a multiple tube finite element model. In this model, three adjacent absorber tubes were pressurized. A stress intensity distribution is shown below. As shown, the maximum stress is [[

]]. The effect of the adjacent pressurized tubes is to produce compressive rather than tensile stresses in the flat portions of the tube that are welded together. In this way, the opposing pressures from opposite sides of this welded ligament is actually beneficial in terms of the pressurization capability of the tubes.

[[

]]

Stress Intensity Distribution, Multiple Tube Model, All Tubes Pressurized

[[

]] Therefore, the single tube model is used to determine design basis allowable pressures.

[[

]].

c.7) The Marathon and Marathon-5S Control Rod Blades (CRB) are manufactured using very low heat input laser weld processes. The resulting regions of microstructural change including the associated heat affected zones (HAZ) are very small (see response to RAI #10). Based on general understanding, the fine HAZ microstructure will have mechanical properties that are equivalent to, or exceed, those of the wrought base material. Therefore, the HAZ will have mechanical properties that exceed the required minimum properties of the associated wrought material.

Two potential issues arise from welding of the absorber section: (1) sensitization and (2) residual stress. These issues are addressed below:

Sensitization: The low heat input laser welding processes have minimal impact on the wrought tube material, in that they typically do not result in sensitized material. To confirm this conclusion, the processes are continually evaluated metallographically to confirm the acceptability of the weld region (i.e., lack of sensitization). In addition, [[

]] Note also from the response to RAI #1 that these hoop stresses (and associated strains) have been eliminated for the Marathon-5S control rod.

Residual stress: One major effect of the welding process is that it will introduce tensile residual stresses in the narrow weld/HAZ region. These stresses are not a significant concern for two reasons: (1) The field cracking has not been associated with the weld HAZ and (2) the irradiation experienced by the CRB over the initial time of operation can significantly reduce these stresses by 60% or more through radiation creep processes [1]. At this level of reduced stress, there is little concern for any effect on stress corrosion cracking (SCC) initiation or their applied stresses and strains. In that the major concern are strains from swelling, this level of stress is well below those levels required to even produce yielding. See also response to RAI#26.

c.8) The method in which corrosion is modeled depends on which finite element analysis is being discussed. For the pressurization analysis, a thinner tube will generally produce higher stresses for the same internal pressure. Therefore, corrosion and wear are modeled as a loss of material. Both processes can affect the thickness of the tube, which must be assumed to maintain the strength properties of the austenitic stainless steel. Wear will lead to reduction in thickness consistent with the modeling approach. While corrosion can lead to a physical increase in thickness, the resultant oxide will include metallic atoms from the primary stainless steel constituents such as Chromium. The base metal will be the source of these atoms and will effectively change the characteristics of the thin surface. Therefore it is appropriate to assume the metal will behave mechanically as if were thinner, even if it is related to the oxide thickness. It should also be recognized that elements such as Nickel will actually be removed at the surface. Again, this will change the surface characteristics supporting the loss of material assumption. Therefore, this is a conservative approach for evaluating this external surface process.

The thermal analysis evaluates the temperature of the boron carbide due to heat generated by the neutron capture reaction. Analyses which result in higher temperatures are conservative [[

]] Further, higher internal temperatures will increase the thermal stress experienced by the absorber tube. Therefore, for the thermal analysis, corrosion of the absorber tube is combined with the deposition of other corrosion products (crud) as an insulating layer. A very conservative crud layer of [[ ]] is applied, which is twice that used on previous analyses.

c.10,11,12) As noted above, corrosion is modeled in the thermal analysis as combined with deposited crud as a build-up of insulating material. Worst-case, thickest-wall tube dimensions are used. Since a removal of material would generally result in less conservative, lower temperatures, surface defects and wear are not considered in the thermal analysis.

Results are shown below for the D/S lattice case. The model used assumes that the tube is interior to the wing, in that there is another absorber tube to the left and right. The boundary on the left and right is conservatively assumed to be insulated (zero heat flux).

[[

]]

D/S Lattice Thermal Model Temperature Distribution

Location	Nominal Dimensions		Worst Case Dimensions	
	Radius (in)	Nodal Temp (°F)	Radius (in)	Nodal Temp (°F)
Centerline	[[			
Ring1 OD				
Ring2 OD				
Ring3 OD				
Ring4 OD				
Ring5 OD				
Ring6 OD				
Ring7 OD				
Ring8 OD				
Capsule ID				
Capsule OD				
Abs Tube ID				
Abs Tube OD				
Crud Surface				
Avg B4C				
Avg He Void				]]

D/S Lattice Thermal Analysis Results

[[

]]

D/S Lattice Thermal Analysis Results

Location	Nominal Dimensions		Worst Case Dimensions	
	Radius (in)	Nodal Temp (°F)	Radius (in)	Nodal Temp (°F)
Centerline	[[			
Ring1 OD				
Ring2 OD				
Ring3 OD				
Ring4 OD				
Ring5 OD				
Ring6 OD				
Ring7 OD				
Ring8 OD				
Capsule ID				
Capsule OD				
Abs Tube ID				
Abs Tube OD				
Crud Surface				
Avg B4C				
Avg He Void				]]

C Lattice Thermal Analysis Results

[[

]]

C Lattice Thermal Analysis Results

The following conservatisms are applied to the thermal model:

- Peak beginning-of-life heat generation rates are used, these are combined with:
- End-of-life combined corrosion and crud build-up of [[ ]], twice that used in previous analyses.
- Peak heat generation rates are used from the highest heat generation tube, which is actually the outermost edge tube. In reality, this tube will have coolant on one side, rather than be insulated. Further some heat transfer will occur from the peak heat generation tube to the adjacent tube, rather than be perfectly insulated.
- Maximum wall thickness dimensions are used.

RAI #4

Section 3.1 paragraph 2 states: "As in reference 1, effective stresses and strains are determined using the distortion energy theory (Von Mises)..."

a) For in-reactor temperature and pressure conditions, provide data to map the dominant deformation mode. Demonstrate that Von Mises analyses are adequate if the failure mode may be via either ductile, fatigue, or crack propagation?

b) A conservatism of 0.5 UTS may still be low, if failure is by fatigue or another mechanism. Provide data supporting why 0.5 UTS is conservative.

c) Provide data to show why UTS is employed, rather than yield strength as a design criterion. Demonstrate that continued operation with plastic strain (up to UTS) is achievable with no channel / blade interference.

d) Provide mechanical test data to support FEA results.

e) Provide data to demonstrate that radiation effects do not induce a ductile-to-brittle transition, which may invalidate the FEA analysis for higher burnup materials.

f) Provide surveillance data from Reference 1, pertaining to GHNE's un-irradiated stainless steel properties which were presented at the time (said properties which are not for the same material of which neither the marathon nor the marathon-5S are constructed). Justify that this data supports past and present calculations for marathon (since the 5S design references the original marathon topical report) and Marathon-5S designs.

g) Provide data, including mechanical test results, to verify that radiation embrittlement is not a safety issue.

h) Provide data, including mechanical test results, to verify that radiation induced changes in the ductile-to-brittle transition temperature is not a safety issue.

Response

a) For many analyses, current methods for calculating stresses in components employ stress intensity or effective stress calculations to include the evaluation of all principal stress components. The choice of the effective stress criterion was selected to accurately evaluate the stress levels in the context of yielding the material. This criterion was accepted as appropriate in the original evaluation of the marathon CRB as discussed in Reference 1. Additionally, the criterions used were all based on the un-irradiated properties of stainless steel.

Given this background, the effects of irradiation are well known. Specifically, the material will have a significant increase in yield strength and ultimate strength. Therefore, the design criteria used, one based on un-irradiated properties, will insure that as fluence is accumulated, the component continues to remain elastic and well below the actual yield strength. As stated in Reference 1, this approach has been previously accepted.

The use of the von Mises criterion takes into consideration the hydrostatic component of stress and the corresponding strain value. It should be recognized that failure modes in these thin walled structures are initiated at the surface, a location where one of the three principal stresses is zero. The use of the von Mises criterion is therefore adequate to evaluate the potential for any of the important failure modes. First, ductile failure is associated with plastic flow. The criterion was developed to best assess that mode. Fatigue and crack growth processes would initiate on the surface. Again, plastic flow at the surface is necessary for these processes to start. As supported by the stress analyses results in Reference 2 in Section 3, the stresses are below the un-irradiated stress limits. Therefore, the absorber tubes will only experience elastic deformation. This condition is also true in the irradiated condition where the stress ratio will decrease when compared to the actual irradiated yield strength value.

Both Von Mises and Tresca stress criteria are used to predict the conditions for yielding under both uniaxial and multiaxial stress states. The Tresca Criterion can be called the maximum shear criterion since it measures the maximum shear stress present The von Mises, or Mises Criterion, also known as the distortion energy, takes into account all principal stresses in the calculation of the conditions where yielding occurs. For thin walled tubes, under combined loads, the Mises Criterion appears to more accurately represent the condition under which yielding occurs (reference 8). For this reason, this criterion has been used as the basis for assessing yielding in the control rod blade tubes.

b) It is well known that the cycles for fatigue initiation are dependent on the stress or strain range. The number of loading cycles that the control rod blade experience are limited to 100 for all of the different designs. The stress amplitudes are all in the elastic range. As shown in Section 3 of Reference 2, based upon the ASME Section III fatigue design curve for un-irradiated austenitic material (ref. 3), the low number of cycles represents only a small amount of cumulative damage, well below the design limit. The 0.5 UTS value represents the ASME design limit for ~30,000 cycles. It has been established that an increase in the strength level, consistent with the effect of irradiation, would only increase the margin. This is supported by data on high strength materials, which confirm that the endurance limit is close to 0.5 of the UTS (ref. 4).

   The last consideration with regard to fatigue is an evaluation of whether there is any flow-induced vibration that could in turn provide the potential for fatigue initiation. An assessment was performed to evaluate the loads induced by transverse loading. The evaluation that treated the control blade as a cantilever beam, found that the loads were very small and would not be sufficient to even close the gap between the blade and the fuel assembly. This load is considered so small as to be negligible, and would not lead to any risk of fatigue.

c) As discussed in response to 4a, the 0.5 UTS value used is well below the stress to produce plastic strains. This value was set based upon the un-irradiated properties of stainless steel. The maximum outer edge strain value for the worst design conditions is [[ ]] as given in Table 3-8 in Reference 2. This value is well below the design value of [[ ]], which was based on irradiated material properties, and a value that is below the value measured for the Type 304S material as discussed in Reference 1. Therefore, the report has adequately answered the RAI.

d) Destructive burst pressure tests have been previously performed on the 'square' type absorber tube described in NEDE-31758P-A (ref. 1) to validate the finite element analysis method to determine allowable absorber tube pressures. These tests were conducted

using test specimens consisting of square absorber tubes welded together to form a panel. The test specimens were pressurized until they ruptured, and the rupture pressure was compared to the finite element analysis predictions. The results were that the pressure at which the test specimens ruptured was approximately [[ ]] less than the finite element model predicted, using nominal dimensions with no surface defects. To accommodate the test results, a [[ ]] scaling factor was applied to the results of the finite element model of the square type absorber tube, along with a safety factor of 2.0, in determining an allowable pressure for the tube.

The allowable pressure for the 'round' type absorber tube for the Marathon-5S is based on a finite element model incorporating worst-case dimensions, along with maximum specification permitted surface defects and expected wear. The finite element analysis shows that the worst-case burst pressure, on which the allowable pressure of the Marathon-5S tube is based, is [[ ]] lower than the burst pressure using nominal dimensions and no surface defects (see table below).

To confirm the finite element results, burst pressure tests were performed on two test specimens consisting of a short panel of welded absorber tubes, in which all tubes are pressurized (see Figure below). The resulting tested burst pressures are compared to the finite element calculated burst pressures in the following table.

Parameter (D/S Lattice)	Burst Pressure (psia)
Nominal Dimensions (FEA)	[[
Worst-Case Dimensions and Maximum Surface Defects (Design Basis) (FEA)	
Specimen 1 Tested Burst Pressure	
Specimen 2 Tested Burst Pressure	]]

D/S Lattice Burst Pressure Results from FEA and Testing

As shown, the test results exceed the nominal predicted burst pressure by approximately [[ ]], and exceed the worst-case burst pressure (worst-case dimensions and surface defects) by a wide margin (~40%). Since the design basis allowable pressure for the absorber tube is based on the worst-case burst pressure combined with a safety factor of 2.0, the design is conservative.

e) Data was presented earlier in Reference 1 that established that the material exhibited ductile behavior at high fluence levels. Likewise, References 5 and 6 provide tensile data that shows high total elongation for these types of stainless steel when exposed to similar fluence levels. References 5 and 6 also present fracture toughness data that establishes that even in the presence of a sharp notch, there is no brittle behavior. Finally, it is general knowledge, that austenitic materials exhibit ductile behavior at elevated temperatures.

f) GEH requires that the mechanical properties of all material used in the fabrication of control rods be certified as meeting material specification limits. The mechanical properties for control rod materials are shown in Table 3-1 of the LTR (reference 2). For example, the mechanical properties of finished, annealed, and un-irradiated type 304S absorber tubes is defined by a fabrication specification. These mechanical limits, along with the certification results of three recent absorber tube lots are shown in the following table.

Property	Room Temperature Yield Stress (ksi)	550 °F Yield Stress (ksi)	Room Temperature Ultimate Tensile Stress (ksi)	550 °F Ultimate Tensile Stress (ksi)	Room Temperature Elongation (% in 2 inches)
Specification Requirement*	[[				
Lot 1					
Lot 2					
Lot 3					]]

* These material requirements are specified in the fabrication specification for the absorber tubes. The tubing supplier certifies each lot of absorber tubes as meeting these requirements.

Type 304S Absorber Tube Mechanical Properties

These specification mechanical properties are used in the analyses for both the Marathon and Marathon-5S control rods. As shown in the table above, all mechanical properties met the specification requirements. Therefore, analyses using the specification requirements are conservative.

g,h) Ferritic pressure vessel steels do exhibit a loss of toughness with a decrease in temperature (the ductile to brittle transition temperature [DBTT]). The effect of irradiation on the DBTT is to increase the DBTT as a function of fluence. Austenitic stainless steels, however, do not exhibit this behavior. The material fracture toughness and ductility (in the unirradiated condition) does not vary significantly in the temperature range of interest (70 - 550°F). In turn, the effect of irradiation on austenitic stainless steel is to reduce the toughness and ductility somewhat; however, austenitic stainless steel still retains ductility after irradiation. There are existing data at high fluence that confirm the tensile ductility and fracture toughness. Specifically, ductility levels and fracture toughness data for irradiated components are documented in Reference 6. These data substantiate their ductile behavior at both room temperature as well as operating temperature.

[[

]]

Burst Test Specimen #1 – After Test

[[

]]

Burst Test Specimen #2 - Rupture

RAI #5

Table 3-1 lists the Marathon-5S material properties. Tensile strength may not be uniaxially equal after forging, rolling, extrusion, pilgering or other mechanical and thermal processing. Provide mechanical test results demonstrating axial and radial tensile strength, especially across welded interfaces.

Response

The austenitic stainless steel wrought product that was used to construct the control rod blade absorber tubes and other components has been manufactured using standard processing followed by solution annealing. There is no significant anisotropy in the wrought product form of this alloy. Photos at 300X magnification and different orientations are shown below. Secondly, the axial loading direction is the direction of concern and it is aligned with the standard testing direction that have been evaluated in tests of other irradiated stainless steel materials. In that the absorber tube components are thin walled structures, there would be no acceptable method to measure the tensile properties in the radial direction. However, the tri-axial state associated with necking that occurs in standard tensile tests supports the adequacy of the tensile strength in the radial direction and the isotropic characteristics of the material.

[[

]]

[[

]]

[[

]]

RAI #6

Section 3.2 paragraph 1 states: "The limiting unirradiated material strengths are first identified for structural materials, as shown in table 3.1."

a. Provide mechanical test data showing that these *unirradiated* property limits hold for *irradiated* materials.
b. Address the embrittlement questions of RAI 4.g and 4.h above.

Response

a. As stated, References 5 and 6 as well as the data referenced in Reference 1 substantiate that the un-irradiated tensile strength properties are lower than those for the irradiated stainless steel. Since the lower strengths are used as the basis of the design, the data confirms their use as lower limits. For strain, the values used are based on irradiated properties. The values are much less than the values for un-irradiated stainless steel.

b. Please see response to RAI #4.g and 4.h.

RAI #7

Section 3.8, paragraph 1, provides the assumed lifetime on which the fatigue analysis is based. Explain the numbers of fatigue cycles. Are the fatigue cycle numbers based only upon insertion into the core (e.g. 1 scram = 1 cycle, or 1 seismic event = 1 cycle)? Or are fatigue cycle numbers based upon turbulent flow vibrations, or other cyclic stresses? For example, 1 scram may be equivalent to 1 rod insertion for 72 hours duration, during which the blade tips may deflect in an oscillating motion for thousands of cycles.

Response

For scram, each cycle represents a single scram insertion. Scram simulations show that the oscillations in the control rod structure damp out quickly. Further, it is extremely conservative to assume [[ ]] scrams with a 100% inoperative control rod drive buffer, as the loads experienced by the control rod in a normal buffered scram are much less severe.

Consistent with previous analyses, for the Operational Basis Earthquake (OBE), a total of [[ ]] seismic events, in which each event consists of [[ ]] cycles of control rod lateral bending. The assumption of [[ ]] lifetime OBE events is also considered very conservative. After making these very conservative assumptions, the usage factors shown in Tables 3-14, 3-15 and 3-16 of NEDE-33284P (ref. 2) are very small.

For a discussion of cyclic metal fatigue loading due to vibrational loads, please see the response to RAI #4b.

RAI #8

Section 3.6, paragraph 4 states: "...the capsule tube dimensions are sized such that [[

]]..."

a) Provide data for the calculations showing that 100 percent burnup B_4C capsules [[ ]].

b) Provide mechanical test data to support the analysis. Identify the tests, and verify that the data is acceptable.

c) Identify examination methods, and verify that they are accepted standards.

d) Provide radial and axial data.

e) What are the volumetric expansion interactions of stresses and strains?

Response

a. Please see the response to RAI #1 for the calculation showing [[ ]]. As noted, the upper bound diametral swelling is based on mechanical test data.

b,c,d: Mechanical test data of the irradiated behavior of boron carbide was obtained by irradiating test capsules for a period of approximately ten years in a reactor. Test capsules were placed in neutron monitor tubes and irradiated in a reactor. The configurations of two types of test capsules used are shown below.

[[

]]

Irradiated Test Capsule Configurations

The dimensions of the test capsules were measured prior to irradiation using standard laboratory practice. The irradiated test specimens were examined post-test in a hot cell, also using laboratory standard practices. For test capsules with a

mandrel, the diametral strains were mathematically corrected to compensate for the mandrel, resulting in an increase of reported strain value.

Diametral swelling results are shown in the following table and statistical summary. As discussed in the response to RAI #1, the Marathon-5S swelling analysis conservatively used a +3σ upper bound value of [[ ]].

Descriptive Statistics

[[

]]

Irradiated Boron Carbide Diametral Swelling Data

[[

]]

Irradiated Boron Carbide Diametral Swelling Data

Axial swelling data is shown in the following table and was found to be comparatively smal

[[

]]

Irradiated Boron Carbide Axial Swelling Data

e. No clear relationship between the volumetric, diametral, and axial expansion rates is apparent. The photo below is a neutron radiograph of a highly irradiated Marathon control rod. As shown in the photo, after irriadiation, an axial gap remains above the column of irradiated boron carbide powder, below the capsule end cap. Therefore, no strain has been imposed on the capsule due to the axial expansion of the boron carbide powder.

[[

]]

Neutron Radiograph of Irradiated Marathon Absorber Capsules

As discussed in the response to RAI #1, the Marathon-5S absorber tube and capsule combination is designed with a larger gap, such that [[

]]

RAI #9

Section 3.6, paragraph 5 refers to: "...the largest allowable surface defects (see Figure 3-5)."

a. What are the criteria for quantifying the largest allowable defect?
b. Define the term "manufacturing capability."
c. What calculations and methods are used to determine the maximum allowable depth of a surface defect?
d. Besides depth, what are the other dimensional maximum allowable defect sizes (length, width, radius, area)?
e. What are the other inputs to the FEA for surface defects? How are these determined?
f. What are the FEA results? Provide justification for the acceptability of the results.

Response

a. The largest sized allowable surface defects are based on the manufacturing capability of the absorber tube. The maximum allowable surface defect size as specified by the drawing as not to exceed [[ ]] in depth. Then, the finite element analysis that analyzes the pressurization capability of the absorber tube incorporates this size of surface defect in the analysis (see Figure 3-5 of NEDE-33284P, ref. 2).

b,c. "Manufacturing capability" means the ability of the tubing manufacturer to produce tubes to the absorber tubing drawing and specification with reasonable yield rates which in part affects the part cost. A collaborative effort was undertaken to determine a maximum surface defect size that would maintain reasonable yield rates at the tubing manufacture, but would not reduce the pressurization capability of the tube below acceptable values. A surface defect limit of [[ ]] in depth was determined, then factored into the pressurization analysis.

d. The acceptance criteria for surface defects is based primarily on the depth of the defect. Additionally, matching sets of visual standards are used by both the supplier and by GEH to identify and acceptable and unacceptable surface features.

e. The finite element analysis shows that smaller diameter defects result in larger stress concentrations around the defect. A survey was performed of surface defects, and the smallest area defect was found to be [[ ]] in diameter. Therefore, a diameter of [[ ]] was used for the finite element model surface defects.

f. For a summary of the finite element results, please see the response to RAI #3c.

RAI #10

Section 3.2, paragraph 6 states: "For welded connections, a weld quality factor, q, is used..."

a) Since Marathon-5S channel thicknesses have changed from the previous design, provide data to support why laser welding parameters were changed, or why they were not changed.
b) Provide mechanical test data to show that laser welding techniques and annealing are adequate, regarding the base metal, weld, HAZs, and stress relaxation.
c) Provide a statistically adequate amount of micrographs used for the examination of a statistically adequate sampling of weld cross-sections.
d) Characterization the micrographs.
e) Identify the micrograph magnifications.
f) Present supporting information that the magnification is sufficient, and conforms to accepted standards.
g) Present data to support that microstructural composition did not adversely change with temperature during welding or other fabrication techniques.
h) Verify that microstructural changes, such as grain boundary segregation of precipitates and precipitate free zones, i.e. strength and toughness degradation due to welding, will not affect performance and safety.
i) Present microstructural and mechanical test data to demonstrate that stress corrosion cracking will not degrade the materials.

Response

a) Welding processes for control rods are developed and qualified against a set of acceptance standards which includes: (1) meeting minimum penetration requirements, (2) smooth blends between welded members, and (3) no cracks, holes, lack of fusion or porosity. During weld process development for the Marathon-5S control rod, it was found that good results for the absorber tube-to-tube laser welds were achieved using the same parameters as the Marathon control rod.

b) As a result of the complexity of the control rod geometry, GEH qualified the welding process in a manner meeting the intent of the ASME Code. The qualification method selected was to confirm the mechanical properties of the weld by using a representative mockup of the laser weld. Mechanical tests confirmed that the mechanical properties of the weld were higher than the minimum properties of the base metal. See also response (a) above.

The weld quality factor (q) provides a safety margin against manufacturing defects during processing. The critical to quality components of the weld are defined by ASME B&PV code weld procedure QW-264.1, Welding Procedure Specifications, Laser Beam Welding (LBW). GEH further refines its internal critical to quality requirements from the ASME B&PV code for its day-to-day operations. Over the past 4 years no samples have been rejected for carbide formation.

To evaluate the strength of the absorber section to handle/velocity limiter laser weld, test panels consisting of four edge-welded absorber tubes and end plates representing the handle/fin were fabricated. These test specimens used the same weld processes and

parameters as production welds in order to provide a real-world test of the weld strength. A tensile test was then performed.

The results of this test showed that the test specimens ruptured first in the absorber tube material, prior to the rupturing of the laser weld, as shown in the figure below.

[[

]]

Absorber Tube Panel Tensile Test Result

c-f) GEH performs metallographic evaluation of the laser welds on a weekly basis to confirm that the welding process is within expected parameters, and these results are documented. Attached is a photomicrographs of a typical laser weld, taken as part of a recent qualification test. Comparing the etched grain structure at the edge of the weld to an area away from the weld, the conclusion is that there is a very small metallurgical heat affected zone for a laser weld. Based on this examination, the observed maximum amount of melting of grain boundaries is less than 0.001 inch wide.

[[

]]

Typical Autogenous Laser Weld of 304S Absorber Tube

g-i) Welding of austenitic stainless steels has been performed for many years. With no inherent age hardening capability, austenitic stainless steels lend themselves readily to the welding process. GEHs' proprietary Type 304 S composition is as follows:

[[

]]

The primary concern in austenitic stainless steel welds is carbide precipitation that can enhance stress corrosion cracking initiation by depleting chromium in the grain boundaries as a result of the formation of chromium carbide ($Cr_{23}C_6$). The resulting localized chromium depletion at the grain boundaries reduces the chromium content to below that needed to form a passive corrosion resistant layer (~12%).

For the Type 304S material, control of chromium carbide formation is inherent to the material composition and fabrication process. Carbide precipitation abides by Fick's laws of diffusion and is a function of both carbon concentration and heat input. As temperature and/or carbon concentration increase, the driving force for precipitation increases exponentially, correspondingly as these parameters are lowered the driving force is reduced exponentially. GEH minimizes both driving forces in three ways: (1) placing stricter tolerances on carbon content in the type 304S stainless steel tubing and tie rod material (.04 max vice .08 max) than specified by a standard ASME material specification for Type 304 stainless steel (e.g. SA-240 Type 304); (2) stabilizing elements (e.g. Ta) that preferentially form carbides; and 3) utilizes the laser welding process to reduce the heat input. The highest rate for carbide precipitation occurs at temperatures between 425 and 825 degrees Celsius, and coupled with a large heat sink (the base absorber section material) the result is a heat affected zone (HAZ) that is less than 0.001" (see Figure). Therefore, there is neither time nor temperature gradient enough for significant diffusion, hence the driving force for chromium carbide precipitation mechanism is minimized, and the resultant microstructure is considered resistant to stress corrosion cracking.

RAI #11

Figure 2.2 illustrates Marathon-5S absorber wing weld locations. In the previous design, Marathon blades had gaps between each of the channels, which are welded to form a wing. If expansion occurred, the gaps could accommodate some expansion. Marathon-5S blades do not have gaps.

a. Provide test data to show that expansion in a blade will not exceed tolerances.
b. Present mechanical test data and calculations for both radial and axial expansion.
c. Explain the interaction of expansion in each direction upon expansion in the other.
d. Present data to show that crud build-up in any portion of the control rod blade (CRB) (such as at any spaces between adjoining surfaces, or against any protruding or flow resistant areas where excess crud may deposit) does not result in additional heat build-up and thermal expansion in localized areas.

Response

a) As discussed in RAI #1, the Marathon-5S absorber tube and capsule combination is designed [[ ]]. This eliminates the major source of expansion of the absorber tubes in a control rod wing. The only other source of significant expansion is due to the pressurization of the absorber tube.

As part of the finite element analysis that determined the pressurization capability of the absorber tube, models were analyzed consisting of several adjacent pressurized absorber tubes. It was found that a single tube model was more limiting than the multiple tube model. As discussed in the response to RAI #3c.6, the finite element results showed that the effect of opposing internal pressures from adjacent tubes actually reduced the stress seen in the flat portion of the tube. The burst pressure test results shown in the response to RAI #4d corroborate this result in that both tube panels tested failed in the outer tube. Therefore, there is no degrading effect due to the lack of gaps between the absorber tubes in the Marathon-5S design.

b) The radial expansion of the absorber tube is evaluated using the two-dimensional finite element pressurization model. For this evaluation, the maximum allowable internal pressure is applied. The model showed that the maximum expansion of the width of the tube is [[ ]] for D/S lattice and [[ ]] for C lattice. This amount of expansion is very small, and will have no adverse effect on the fit, form or function of the control rod.

The pressurization of the absorber tubes will also cause an axial expansion of the tubes. This is due to the internal pressure pushing against the end plugs that seal the absorber tubes. Using the maximum allowable internal pressure, the area of the end plugs, and the number of pressurized tubes in the absorber section, the maximum axial load is calculated and shown in the table below.

Assuming stresses remain in the elastic range, the axial strain on the absorber tubes is calculated as $\varepsilon = \sigma/E = P/AE$, with the elongation being $\Delta L = \varepsilon L$. For an absorber section that is nominally [[ ]] long, the total elongation is also shown in the table. These

maximum elongations are relatively small, and will not affect the fit, form or function of the control rod.

Parameter	D Lattice	C Lattice	S Lattice
Axial Load due to Pressurization (kips)	[[		
Absorber Section Cross-Sectional Area (in^2)			
Modulus of Elasticity, E (ksi)			
Strain (in/in)			
Elongation, ΔL (inch)			]]

c) The analyses presented in part b above independently evaluate the diametral and axial expansion of the absorber tubes due to the internal pressure in the tubes. In reality, expansion in the diametral direction will generally reduce expansion in the axial direction, and vice versa. Therefore, the strains and displacements shown in part b above are conservative.

d) The Marathon-5S is a crevice-free design such that there are no spaces between adjoining surfaces that are exposed to reactor coolant. The uniform [[ ]] thick crud layer applied in the thermal analysis, which is twice that applied in previous analyses, is judged to be sufficiently conservative to bound any crud build-up in localized areas.

RAI #12

Section 3.2 states: "The width of the absorber tube and the width of the control rod wing of the Marathon-5S CRB are identical to the Marathon CRB (see Table 2-1). Plus, all other envelope dimensions, including tie rod, handle, and velocity limiter are identical. Therefore, the fit and clearance of the Marathon-5S CRB in the fuel cell is identical to the Marathon CRB." Provide data to account for dimensional stability and integrity during longer refueling times.

Response

The attached letter to NRC, MFN 07-138 (ref. 7) provides a summary of the inspection history of the Marathon control rod. For all of these inspections, no issues have been identified with respect to the lack of dimensional stability of the Marathon control rod assembly. The inspections have not shown signs of excessive wear on the control rod due to any distortion of the control rod assembly.

Therefore, the inspection history of the Marathon control rod demonstrates that the Marathon design is dimensionally stable, even with significant amounts of irradiation and residence time.

RAI #13

Section 2.2 states: "The Marathon-5S CRB uses a capsule body tube geometry with a thicker capsule body tube wall." The surface geometry is changed.

a) Provide test data to show that the new surface geometry of the blades does not adversely affect thermal hydraulics.
   1. Present data for displaced volume differences.
   2. Present data for topographic changes.

Response

a,1) The surface geometry of the Marathon-5S is different than the Marathon control rod due to the different outer absorber tube geometry. In order to evaluate the effect on the thermal hydraulics of the fuel cell, the total displaced volume of the Marathon-5S control rod is compared to the Marathon control rod, approved in NEDE-31758P-A (ref. 1). The S lattice, BWR/6 version of these control rods are chosen for this comparison.

The total displaced volume for the Marathon control rod is [[ ]]. The total displaced volume of the Marathon-5S control rod is [[ ]], for a difference of [[ ]]from the Marathon control rod. This small difference is judged to be negligible in its effect on the thermal hydraulics of the fuel cell.

a,2) The topographic differences between the Marathon-5S and the Marathon control rods is less significant than the differences between the Marathon control rods and DuraLife type control rods and control rods from other vendors. These small topographic changes will have no significant effect on the thermal hydraulics of the fuel cell.

RAI #14

Section 3.2, paragraph 5 states: "Resulting allowable stresses for primary loads are shown in Table 3-2 for both the ASME [American Society of Mechanical Engineers boiler and pressure vessel] code method, and the ½ ultimate tensile strength criteria from Reference 1."

a. Provide examples of maximum and allowable stress calculations from different locations on the CRB.
   1. Include all the highest ASME and alternate design ratio results for all locations on a blade, especially for the S lattice.
b. Justify why the alternate design ratio criteria from Reference 1 is a valid methodology.

Response

a) Failed buffer scram stress calculations for all cross-sections shown in Figures 3-1 and 3-2 of NEDE-33284P, reference 2. During a control rod scram, large axial loads are imparted on the control rod. These axial loads are determined using a dynamic spring and mass model, the results of which are presented in Table 3-4 of NEDE-33284P (ref. 2). For this analysis, the scram loads are determined assuming a 100% inoperative control rod drive buffer. The following cross-sections are analyzed.

Socket Minimum Cross-Sectional Area (NEDE-33284P, Fig. 3-1)

The minimum cross-sectional area of the socket is calculated from the drawing to be [[ ]]. Actual and allowable stress calculations are shown in the following table.

Description	Source	D Lattice		C Lattice		S Lattice	
		70 °F	550 °F	70 °F	550 °F	70 °F	550 °F
Max Failed Buffer Scram Load (kips)	Table 3-4 of NEDE-33284P	[[					
Max Failed Buffer Scram Stress (ksi)	=P/1.919 in^2						
Allowable Stress (ksi), ASME	Table 3-2 of NEDE-33284P (XM-19)						
Allowable Stress (ksi), Alternate	Table 3-2 of NEDE-33284P (XM-19)						
Design Ratio, ASME	=stress/allow						
Design Ratio, Alternate	=stress/allow						]]

Socket Axial Stress Calculations

As shown, all design ratios are less than 1.0. Therefore, the structure is acceptable.

Socket to Transition Piece Weld (NEDE-33284P, Fig. 3-1)

The socket to transition piece weld is a full penetration groove weld. It joins the XM-19 socket to the type 316 transition piece, with ER 308L filler metal required. The minimum cross-sectional area is shown in the following table.

Description	Source	All Lattice Types
Minimum Socket/Transition Piece OD (in)	Drawings	[[
Maximum Socket/Transition Piece ID (in)	Drawings	
Min Cross-sectional Area (in^2)	$=PI/4(OD^2-ID^2)$	]]

Socket to Transition Piece Weld Geometry

The following table shows the actual and allowable stresses for this weld.

Description	Source	D Lattice		C Lattice		S Lattice	
		70 °F	550 °F	70 °F	550 °F	70 °F	550 °F
Max Failed Buffer Scram Load (kips)	Table 3-4 of NEDE-33284P	[[					
Max Failed Buffer Scram Stress (ksi)	=P/A						
Allowable Stress (ksi), ASME	Table 3-2 of NEDE-33284P (ER 308L)						
Allowable Stress (ksi), Alternate	Table 3-2 of NEDE-33284P (ER 308L)						
Weld Quality Factor	Table 3-3 of NEDE-33284P						
Allowable Weld Stress (ksi), ASME	$=S_m*q$						
Allowable Weld Stress (ksi), Alternate	$=S_m*q$						
Design Ratio, ASME	=stress/allow						
Design Ratio, Alternate	=stress/allow						]]

Socket to Transition Piece Weld Stress Calculations

As shown, all design ratios are less than 1.0. Therefore, the weld is acceptable.

Velocity Limiter Transition Piece to Fin Weld (NEDE-33284P, Fig. 3-1)

The transition piece to fin welds are double fillet welds, joining the type 316 transition piece and fins, with ER 308L filler metal required.

For the calculation of the area of these welds, on the vertical portions of the welds are considered. The angled portions of the welds are conservatively neglected (NEDE-33284P, Fig. 3-1). Also, since the welds are in shear, the resulting area is multiplied by $(1/\sqrt{3})$ to calculate an equivalent normal area. The minimum equivalent normal weld area is calculated to be [[

]].

The following table shows the actual and allowable stresses for this weld.

Description	Source	D Lattice		C Lattice		S Lattice	
		70 °F	550 °F	70 °F	550 °F	70 °F	550 °F
Max Failed Buffer Scram Load (kips)	Table 3-4 of NEDE-33284P	[[					
Max Failed Buffer Scram Stress (ksi)	=P/A						
Allowable Stress (ksi), ASME	Table 3-2 of NEDE-33284P (ER 308L)						
Allowable Stress (ksi), Alternate	Table 3-2 of NEDE-33284P (ER 308L)						
Weld Quality Factor	Table 3-3 of NEDE-33284P						
Allowable Weld Stress (ksi), ASME	$=S_m*q$						
Allowable Weld Stress (ksi), Alternate	$=S_m*q$						
Design Ratio, ASME	=stress/Allow						
Design Ratio, Alternate	=stress/Allow						]]

Transition Piece to Fin Weld Stress Calculations

As shown, all design ratios are less than 1.0. Therefore, the weld is acceptable.

Velocity Limiter Fin Minimum Cross-Sectional Area (NEDE-33284P, Fig. 3-1)
The minimum cross-sectional area of the fins is calculated from the drawing to be [[ ]].
Actual and allowable stress calculations are shown in the following table.

Description	Source	D Lattice		C Lattice		S Lattice	
		70 °F	550 °F	70 °F	550 °F	70 °F	550 °F
Max Failed Buffer Scram Load (kips)	Table 3-4 of NEDE-33284P	[[					
Max Failed Buffer Scram Stress (ksi)	=P/A						
Allowable Stress (ksi), ASME	Table 3-2 of NEDE-33284P (316 plate)						
Allowable Stress (ksi), Alternate	Table 3-2 of NEDE-33284P (316 plate)						
Design Ratio, ASME	=stress/allow						
Design Ratio, Alternate	=stress/allow						]]

Minimum Fin Area Stress Calculations

As shown, all design ratios are less than 1.0. Therefore, the structure is acceptable.

Velocity Limiter to Absorber Section Weld (NEDE-33284P, Fig. 3-2)
The weld connecting the absorber section to the velocity limiter is analyzed using the combined loading of the scram loads and axial loads due to the maximum allowable internal pressure of the absorber tubes.

Since both the scram loads and the load due to the internal pressure of the absorber tubes is considered, a combined weld area of the absorber section to handle weld, and the end plug to absorber tube weld is calculated. Since the end plug weld is in shear for this loading, the weld area is multiplied by $(1/\sqrt{3})$ to calculate an effective normal weld area. This is added to the minimum absorber section to velocity limiter weld area, which is determined using CAD software:

A_{normal} = (# of tubes){$(1/\sqrt{3})(\pi)OD_{plug,min}$(weld penetration) + (absorber section to handle/VL area per tube)}.

The weld area per tube is then multiplied by the number of tubes. The weld area calculation is summarized in the following table.

Description	Reference	D Lattice	C Lattice	S Lattice
Absorber Tube to VL Weld Area (in^2)	CAD analysis	[[		
Min End Plug OD (in)	Drawing			
Max End Plug OD (in)	Drawing			
Min End Plug Weld Penetration (in)	Assembly Drawing			
Total Normal Weld Area Per Tube	Equation above			
Number of Absorber Tubes per Assembly	Assembly Drawing			
Total Weld Area (in^2)	=(# tubes)(area)			]]

Velocity Limiter to Absorber Section Weld Geometry

[[

]]

Once the effective normal weld area is known, the combined maximum stresses due to scram and internal pressure are calculated as described in the following table.

Description	Source	D Lattice		C Lattice		S Lattice	
		70 °F	550 °F	70 °F	550 °F	70 °F	550 °F
Max Failed Buffer Scram Load (kips)	Table 3-4 of NEDE-33284P	[[					
Maximum Allowable Internal Pressure (ksi)	Finite Element Analysis						
End Plug Pressure Area (in^2)	$=\pi/4*(OD_{plug})^2$						
Number of Pressurized Tubes	Assembly Drawing						
Total Axial Load (kips)	=Scram Load + (press)(area) (# tubes)						
Total Weld Area (in^2)	Previous Table						
Max Failed Buffer Scram + Internal Pressure Stress (ksi)	=Ptot/A						
Allowable Stress (ksi), ASME	Table 3-2 of NEDE-33284P (340S Tubes)						
Allowable Stress (ksi), Alternate	Table 3-2 of NEDE-33284P (340S Tubes)						
Weld Quality Factor	Table 3-3 of NEDE-33284P						
Allowable Weld Stress (ksi), ASME	$=S_m*q$						
Allowable Weld Stress (ksi), Alternate	$=S_m*q$						
Design Ratio, ASME	=Stress/Allow						
Design Ratio, Alternate	=Stress/Allow						]]

Velocity Limiter to Absorber Section Weld Stress Calculations

As shown, all design ratios are less than 1.0. Therefore, the weld is acceptable.

Absorber Section (NEDE-33284P, Fig. 3-2)
The minimum cross-sectional area of the absorber section is calculated in the following table.

Description	Source	D Lattice	C Lattice	S Lattice
Min Absorber Tube Area (in^2)	CAD Analysis	[[		
Min Tie Rod Area (in^2)	CAD Analysis			
Number of Absorber Tubes	Assembly Drawing			
Total Minimum Absorber Section Cross-sectional Area (in^2)	=(# tubes)(tube area) + tie rod area			]]

Absorber Section Geometry Calculation

Actual and allowable stresses are shown in the following table.

Description	Source	D Lattice		C Lattice		S Lattice	
		70 °F	550 °F	70 °F	550 °F	70 °F	550 °F
Max Failed Buffer Scram Load (kips)	Table 3-4 of NEDE-33284P	[[					
Max Failed Buffer Scram Stress (ksi)	=P/A						
Allowable Stress (ksi), ASME	Table 3-2 of NEDE-33284P (340S Tubes)						
Allowable Stress (ksi), Alternate	Table 3-2 of NEDE-33284P (340S Tubes)						
Design Ratio, ASME	=stress/allow						
Design Ratio, Alternate	=stress/allow						]]

Absorber Section Stress Calculation

As shown, all design ratios are less than 1.0. Therefore, the structure is acceptable.

Absorber Section to Handle Weld (NEDE-33284P, Fig. 3-2)
The weld connecting the absorber section to the handle is analyzed using the combined loading of the scram loads and axial loads due to the maximum allowable internal pressure of the absorber tubes.

Since both the scram loads and the load due to the internal pressure of the absorber tubes is considered, a combined weld area of the absorber section to handle weld, and the end plug to absorber tube weld is calculated. Since the end plug weld is in shear for this loading, the weld area is multiplied by $(1/\sqrt{3})$ to calculate an effective normal weld area. This is added to the minimum absorber section to handle weld area, which is determined using CAD software:

A_{normal} = (# of tubes}{$(1/\sqrt{3})(\pi)OD_{plug,min}$(weld penetration) + (absorber section to handle/VL area per tube)}.

The weld area per tube is then multiplied by the number of tubes. The weld area calculation is summarized in the following table.

Description	Source	D Lattice	C Lattice	S Lattice
Absorber Tube to Handle Weld Area (in^2)	From CAD analysis	[[		
Min End Plug OD (in)	From drawing			
Max End Plug OD (in)	From drawing			
Min End Plug Weld Penetration (in)	From assembly drawing			
Total Normal Weld Area Per Tube (in^2)	Equation above			
Number of Absorber Tubes per Assembly	From assembly drawing			
Total Weld Area (in^2)	=(# tubes)(area)			]]

Absorber Section to Handle Weld Area Calculation

[[

]]

Once the effective normal weld area is known, the combined maximum stresses due to scram and internal pressure are calculated as described in the following table.

Description	Source	D Lattice		C Lattice		S Lattice	
		70 °F	550 °F	70 °F	550 °F	70 °F	550 °F
Max Failed Buffer Scram Load (kips)	Table 3-4 of NEDE-33284P	[[					
Maximum Allowable Internal Pressure (ksi)	Finite Element Analysis						
End Plug Pressure Area (in^2)	$=\pi/4*(OD_{plug})^2$						
Number of Pressurized Tubes	From assembly drawing						
Total Axial Load (kips)	=Scram Load + (press)(area) (# tubes)						
Total Weld Area (in^2)	Previous table						
Max Failed Buffer Scram + Internal Pressure Stress (ksi)	=Ptot/A						
Allowable Stress (ksi), ASME	Table 3-2 of NEDE-33284P (340S Tubes)						
Allowable Stress (ksi), Alternate	Table 3-2 of NEDE-33284P (340S Tubes)						
Weld Quality Factor	Table 3-3 of NEDE-33284P						
Allowable Weld Stress (ksi), ASME	$=S_m*q$						
Allowable Weld Stress (ksi), Alternate	$=S_m*q$						
Design Ratio, ASME	=Stress/Allow						
Design Ratio, Alternate	=Stress/Allow						]]

Absorber Section to Handle Weld Stress Calculations

As shown, the D and C lattice analysis meets the ASME code criteria, therefore the design is acceptable. The S lattice analysis does not meet the ASME code criteria, but does meet the alternate criteria of ½ ultimate tensile strength. Therefore, the design is acceptable.

Handle Minimum Cross-Sectional Area (NEDE-33284P, Fig. 3-2)
The minimum cross-sectional areas of the handle, and actual and allowable stresses, are shown in the following table.

Description	Reference	D Lattice		C Lattice		S Lattice	
		70 °F	550 °F	70 °F	550 °F	70 °F	550 °F
Max Failed Buffer Scram Load (kips)	Table 3-4 of NEDE-33284P	[[					
Handle Minimum Cross-Sectional Area (in^2)	Calculated from Drawings						
Max Failed Buffer Scram Stress (ksi)	=P/A						
Allowable Stress (ksi), ASME	Table 3-2 of NEDE-33284P (316 plate)						
Allowable Stress (ksi), Alternate	Table 3-2 of NEDE-33284P (316 plate)						
Design Ratio, ASME	=stress/allow						
Design Ratio, Alternate	=stress/allow						]]

Handle Scram Stress Calculations

As shown, all design ratios are less than 1.0. Therefore, the structure is acceptable.

b) The ½ ultimate strength criteria is well established for control rod design, most recently approved in the Safety Evaluation Report (reference 1) for the Marathon control rod. A factor of safety of 2.0 to the ultimate strength of the material is judged to be a sufficiently conservative criteria.

RAI #15

In section A-1.4, a "conservatively estimated" maximum added friction force of [[ ]]is stated.

a) Provide calculations of how this number was determined.

b) Why it is conservative as a percentage of maximum?

c) What is the maximum allowable amount?

d) Across which area is this force applied?

e) Provide mechanical test data to verify that the estimate is conservative.

Response

a,b,c,d) Lateral loads on the handle rollers were determined during testing of alternate roller materials. The tests showed that the lateral loads on the rollers were small, typically between [[ ]], with a maximum of [[ ]]. To determine the axial friction load at this contact, the lateral load is multiplied by a friction coefficient between stainless steel and zircaloy (fuel channels) of [[ ]] (see Figure below). This results in a maximum axial friction load of [[ ]]. For conservatism, this load is rounded up to [[ ]].

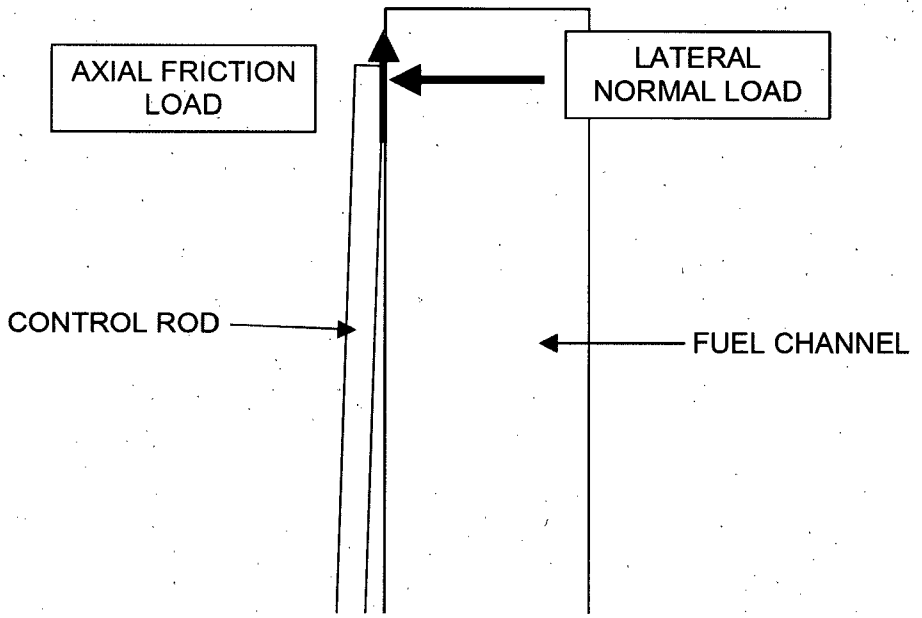

Diagram of Lateral and Axial Friction Loads on the Control Rod (Control Rod Lean Exaggerated)

e) GE has completed seismic scram testing for the Marathon control rod. This test uses a simulated reactor pressure vessel, including fuel bundles and other reactor internals. In the test, the core plate is oscillated to produce fuel bundle oscillation that would be experienced during a seismic event.

The Marathon-5S prototypes used for the test incorporated plain, roller-less handles. The acceptance criterion for the test was that scram time requirements were to be met up to fuel bundle oscillation consistent with an OBE (Operational Basis Earthquake) event. The results of the tests were very successful, in that scram time requirements were met through the much more severe SSE (Safe Shutdown Earthquake) event for both the C lattice and S lattice applications. This is further evidence that the implementation of the plain, roller-less handle will not degrade the ability of the control rod to scram.

Additional comment:
In August 2007, the maximum control rod deflections due to channel bow used in the Marathon-5S analysis are reviewed against current data. The result of this review is that the deflection values remain valid with the latest inspection data.

RAI #16

For the paragraph titled "Flow Induced Vibrational Effects" in section A-3, on page A-5, provide data to demonstrate no adverse change in CRB vibration.

Response

The likelihood that removal of the control rod handle rollers would cause flow-induced vibrations (FIV) was evaluated analytically. The conclusion [[

]] Therefore, the removal of the handle rollers results in no adverse change in control rod FIV.

RAI #17

The last sentence on page A-7 states: "GE has supplied over 100 roller-less handle control rod blades to European BWRs [boiling water reactors], with no reported issues."

a. Expand the definition of "issue" to include any change which has occurred, which may be considered by the NRC to become a safety problem. "Issues" should include both operational and non-operational issues, such as cracking, neutronics problems, corrosion, excessive crud formation, or any other unanticipated or anticipated problems or degradation at any location.
b. Provide surveillance test data showing that this design has worked well in operation.
c. Include all surveillance data, foreign and domestic. Particularly, provide all information pertaining to any marathon or marathon-5S, control blade problems experienced in Taiwan.
d. Have there been unreported issues or other problems?
e. "Over 100" means exactly what number?
f. What is the total number of control blades supplied to all customers worldwide?
g. What problems have been encountered world-wide, and what is the number of these problems?
h. Were any warrantied blades replaced? Why?
i. For the data, indicate the dates put into service and the dates of the examinations.
j. For the data, provide reactor power and burn-up, as well as outage times included in the overall time periods.
k. For the data, present information regarding time and position in the reactor. Also state how far into the core the blades were inserted, and the duration of insertion.
l. Identify the types of inspections.
m. Present information to support that the inspection techniques are adequate and adhere to acceptable standards.
n. Present data from a statistically significant amount of reactors at different locations.
o. Identify the reactor locations, and verify if the inspection procedures at each location adhere to NRC guidelines.

Response

a,b) The following table contains a list of 16 inspections of plain, roller-less handle Marathon control rods at an international BWR. As shown, the inspections have not identified any issues with the plain handle design. There has been no reported cracking, neutronics problems, corrosion, excessive crud formation, nor any other unanticipated or anticipated problems or degradation at any location.

Manufacture Year	Inspection Date	¼ Segment % Depletion	¼ Segment % Depletion Limit	% of Nuclear Life	Inspection Results
1990	7/92	[[		~0	No issues identified
1990	9/93			~0	No issues identified
1993	9/95			19%	No issues identified
1993	9/96			33%	No issues identified
1993	9/97			49%	No issues identified
1993	7/98			65%	No issues identified
1996	2/99			Unknown	No issues identified
1993	3/00			65%	No issues identified
1993	4/01			65%	No issues identified
1996	9/03			56%	No issues identified
2000	9/03			13%	No issues identified
2000	9/03			25%	No issues identified
2000	9/03			16%	No issues identified
1996	9/04			58%	No issues identified
2000	9/04			47%	No issues identified
2000	9/04		]]	47%	No issues identified

Plain Handle Control Rod Inspection Results

c) GEH has not supplied plain handle control rods to Taiwan. There has been significant issues with handle cracking in the region of the roller hole, on control rods in Taiwan which incorporate handle rollers. One cause of the cracking is the crevice condition between the pin and drilled pin-hole. Eliminating this type of cracking is the primary motivation in transitioning to roller-less handle designs.

d) GEH can only be aware on any problems that have been reported to us. GEH maintains open communication with our customers to ensure we are made aware of any problems. GEH is aware of no problems with plain handle control rods.

e,f) As of July 2007, GEH has delivered 248 plain handle control rods to 9 BWRs world-wide.

g) GEH is aware of no problems world-wide with plain handles for control rods.

h) No plain handle control rods have been replaced due to a warranty claim.

i) The table above shows the year of manufacture of each control rod and the inspection date. The control rods will generally have been put in service shortly after the manufacture date.

j) The ¼ segment depletions of each control rod at the time of inspection are shown in the table above. Also shown in the table is the ¼ segment depletion limit, as well as the percent of the nuclear lifetime at the time of the inspection. GEH does not compile data on plant outage times, but they are very short compared to the cycle times.

k) GEH does not have data on the insertion patterns and location history of these control rods in the reactor.

l) The inspections are visual inspections using high-resolution underwater cameras.

m) The latest camera technology is used for all visual inspections. The inspections are performed and are reviewed by inspectors trained in GEH/GNF visual inspection standards.

n) All inspection data for plain handle control rods is shown in the table above.

o) All inspections shown in the table above were performed by GEH/GNF inspectors at a European BWR. GEH is aware of no NRC guidelines for the visual inspection of control rods.

RAI #18

During manufacturing, how do you ensure that metal shavings are not accumulating in pockets within CRB assemblies, as occurred in the SCO shop in Wilmington, NC, prior to August 10, 2006, as referenced in a letter from Thomas Carter, GE Manager RPM&D, to Tim Raush, NGS Site VP, Oyster Creek?

Response

With the incorporation of the roller-less handle, the Marathon-5S is a crevice-free, or pocket-free design in the irradiated portions of the control rod: the absorber section and handle. Therefore, there is no opportunity for foreign material to be trapped in a coolant-accessible location in the handle and absorber section.

The velocity limiter does, however, include some potential foreign material entrapment locations. As a result of the foreign material entrapment discussed in the referenced letter, GE quality has taken the following steps:

- Upgraded entrapment area inspection equipment to a new, state-of-the art video boroscope.
- Revised the inspection procedure to include a second, one-over-one inspection of the velocity limiter cavity by a second quality control inspector.
- Conducted training on the new equipment and inspection processes.
- Reviewed all other shop manufacturing process to determine if there was a potential for foreign material. Similar preventative actions were put in place as needed.

These corrective actions are put in place to ensure that no foreign material is left in coolant accessible regions of control rod assemblies.

RAI #19

What is the operational experience of the M-5S predecessor in regards to any nuclear lifetime failures? *If* earlier than predicted failures did occur, how has the analysis process for M-5S been improved to eliminate the possibility of similar shortcomings in the analysis process?

Response

The attached letter to the NRC (MFN 07-138, ref. 7) contains a summary of the inspection history of the Marathon control rod, including the status of the surveillance program. As noted in the letter, while there have been isolated instances of crack indications, GE has not recommended a reduced lifetime for the Marathon control rod. As a result of these inspections, no shortcomings have been identified in the nuclear analysis process.

The design and analysis of the Marathon-5S control rod has been significantly improved to reduce the likelihood crack indications. In the Marathon design, a large portion of the stress and strain imposed on the outer absorber tube is due to the swelling of the capsule until contact is made with the absorber tube, and continued expansion as the capsule reaches higher depletions. As discussed in MFN 07-138 (ref. 7), the gap between the capsule and absorber tube for the Marathon-5S design has been significantly increased. This results in increased volume to contain the helium gas release by the irradiation of the boron carbide. Further, calculations using worst-case dimensions and helium release show that [[

]].

The increase in the size of the initial gap between the capsule and absorber tube in the Marathon-5S design is a significant improvement in the reliability of the control rod.

The only process change from the original Marathon nuclear analysis to current is that the Monte Carlo computer code used for the neutron transport calculation was changed from MERIT to MCNP. Depletion calculations remain unchanged following the same equations documented in the control rod lifetime document NEDE-30931-8-P, Appendix B.

RAI #20

Section 4.2 discusses the methodology used to calculate the B-10 depletions.

a. Is ^{10}B drift accounted for in the MCNP calculations of boron depletion?
b. Please state the Name/Version of the GE-MCNP that was used.
c. Please list any/all codes (and versions) coupled with the GE-MCNP code (e.g. ORIGEN, TGBLA, etc.).
d. Please discuss any programs for the operator to monitor neutron flux/fluence over the lifetime of the CRB.
e. Please discuss any inspection programs planned to validate lifetime predictions.

Response

a. B-10 drift, defined as the faster depletion of B-10 on the outer edge of B_4C pin than the average pin due to spatial self-shielding of B-10, was not accounted for in the MCNP calculations. This effect has been evaluated recently for the Marathon-5S control rod with new MCNP calculations. These new calculations use a ring model that divides each B_4C pin into four concentric rings of equal cross-sectional area. The results of these new calculations show that, compared to the one-lump model, the four-ring model results in about [[ ]]reduction in the nuclear lifetime of Marathon-5S, depending on the fuel lattice type. Tables and figures in Section 4 of the LTR should be updated with the new results as attached at the end of this document.

   The radii of the boron carbide rings used in the updated analysis are shown in the following table.

Ring Number	Ring Radial Thickness (cm)	
	Marathon-5S, D and S Lattice	Marathon-5S, C Lattice
1 (inner)	[[	
2		
3		
4 (outer)		]]

b. The version of MCNP used in the calculation is GE Level 2 (controlled) code MCNP01A, which is based on MCNP4A.

c. GE utility code "MODL" is used to set up the MCNP input deck, based on lattice design data and control rod design data. GE utility code "HO" is coupled to MCNP for the depletion calculation. It reads the MCNP tallies (cell fluxes and absorber cross sections) and then performs the control blade depletion calculation. The depleted absorber atom densities are then used to update the MCNP inputs for the next time step. MCNP input data for cold case are also generated with "HO" by modifying the input data from the hot inputs.

d. The nuclear depletion calculation summarized in Section 4 of NEDE-33284P (ref. 2) is performed to establish limits on the lifetime of the control rod, expressed as a maximum ¼ -segment depletion. The nodal and ¼ -segment depletions for each control rod are then tracked by the core monitoring computer. As part of a

destructive examination of a DuraLife type control rod, the nodal depletions taken from the monitoring computer were compared to measured values from the control rod being examined. The two sets of depletions were found to be in good agreement.

From the depletion calculation of control rod in a two-dimensional planar geometry, depletion profile by absorber rod can be established, along with the average B-10 depletion (without the presence of hafnium rod) or equivalent B-10 depletion (with the presence of hafnium rod). Combining the rod profile with a typical axial depletion profile (Conventional Sequence Exchange or Control Cell Core, for example), "nodal depletion" values are defined for each axial node (typically 24) of each rod.

"Quarter-segment depletion" is defined as the average depletion of nodal depletion values in a given axial ¼ segment (6 nodes) of the control rod, averaged over four wings. So for any depletion time step, there are 4 quarter-segment depletion values for a given axial depletion profile. In GEH control rod design, the nuclear lifetime is defined as the depletion value of any quarter segment at which the control rod cold worth is 10% less than the zero-depletion cold worth of the Original Equipment.

"Local depletion" is normally defined as the depletion value for each absorber rod in a one-inch segment.

For those plants that use GNF's 3D Monicore for core monitoring, control rod depletions are updated hourly.

e. The proposed surveillance program for the Marathon-5S is described in Section 6.5.2 of the NEDE-33284P Licensing Topical Report. In accordance with this, GE will negotiate with a BWR to insert two Marathon-5S control rods in high-duty locations. GE will further negotiate with the BWR to monitor for boron containment failures by tracking coolant boron and tritium levels, and to visually inspect these lead control rods when they have reached as close to end of life as practical.

RAI #21

In section 2.2 there is a discussion which indicates that due to the new capsule dimensions, there is slightly less B_4C powder mass in each capsule (a trade-off to increase mechanical lifetime). In Tables 4-5, 4-6, and 4-7 there is an increase in initial reactivity worths listed (except for cold conditions in the S lattice).

a. Please discuss how the initial reactivity worth was increased while decreasing the amount of B_4C contained in each capsule.
b. Please provide either a brief description of the OE equipment and/or reference, to further clarify the nuclear calculations, which compares OE and Marathon-5S initial reactivity worths. This is needed to verify that the MCNP input deck geometries are correct. In particular, dimensions for the sheath, the stainless steel block in the middle of the CRB wing, and the absorber rods as modeled in MCNP should be provided.

Response

a. The discussion in section 2.2 on NEDE-33284P (ref. 2) compares the inside diameter of the Marathon-5S capsule to the Marathon capsule. As shown, there is slightly less boron carbide per capsule in the Marathon-5S design, which does reduce the lifetime relative to the previous Marathon design. In contrast, the results shown in Tables 4-5 through 4-7 of NEDE-33284P (ref. 2) compare the initial reactivity worth of the Marathon-5S control rods to the original equipment, which is the design basis for the matched worth criterion discussed in Section 4.1 of NEDE-33284P (ref. 2).

b. As shown in the following figures, the original equipment (DuraLife 100) control rod wings consist of thin sheaths enclosing boron carbide filled tubes. The sheaths are welded to a central tie rod to form the cruciform shape of the control rod.

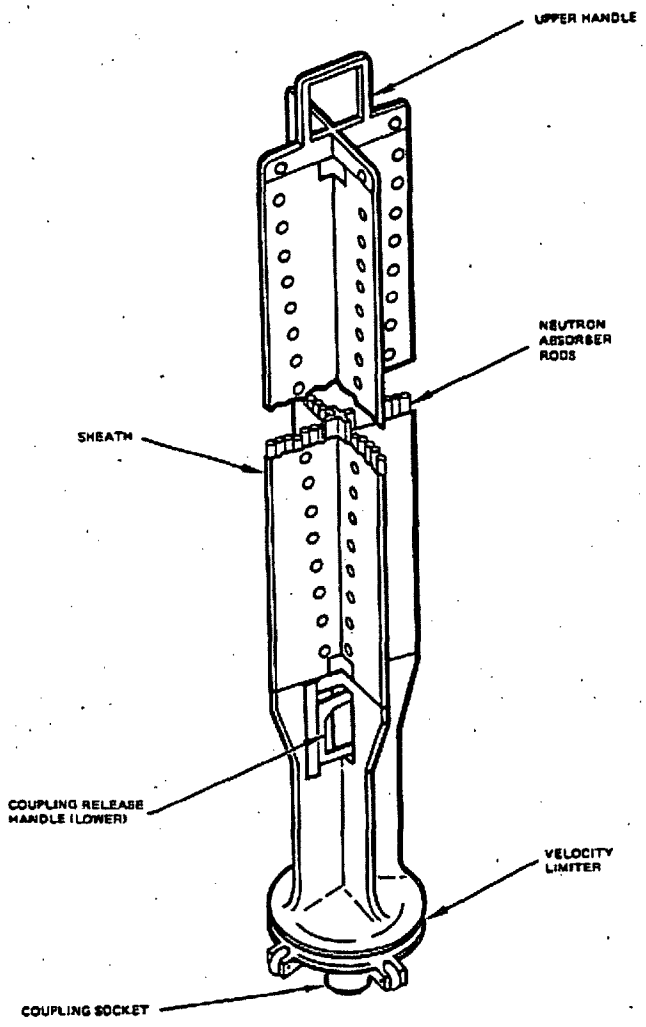

ORIGINAL EQUIPMENT CONTROL ROD DESIGN

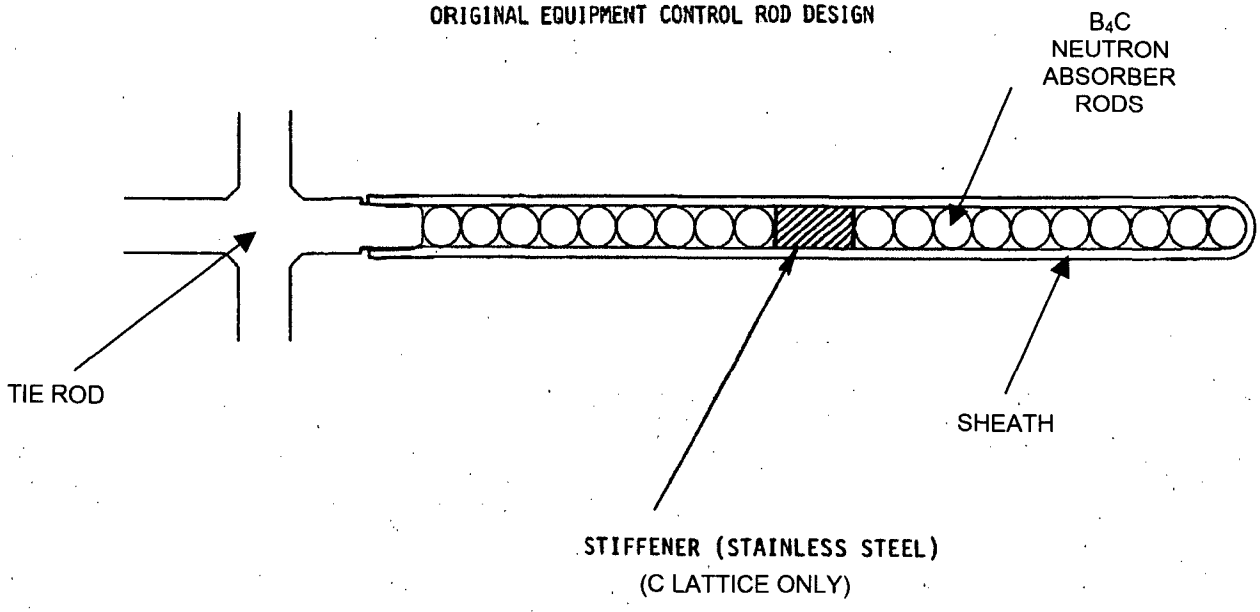

The following tables show the input parameters used to model the original equipment and Marathon-5S control rods.

Description		DuraLife 100 D		Marathon-5S D	
		(inches)	(cm)	(inches)	(cm)
Span		[[			
Half Span	SBL				
Wing Thickness (Square Tube Width)					
Half Wing Thickness	TBL				
Tie Rod Half Thickness	TTR				
Radius of Central Support Filet	RBLF				
Radius of Blade Tip	RBLT				
Span of Central Support (Tie Rod)					
Half Span of Central Support	SCS				
Thickness of Sheath	TSH				
Inner Diameter of Tube (Capsule)	**TID**				
Outer Diameter of Tube	TOD				
Wall Thickness of Tube					
Type	IBLADE				
Number of B4C Tubes (Capsules)	**NOPT**				
Number of Hafnium Rods	NOHFT				
Number of Empty Tubes	NOBT				]]

D Lattice Original Equipment and Marathon-5S Dimensions

Description		DuraLife 100 C		Marathon-5S C	
		(inches)	(cm)	(inches)	(cm)
Span		[[			
Half Span	SBL				
Blade Thickness (Square Tube Width)					
Half Blade Thickness	TBL				
Tie Rod Half Thickness	TTR				
Radius of Central Support Filet	RBLF				
Radius of Blade Tip	RBLT				
Span of Central Support (Tie Rod)					
Half Span of Central Support	SCS				
Thickness of Sheath	TSH				
Inner Diameter of Tube (Capsule)	**TID**				
Outer Diameter of Tube (Hafnium Rod)	TOD				
Wall Thickness of Tube					
Type	IBLADE				
Number of B4C Tubes (Capsules)	**NOPT**				
Number of Hafnium Rods	NOHFT				
Number of Empty Tubes	NOBT				]]

C Lattice Original Equipment and Marathon-5S Dimensions

Description		DuraLife 100 S		Marathon-5S S	
		(inches)	(cm)	(inches)	(cm)
Span		[[			
Half Span	SBL				
Wing Thickness (Square Tube Width)					
Half Wing Thickness	TBL				
Tie Rod Half Thickness	TTR				
Radius of Central Support Filet	RBLF				
Radius of Blade Tip	RBLT				
Span of Central Support (Tie Rod)					
Half Span of Central Support	SCS				
Thickness of Sheath	TSH				
Inner Diameter of Tube (Capsule)	**TID**				
Outer Diameter of Tube	TOD				
Wall Thickness of Tube					
Type	IBLADE				
Number of B4C Tubes (Capsules)	**NOPT**				
Number of Hafnium Rods	NOHFT				
Number of Empty Tubes	NOBT				]]

S Lattice Original Equipment and Marathon-5S Dimensions

RAI #22

Throughout the report, it states that the more restrictive ASME code limits were met for all stress analyses. In Tbl. 3-7, the handle to absorber section weld was analyzed vs. a 1/2 ultimate strength stress criterion.

a. Is that statement still accurate?
b. Please update the table to analyze this with the ASME code limits to match the text.

Response

NEDE-33284P has been revised to only use the ½ ultimate stress criteria. All text and tables in NEDE-33284P have been appropriately updated.

RAI #23

The calculation of the pressure in the absorber tube due to helium release includes worst-case variables. What is the helium release faction used and what was the basis for this value?

Response

Helium release fractions are based on models developed using data from multiple sources. The data shows [[
]] The model is based on data from 500 °F to 1000 °F.

The finite element thermal analysis discussed in Section 3.6 of NEDE-33284P (ref. 2) is used to determine the temperature of the boron carbide powder. This analysis conservatively combines maximum heat generation rates that occur at beginning of life, with the 32-year crud build-up discussed in RAI #3.

The table below shows the worst-case average boron carbide temperatures calculated using the thermal model, and the corresponding helium release fractions from the helium release model. As shown, the temperatures of interest are within the bounds of the model (500 °F to 1000 °F). The temperatures shown in the table below are based on peak beginning-of-life boron carbide heat generation rates, are from the peak heat generation absorber tube at the peak axial location. They are radially averaged only across the cross-section of the boron carbide.

Parameter	D/S Lattice	C Lattice
Average B4C Temperature (°F)	[[	
Helium Release Fraction		]]

Marathon-5S Helium Release Fractions

RAI #24

Section A-1.1 indicates that the nuclear effect of the CRB leaning slightly closer to one bundle and away from another had been reviewed. Please provide the documentation for this review.

Response

GEH evaluated the nuclear effect of eliminating the handle pins and rollers for both C and S lattice applications. The review considered two possible effects: (1) the effect of the control rod leaning closer to one set of fuel bundles, (2) the effect of additional stainless steel due to not having drilled roller holes in the handle.

The conclusion for the effect of the small amount of lean of the control rod was that the effect of leaning slightly closer to one set of fuel bundles would be offset be leaning slightly further away from the opposite set of fuel bundles. The conclusion is that the net effect would not be observable in any neutron transport calculation performed.

The evaluation of the additional stainless steel in the handle plate concluded that the effect would be offset by the removal of the handle rollers. The evaluation concluded that even if the entire core of control rods were replaced with plain handles, no net change in reactivity would be expected.

RAI #25

The ASME Boiler and Pressure Vessel Code, Section III, cited by GHNEA doesn't account for the effects of coolant and all stressing modes.

a. Please justify why these effects are not relevant in your analyses, and explain why both or either the ASME stress ratio and the Alternate ½ UTS design ratio calculations are still valid.
b. Cite the applicability of ASME pressure vessel code calculations to comparatively thin CRB materials relative to actual pressure vessel thicknesses.
c. It is acceptable that thick PV materials can accommodate crack propagation up to certain lengths. Verify that this does not occur in GHNE control blade material.
d. Present mechanical tests to support the reasoning and calculations.

Response

a,b) The control rod is not an ASME code part, since it does not form part of the pressure boundary for the reactor. The ASME Boiler and Pressure Vessel Code is, however, used for two limited purposes:

(1) Material property values from the ASME code are used.
(2) For the Marathon-5S analysis, the more conservative ASME code stress criteria is used in addition to the established ½ ultimate tensile strength criteria.

c) The likelihood of cracking of the Marathon-5S control rod absorber tubes is reduced by two methods:
(1) The use of high-purity, stabilized stainless steel (type 304S), which has shown to have crack-resistant properties.
(2) A mechanical design that eliminates strain in the absorber tube due to the swelling of irradiated boron carbide. As discussed in the response to RAI #1, [[

]] This is a significant reliability improvement over previously approved control rod designs.

d) The inspection history of the Marathon control rod, which uses the same absorber tube material as the Marathon-5S control rod, is contained in the attached letter to the NRC, MFN 07-138. Note that the mechanical design of the Marathon-5S control rod offers a significant reliability advantage over the Marathon control rod due to the large gap between the capsule and the outer absorber tube as described in MFN 07-138 and in the response to c(2) above.

RAI #26

There appears to be extensive elongation and variability in absorber tube lengths during and after welding.

a. Please provide measurement data of the maximum changes in elongation due to welding.
b. Present microstructural and mechanical characterization verifying that dimensional changes due to welding or any other manufacturing process do not degrade mechanical properties and that mechanical properties will remain sufficient throughout use and irradiation.
   1. Include radiation embrittlement factors.

Response

a. Prior to welding, the length of the absorber tubes are [[ ]]. The lengths of the absorber tubes after welding were measured on a production Marathon control, and are recorded below.

Case	Absorber Tube Length (in)
Prior to Welding	[[
Longest Tube After Welding	
Shortest Tube After Welding	]]

As shown in the table above, the biggest difference in relative length between the absorber tubes after welding is [[ ]]

The length of the finished absorber section is 143.68". Therefore, the maximum axial strain due to the differential weld shrinking of the absorber tubes is:

Strain (ε)= $\Delta L/L_{initial}$ = [[ ]]

A [[ ]] strain is insignificant.

b. The minimal induced strain from the laser welding process as shown in response to 26.a) indicates that no microstructural change in the bulk tubing material occurred. Please see RAI response 10 for further discussion with regard to the mechanical properties of the laser welds.

Radiation induced strain hardening is not an "embrittling" mechanism. Rather, it is beneficial as the mechanical strength of the material is enhanced over the course of "in service use". Therefore, the mechanical design is considered conservative based on the use of non-strain hardened values for the mechanical design basis.

RAI #27

Section 3.6 states "The in-service performance, and inspection history of the Marathon CRB has proven the crack resistant properties of Rad Resist 304S."

a. Please provide the supporting data of the inspection history, in accordance with the criteria detailed in RAI#17.
b. Discuss all relevant forms of stress corrosion cracking, and verify that it is not and will not become a significant problem.

Response

a) The inspection history for the Marathon control rod is contained in the attached summary letter to NRC: MFN 07-138. The licensing topical report (reference 2) has been revised to delete the referenced sentence.

b) In order for the stress corrosion cracking mechanism to activate it requires a material that is susceptible, a conducive environment and a sustained tensile stress. If one of these three mechanisms is not present to a sufficient degree, the likelihood of a stress corrosion crack to form is significantly reduced.

The following measures are taken in the design of the Marathon-5S to reduce the likelihood of stress-corrosion cracking:

(1) The absorber tubes are made from the same low carbon, high purity, stabilized GE proprietary type 304S stainless steel as the Marathon control rod.
(2) As discussed in the response to RAI #1, the Marathon-5S is designed such that [[

]]

Additional LTR Change

Since the submittal of the NEDE-33284P Marathon-5S Licensing Topical Report (ref. 2), manufacturing process development for the tie rod revealed that the material properties shown in Table 3-1 of NEDE-33284P (ref. 2) could not be met. Testing of the tie rods, which are delivered in the fully annealed state, showed that the minimum yield stresses could not be met.

As a response, the specification for the type 304S tie rods was changed, lowering the strength requirements to match those of the type 304S absorber tubes. Table 3-1 and Table 3-2 have therefore been changed as shown.

Table 3-1
Marathon-5S Material Properties

Material Type	Control Rod Components	Ultimate Tensile Strength, S_U (ksi)		Yield Strength, S_Y (ksi)		Modulus of Elasticity, E (x 10^6 psi)		Poisson's Ratio, v	
		70 °F	550 °F	70 °F	550 °F	70 °F	550 °F	70 °F	550 °F
304S Bar (Rev. 0)	Tie rods	[[							
304S Bar (Rev. 1)	Tie rods								
304S Tubing (no change)	Absorber Tubes								]]

Table 3-2
Design Allowable Stresses for Primary Loads

Material Type	CR Components	ASME Code Method S_m (ksi)		½ Ultimate Tensile Stress S_m (ksi)	
		70 °F	550 °F	70 °F	550 °F
304S Bar (Rev. 0)	Tie rods	[[			
304S Bar (Rev. 1)	Tie rods				
304S Tubing (no change)	Absorber Tubes				]]

Prior to making the material specification change, the structural analyses involving the tie rod were thoroughly reviewed. This review showed that all analyses involving the tie rod use the more limiting material properties of the absorber tubes. Therefore, since the new material property requirements for the tie rod are the same as those of the absorber tubes, there are no changes to the results of the structural analyses shown in NEDE-33284P (ref. 2).

References

1. "GE Marathon Control Rod Assembly," NEDE-31758P-A, Class III, October 1991.
2. "Licensing Topical Report: Marathon-5S Control Rod Assembly," NEDE-33284P. Revision 0, September 2006.
3. 1989 ASME Section III, Division 1, Appendix I, Figure I-9.2.1.
4. JA Bannantine, JJ Comer and JL Handrock, 'Fundamentals of Metal Fatigue Analysis', Prentice Hall, 1990.
5. BWR Vessel and Internals Project: Fracture Toughness and Tensile Properties of Irradiated Austenitic Stainless Steel Components Removed from Service (BWRVIP-35)," EPRI TR-108279, June 1997.
6. BWR Vessel and Internals Project: Review of Test Data for Irradiated Stainless Steel Components (BWRVBIP-66)," EPRI TR-112611, March 1999.
7. MFN 07-138, "Marathon Control Rod Assembly Surveillance Program Status", February 26, 2007.
8. *Mechanical Behavior of Materials*, F. A. McClintock and A. S. Argon, pages 277-278, Addison-Wesley Publishing Company, Inc., 1966.

Table 4-1
D Lattice Depletion Calculation Results

Irradiation Time (days)	Equivalent B-10 Depletion (%)	Hot, Voided Eigenvalue	Hot Worth (Δk/k)	Hot Change in Worth (%)	Cold Eigenvalue	Cold Worth (Δk/k)	Cold Change in Worth (%)
[[							]]

Table 4-2
C Lattice Depletion Calculation Results

Irradiation Time (days)	Equivalent B-10 Depletion (%)	Hot, Voided Eigenvalue	Hot Worth (Δk/k)	Hot Change in Worth (%)	Cold Eigenvalue	Cold Worth (Δk/k)	Cold Change in Worth (%)
[[							]]

Table 4-3
S Lattice Depletion Calculation Results

Irradiation Time (days)	Equivalent B-10 Depletion (%)	Hot, Voided Eigenvalue	Hot Worth (Δk/k)	Hot Change in Worth (%)	Cold Eigenvalue	Cold Worth (Δk/k)	Cold Change in Worth (%)
[[							]]

Table 4-4
Marathon-5S Control Rod Nuclear and Mechanical Depletion Limits

Application	End of Life B-10 Equivalent Depletion (%)	
	Nuclear Peak Quarter Segment	Mechanical Four Segment Average
D Lattice, BWR/2-4	[[	
C Lattice, BWR/4,5		
S Lattice, BWR/6		]]

Table 4-5
Initial Reactivity Worth, D Lattice (BWR/2-4) Original Equipment and Marathon-5S CRBs

Condition	Original Equipment Δk/k	Marathon-5S Δk/k	Marathon-5S Change from Original Equipment
Cold	[[		
Hot (40% Void)			]]

Table 4-6
Initial Reactivity Worth, C Lattice (BWR/4,5) Original Equipment and Marathon-5S CRBs

Condition	Original Equipment Δk/k	Marathon-5S Δk/k	Marathon-5S Change from Original Equipment
Cold	[[		
Hot (40% Void)			]]

Table 4-7
Initial Reactivity Worth, S Lattice (BWR/6) Original Equipment and Marathon-5S CRBs

Condition	Original Equipment Δk/k	Marathon-5S Δk/k	Marathon-5S Change from Original Equipment
Cold	[[		
Hot (40% Void)			]]

Table 4-8
Heat Generation Rates

Application	Average Heat Generation Rate (Watts/gram B_4C)	Radial Peaking Factor	Peak Tube Heat Generation Rate (Watts/gram B_4C)
D Lattice, BWR/2-4	[[		
C Lattice, BWR/4,5			
S Lattice, BWR/6			]]

Table 4-9
D Lattice Mechanical Lifetime Calculation

[[

]]

Table 4-10
C Lattice Mechanical Lifetime Calculation

[[

]]

Table 4-11
S Lattice Mechanical Lifetime Calculation

[[

]]

[[

]]

Figure 4-1. D Lattice Fuel Bundle Rod Position and Enrichment

[[

]]

Figure 4-2. C Lattice Fuel Bundle Rod Position and Enrichment

[[

]]

Figure 4-3. S Lattice Fuel Bundle Rod Position and Enrichment

[[

]]

Figure 4-4. D Lattice Control Rod Cold Worth Reduction with Average Depletion

[[

]]

Figure 4-5. C Lattice Control Rod Cold Worth Reduction with Average Depletion

[[

]]

Figure 4-6. S Lattice Control Rod Cold Worth Reduction with Average Depletion